

UC Berkeley
SEMM Reports Series

Title

Damping Characteristics of Prestressed Concrete

Permalink

<https://escholarship.org/uc/item/2nk128q3>

Author

Penzien, Joseph

Publication Date

1962

REPORT TO NAVY

SERIES 100
ISSUE 15

STRUCTURES AND MATERIALS RESEARCH
DEPARTMENT OF CIVIL ENGINEERING

DAMPING CHARACTERISTICS OF PRESTRESSED CONCRETE

BY
J. PENZIEN

Report to
U. S. Naval Civil Engineering Laboratory
Port Hueneme, California

January 1962

INSTITUTE OF ENGINEERING RESEARCH
UNIVERSITY OF CALIFORNIA
BERKELEY CALIFORNIA

DAMPING CHARACTERISTICS OF PRESTRESSED CONCRETE

by

Joseph Penzien

University of California

January 1962

TABLE OF CONTENTS

Foreword	i
Acknowledgment	ii
Notation	iii
I. Introduction	1
II. Experimental Program	1
A. Test Specimens	1
B. Dynamic Testing Equipment	5
C. Dynamic Testing Procedures	8
1. Steady state testing	8
2. Free vibration testing	9
III. Experimental Results	10
A. Steady State Tests	10
B. Free Vibration Tests	11
IV. Discussion of Experimental Results	12
A. Steady State Tests	12
B. Free Vibration Tests	19
V. Conclusions and Recommendations	22
VI. Bibliography	24

LIST OF TABLES AND FIGURES

Table I	-	Beam properties	25
Figure 1	-	Gradation curves for aggregates	27
Figure 2	-	Stress-strain relationships for reinforcing bars	27
Figure 3	-	Prestressing equipment (photograph). . .	28
Figure 4	-	Prestressing bar after removal from beam (photograph).	28
Figure 5	-	Ultimate compressive strength versus age for Mix No. 2	29
Figure 6	-	Unrestrained expansion of grout versus age	29
Figures 7-30	-	Cylinder stress-strain curves	30
Figure 31	-	Free-free beam attached to exciter (photograph)	36
Figure 32	-	Electronic recording equipment (photograph)	36
Figure 33	-	Free vibration testing equipment (photograph)	37
Figure 34	-	Exciter force and velocity oscilloscope record	37
Figure 35	-	Beam deflection versus time oscilloscope record	37
Figures 36-57	-	Resonance curves	38
Figures 58-81	-	Static load-deflection curves	44

Figures 82-89	-	Free vibration response curves	50
Figure 90	-	Dynamic magnification factor versus frequency ratio for a single degree system	58

FOREWORD

The research described in this report, "Characteristics of Prestressed Concrete", was conducted under the supervision and technical responsibility of Joseph Penzien, Associate Professor of Civil Engineering, Division of Structural Engineering and Structural Mechanics, College of Engineering, University of California, Berkeley, California.

This research was performed under the sponsorship of the U. S. Naval Civil Engineering Laboratory, Port Hueneme, California, and is submitted in this final report in fulfillment of Contract No. NBy-32203.

ACKNOWLEDGMENT

The author wishes to express his appreciation and sincere thanks to all those individuals who contributed to the completion of this investigation, especially to Maynard Serbousek for supervising the day-to-day test operations, to Eric Isaacson for his guidance in setting up the electronic recording equipment, to George Hayler for his assistance in establishing the concrete mix designs, to Alex Fattaleh for his assistance in the experimental program and in the preparation of Figures for this report, and to Mrs. Jo Ann Nugent for typing the final report.

The author also wishes to give special thanks to Ronald Dennison and Victor Viets, two high school students sponsored by the National Science Foundation, who contributed a great deal by their assistance in the experimental program.

Finally the author wishes to thank the U. S. Naval Civil Engineering Laboratory, Port Hueneme, California, for the financial assistance which made this investigation possible.

NOTATION

DMF	Dynamic magnification factor
E	Modulus of elasticity of concrete
f'_c	Ultimate strength of concrete
f_t	Modulus of rupture of concrete
L	Length of beam
m	Mass per unit length of beam
M	Total mass of beam
M_1	Generalized mass of the first free-free vibration mode
p_0	Applied static load in free vibration test
\bar{p}	Load amplitude during steady state test
\bar{x}_d	Beam deflection amplitude during steady state test
$\bar{\dot{x}}$	Beam velocity amplitude during steady state test
\bar{x}_s	Static contribution to beam deflection
$x(0)$	Initial beam deflection - free vibration test
t	Time
z	Coordinate along beam axis
λ	Damping coefficient
ω	Circular frequency of harmonic input
ω_1	Circular frequency of first mode of vibration
ϕ	Phase angle between velocity and force, Mode shape function

I. INTRODUCTION

In recent years there has been an increase in the use of prestressed concrete structural elements which must be designed to withstand various types of dynamic loading conditions. These dynamic conditions may be transient in nature as produced by blast loading or earthquake loading or they may be steady state harmonic conditions as produced by heavy rotating equipment. In either case it is desirable in designing such elements that their damping characteristics be known.

Due to the lack of knowledge in this general area, the investigation as reported herein was undertaken to specifically study the damping characteristics of concrete under different types and intensities of prestress.

II. EXPERIMENTAL PROGRAM

A. Test Specimens

A total of 20 prestressed concrete beams and 4 standard reinforced concrete beams (no prestress) having the dimensions 6" x 6" x 90" were tested under dynamic conditions to determine their general damping characteristics. Table I summarizes the important features of each beam by giving the standard properties of the concrete, the location and size of reinforcing bars, and the prestress condition just prior to testing.

All concrete used in the program was manufactured using Santa Cruz Type I cement, Eliot sand, and Fair Oaks gravel. The gradation curves for the aggregates are shown in Figure 1.

Three different concrete mix designs were used in the investigation. The proportions by weight of Type I Santa Cruz Cement, Eliot sand, and Fair Oaks gravel used in each of these mixes were 1.00 : 2.88 : 3.60 (Mix No. 1), 1.00 : 2.31 : 3.29 (Mix No. 2), and 1.00 : 0.96 : 2.04 (Mix No. 3). Water cement ratios by weight were 0.56, 0.475, and 0.28, respectively, which produced ultimate strengths of approximately 4000, 5000, and 6000 pounds per square inch. All concrete when poured produced a slump in the range of 1 to 4 inches. The curing procedure was similar for all concrete specimens and consisted of 7 days in a fog room (100% humidity) followed by 21 days in an air dry condition. All specimens were tested at the age of 28 days.

Three standard control cylinders (6" x 12") and three control flexure beams (6" x 4-7/8" x 20") were poured along with each test beam. These control specimens were tested in accordance with ASTM specifications and gave average compressive strengths and moduli of rupture as presented in Table I. Strain measurements made on two of the three cylinders for each test beam gave the stress-strain curves shown in Figure 7 - 30. The modulus of elasticity for each cylinder tested is summarized in Table I.

Because of the desirability to restrict damping as much as possible to the concrete itself, high strength deformed bars were used as reinforcement rather than standard prestressing cables. Only two bar sizes, namely No. 6 and No. 9, were used in the investigation. While both size bars were of high strength steel, they were rolled from two different grades of steel having the stress-strain properties shown in Figure 2.

In order to maintain better control over the prestress, post-tensioning of the reinforcing bars was employed. This operation necessitated embedding flexible metal tubing (1-7/16" diameter) in the concrete through which the reinforcing bars could later be placed. Post-tensioning was accomplished in a standard manner using an hydraulic jack. Steel bearing plates 1-1/2 inches in thickness were used at the ends of each beam with a 1/4 inch plywood filler plate placed between the steel plate and the concrete to insure an even distribution of prestress. Howlett nuts and wedges were used to grip the bars. The photograph in Figure 3 shows all of the equipment used in the post-tensioning operation.

Post-tensioning of each concrete beam was started within a few days after removal from the fog room. The intensity of prestress applied at this early age was set as close to the design prestress as the strength of the concrete would permit without inflicting damage. Curves of ultimate strength versus age such as shown in Figure 5 for Mix No. 2 were used as a guide in establishing a safe limiting prestress at any age. The prestress was again increased or adjusted several times between the age of 7 and 21 days. At the age of 21 days, final adjustment of prestress was made.

Immediately following final adjustment of prestress, an expansive grouting mixture was pumped into the void space between the reinforcing bar and the flexible metal tubing from one end of the beam until it was forced out a small opening at the opposite end. The formula used to make the grouting mixture was the following: Type I Santa Cruz cement, 10.8 lbs.; Fly Ash, 1.2 lbs.; Interplast C, 55 gms.; 10% solution of plastiment, 6 m.l.; and water, 1944 m.l. An unrestrained

expansion test performed with this material produced the expansion versus age relationship as shown in Figure 6. Compressive strengths of approximately 2890 pounds per square inch at the age of 8 days were observed for this material.

The photograph in Figure 4 shows a reinforcing bar after removal from one of the test beams. In this photograph one will observe that the flexible tubing has been removed over a portion of the bar to expose the hardened grouting material and the grouting material has been removed over a short interval of length to expose the reinforcing bar. Bond between the reinforcing bar, the grout, and the flexible tubing was found to be very good; thus, one could reasonably assume no slippage took place in the immediate region of the reinforcing bars during dynamic testing. This condition was desirable to help restrict the internal damping to the concrete itself.

Several strain gauges were attached to each reinforcing bar prior to their being placed in the flexible tubing. Strains could thus be measured during the prestressing period to provide a check of the magnitude of prestress supplied by the calibrated hydraulic jack. Strains were also measured by these gauges just prior to testing each beam at the age of 28 days so that any loss of prestress, due to creep of the concrete after grouting (21 days), could be determined. However, due to the procedure of prestressing the concrete at as early an age as possible, very little loss of prestress was observed during the period between grouting and testing. These gauges were also used to detect any loss of prestress resulting from the dynamic tests. Because of the large initial strains in the steel bars, this loss was negligible up to the point of complete failure of the concrete.

B. Dynamic Testing Equipment

Each test beam was first subjected to a steady state harmonic excitation as a free-free beam. This free-free condition was obtained by hanging each beam from two relatively soft springs ($k = 17.5 \text{ lb/in}$) which were attached to the beam at its nodal points. The harmonic excitation was obtained by attaching a Model Cl-J, MB exciter to the lower side of the beam at its midpoint, as shown in Figure 31. The attachment of beam to exciter was made through a calibrated load cell which was strain gauged in such a manner that any bending in the load cell itself would not contribute to its output signal. Thus, the signal generated by this load cell was directly proportional to the concentrated load applied to the beam by the exciter driver coil. A velocity generator which is built into the above exciter provides a signal which is directly proportional to the vertical velocity of the driver coil. The above two signals, i.e. the signals from the load cell and the velocity generator, provide a measure of the steady state input and output, respectively.

The photograph in Figure 32 shows the associated electronic equipment used in the steady state testing program. The MB Model T112531 power supply unit for the exciter (Unit No. 1 in photograph) consists of separate power supplies for the driver and field coils, a power supply for the velocity generator, as well as an audio oscillator having a frequency range from 5 - 60,000 cps. The Ellis Model BA2 bridge and amplifier (Unit No. 2) shown in this photograph served as an intermediate element between the load cell and one channel of the Techtronic dual beam oscilloscope (Unit No. 3) shown in this same picture. The purpose of this unit is to balance the strain

gauge bridge on the load cell, amplify its signal before going to the oscilloscope, and to serve as a calibration unit. Two other pieces of equipment are shown in Figure 32, namely, a Hewlett Packard electronic counter, Model 521A (Unit No. 4), which was used only to check the audio oscillator frequency, and a power supply unit (Unit No. 5) for the Techtronic oscilloscope. The output signal from the velocity generator in the exciter is carried directly to one channel of the Techtronic oscilloscope. Shielded cables were used for all connections to ~~eliminate~~ the recording of any stray signals present.

After subjecting each beam to the steady state excitation as previously described, they were supported at their ends as simple beams and subjected to static concentrated loads of various magnitudes at midspan which were then instantaneously released, thus producing a free vibration condition.

This type of loading was accomplished by the system shown in the photograph of Figure 33. As demonstrated in this photograph, the concrete beam is bolted rigidly between two bearing plates at each end. The bottom bearing plates are welded to flexible supporting plates which are in turn welded to a very rigid steel supporting beam. The purpose of these flexible supporting plates is to provide the concrete test beam with supports which are very near to simple supports and which are essentially free of damping. The restraining moments provided by these plates as the ends of the test beam rotate are negligible. The rigid steel supporting beam is clamped into the Baldwin hydraulic testing machine shown in the picture with a force of approximately 15,000 pounds.

The static concentrated load at midspan is applied by a calibrated hydraulic jack which sets on top of a railroad car coil spring which in

turn rests on the upper head of the Baldwin testing machine as shown in Figure 33. The load from the jack is transmitted through a one inch diameter high strength bolt which passed down through the cylinder of the hydraulic jack and on down through the upper head of the Baldwin testing machine with a one-half inch thick plate and a nut being placed on its lower end just under the upper head of the testing machine. To complete the connecting link between jack and concrete test beam, a load bar approximately 9 inches long is threaded into the lower end of the one inch high strength bar. The lower end of this load bar is threaded into a rigid bracket which is in turn bolted rigidly to the test beam. As the hydraulic jack applies a load through the load bar it must be reacted by the railroad car spring ($k = 8.7$ kips/in.). This spring compresses as the load is increased to its desired magnitude and provides the necessary flexibility in the system so that when the load bar is cut no appreciable loss of load will be experienced due to local yielding of the load bar at the point of fracture. Fracture of the load bar is initiated at the desired time using bolt cutters. The one half inch thick plate mentioned above served as a safety element which prevented, upon fracture of the load bar, the sudden release of the strain energy stored in the railroad car spring.

A Bourns linear motion potentiometer, powered with two 45 volt dry cell batteries, was used to measure the center deflection of the concrete test beam immediately following fracture of the load bar. The output signal from this potentiometer was placed directly on one channel of a dual beam Techtronic oscilloscope. Calibration of the

potentiometer was accomplished by measuring the static deflection at the location of the potentiometer using a standard dial gauge.

C. Dynamic Testing Procedures

1. Steady state testing - As indicated in the previous section, each concrete beam was first subjected to steady state harmonic oscillation as a free-free beam. The testing procedure for this loading condition consisted of setting the desired input frequency on the audio oscillator located in the exciter power supply unit and then adjusting the voltage gain on the exciter driver coil to produce the desired force amplitude. This force amplitude was very easily controlled by observing directly on an oscilloscope the signal produced by the calibrated load cell. The response of the beam to this known input was then measured by observing directly on the oscilloscope the signal generated by the velocity generator in the exciter. This signal gave a direct measure of the velocity produced at the center of the beam.

Figure 34 shows two photographs taken directly from the oscilloscope during steady state testing. Each photograph shows two signals as received from the load cell and the signal generator which gave force and velocity conditions, respectively. Photograph A shows, for a particular test condition, a velocity which is leading the force by approximately 80 degrees while photograph B shows a test condition where this phase angle is nearly zero, thus approaching a resonant condition. These example pictures illustrate the method used to measure directly from the oscilloscope (1) the input force amplitude, (2) the velocity amplitude, and (3) the

phase angle between force and velocity. The frequency is read directly off the audio oscillator for each test condition.

Two input parameters were varied during steady state testing, i.e. frequency and amplitude of the input force. The test procedure consisted of holding a constant force amplitude while varying the frequency of the input over a wide range of frequencies (50 - 500 cps). After measuring velocity amplitude and phase angle between velocity and force for many discrete frequencies in this range, the force amplitude was changed and the test repeated as described above.

2. Free vibration testing - The second method of testing each concrete beam, as previously noted, consisted of applying static concentrated loads of various magnitudes at the center of each beam and then suddenly removing these loads so that free vibration of each beam could be observed. In this phase of the program, each load was applied statically in increments up to some prescribed magnitude while noting the resulting static deflection at the center of the beam at each increment. Upon reaching the prescribed load, the load link was fractured, thus inducing free vibration from a known initial deflection.

This free vibration which damps out rapidly was recorded on one channel of a dual beam oscilloscope. The photograph in Figure 35 shows a typical deflection curve recorded during this period. To obtain such a picture it was necessary that the horizontal sweep on the oscilloscope be initiated at the instant of fracture of the load bar. This control was obtained by placing a metal foil along the load bar (but insulated from it), clamping

it to the bar at each end, and connecting it into the sweep circuit of the oscilloscope in such a manner that when fracture of the load bar occurred, the foil would also fracture thus opening a circuit and causing the oscilloscope beam to sweep across the tube at a preset rate.

To establish an accurate time scale for the dynamic response as shown in Figure 35, a 60 cycle signal was placed on the second channel of the dual beam oscilloscope and recorded simultaneously with response during each period of free vibration.

III. EXPERIMENTAL RESULTS

A. Steady State Tests

The pertinent experimental results obtained in these series of tests are shown in Figures 36 - 57. These figures show the relationship between the center deflection amplitude and frequency of vibration over a fairly small range in the vicinity of the frequency of the first mode of vibration. Each individual resonance curve in these figures is for a constant force amplitude (\bar{p}) as indicated; however, this force amplitude is the parameter which changes from one curve to another in each figure. Dynamic magnification factors (DMF) and damping factors (λ) as defined in a subsequent section are given in each of these Figures.

As indicated previously these steady state tests were conducted over the frequency range from 50 - 500 cps. This frequency range was sufficiently high so that resonance of the third mode of vibration (i.e. second symmetrical mode) was observed. However, due to the

small component of input forcing function present to excite this mode it was impossible to get a reliable measure of the damping present in this mode. Therefore, the experimental data obtained outside the frequency ranges indicated in Figures 36 - 57 did not yield any appreciable information regarding damping and as a result will not be included in this report.

Phase angles between the force input and the velocity output were measured throughout the frequency range 50 - 500 cps but again only those data in the region of the frequencies shown in Figures 36 - 57 are considered of any importance. Since these phase angles were observed to agree reasonably well with theory, they have not been included in this report.

B. Free Vibration Tests

Figures 58 - 81 present the static load versus center deflection relationship for each of the 24 beams tested. The continuous curves in these Figures represent the deflections produced during the initial loading while the dashed curves represent the deflections produced during subsequent loadings. The arrows in Figure 58 illustrate the manner in which loading was applied to Beam No. 1. All other load-deflection curves should be interpreted in a similar manner.

Each beam was positioned on its supports with the cross section oriented as shown in Table I and was loaded in an upward direction at its center. Therefore, those beams having an unsymmetrical section were loaded statically in their weak direction. This direction of loading was considered desirable since any inelastic deformation taking place during dynamic testing would be in that direction

regardless of the direction of load application. No attempt was made to measure a static load-deflection relation for negative loading (i.e. downward loading) for these unsymmetrical cases; however, from the geometry of the cross section and the positive loading results one can predict this relation reasonably well in range of loading applied during dynamic testing.

As previously described the free vibration tests were conducted by simply loading each beam statically in the positive or upward direction, suddenly releasing the load, and measuring the subsequent center deflection of the beam as it vibrates and finally comes to rest. Photographs taken directly from the oscilloscope which show this free vibration response are presented in Figures 82 - 89. The test number given on each of these Figures is also given on the static load-deflection curve for each corresponding beam (Figures 58 - 81) to show the static load-deflection condition of each beam when free vibration starts. This initial static load and its corresponding deflection are given for each test as presented in Figures 82 - 89. Effective viscous damping factors (λ) as defined in the subsequent section are also given for each of these tests.

IV. DISCUSSION OF EXPERIMENTAL RESULTS

A. Steady State Tests

The pertinent experimental data obtained during steady state testing consist of the resonance curves shown in Figures 36 - 57. As previously pointed out, each test beam was supported as a free-

free beam and subjected to a concentrated harmonic force of amplitude \bar{p} at midspan. The resulting steady state vertical velocity amplitude \bar{x} at midspan was measured along with the phase angle ϕ as shown in Figure 34. By dividing this velocity amplitude by the known circular frequency ω of the input forcing function, the center deflection amplitude can be obtained.

Several standard methods can be used to measure the amount of damping as represented by a resonance curve. For this investigation the method considered to be most accurate was simply to base the amount of damping on the response amplitude at resonance. Thus, the dynamic magnification factors ($DMF = \bar{x}_d / \bar{x}_s = \text{dynamic deflection} / \text{static deflection}$) as shown in Figures 36 - 57 are based on resonance conditions. In calculating any particular dynamic magnification factor, the measured dynamic deflection \bar{x}_d is taken directly from the resonance curve; however, the static deflection \bar{x}_s is calculated using the equation

$$\bar{x}_s = \bar{p} / \omega_1^2 M_1 \quad (1)$$

where ω_1 is the resonant frequency of the first mode of vibration and M_1 is the generalized mass of the first mode of vibration. This generalized mass can be calculated using the well known equation

$$M_1 = \int_0^L m(z) \phi_1(z)^2 dz \quad (2)$$

where z is the coordinate along the beam axis, L is the length of the beam, $m(z)$ is the beam mass per unit length, and $\phi_1(z)$ is

the first mode shape normalized so that $\phi_1(\frac{L}{2}) = 1$. It has been assumed in calculating this generalized mass for each test beam that the first mode shape corresponds to that of a uniform free-free beam and is given by the equation

$$\begin{aligned} \phi_1(z) = & -0.982 \left(\text{Sinh } 4.75 \frac{z}{L} + \text{Sin } 4.75 \frac{z}{L} \right) \\ & + \left(\text{Cosh } 4.75 \frac{z}{L} + \text{Cos } 4.75 \frac{z}{L} \right) \end{aligned} \quad (3)$$

It has also been assumed in calculating the generalized mass that the mass per unit length $m(z)$ is constant and equal to M/L where M is the total known mass of the test beam. Substituting Equation (3) and M/L for $m(z)$ into Equation (2) will give

$$M_1 = 0.677M \quad (4)$$

It should be recognized that Equation (4) is approximate due to the presence of the steel end plates which change the mode shape $\phi_1(z)$ slightly from that given by Equation (3) and also influence the mass distribution term $m(z)$ appearing in Equation (2). The error introduced by this approximation is small, however, and therefore can be permitted.

In calculating the DMF's in the manner described above, it is assumed that only the first mode of vibration contributes to the dynamic displacement \bar{x}_d . This assumption is, of course, not strictly true; however, for low damped systems, the contributions from higher modes are negligible when first mode resonance is obtained.

The damping factors λ given in Figures 36 - 57 are based on the usual assumption of viscous damping and have been calculated

using the equation

$$\lambda = \frac{1}{2 DMF} \quad (5)$$

The above theoretical considerations are based on linear flexure theory and should be applied only to those beams showing linear response characteristics. As noted in Figures 58 - 81, the beams tested in this investigation are highly non-linear in character if the deflections produced are sufficiently high. However, in conducting the steady state tests all vibrations were limited to small amplitudes. Therefore, these beams generally responded in their initial linear range thus making the above theoretical considerations applicable.

To study the effect of various parameters on internal damping, consider first the results given in Figures 36 - 49 for Beams Nos. 1 - 16 (see Table I). Two important design parameters are involved, namely, magnitude and type of prestress.

It is apparent by comparing the results given in Figures 36 - 38 and also by comparing the results given in Figures 39 - 42, that for these tests magnitude of prestress did not greatly influence damping. In each of these cases, no tension cracks were developed due to the type of prestress and due to the small amplitude oscillations produced. Therefore, based on these results, it would appear that as long as the initial prestress keeps the entire cross section of the beam under compressive stresses during the vibration period, damping will not be affected greatly by the magnitude of the initial prestress. As noted on Figures 36 - 42, the amount of damping for these cases ranged from about 0.5 - 1.0 percent of critical.

Consider now the results presented in Figures 43 - 45 which represent the triangular initial prestress condition. Comparing these results with those discussed in the previous paragraph (Figs. 36 - 42), it is apparent an increased amount of damping is present. It would appear in this case that the tensile stresses produced by the vibration accounts for this increase. As noted, this increase in damping is accompanied by reduced resonant frequencies which indicate cracking of the concrete has taken place. For this triangular type of prestress, damping would seem to be reduced as the intensity of initial prestress is increased. This reduction is to be expected since the initial linear range of the beam is extended somewhat with increased intensity of prestress as indicated by the static load-deflection curves shown in Figures 66 - 69. The amount of damping given in Figures 43 - 45 for this prestress type ranges from approximately 0.75 - 1.50 percent of critical.

Now observe the results presented in Figures 46 - 49 for Beams Nos. 13 - 16. As shown in Table I, these beams have been prestressed so that tensile stresses are also produced by the initial prestress. However, as shown by Table I, the initial prestress for Beams Nos. 15 and 16 were sufficiently great to produce cracking. It is obvious from the resonance curves in Figures 46 - 49, that damping for this prestress type is greater than the damping observed for any of the other three prestress types previously discussed. This increase is due to the greater amount of cracking permitted. From the data presented for this prestress type, it is difficult to make any conclusions as to the effect which magnitude of initial prestress has on damping. Damping factors are observed for these cases in the approximate range of 1.0 - 2.0 percent of critical.

From the previous discussion of the results presented in Figures 36 - 49, it is generally concluded that the important parameter which affects the amount of internal damping in prestressed concrete is the degree to which tension cracks were allowed to develop in the concrete. The two design parameters involved in these cases, namely, magnitude and type of prestress, have an indirect influence on damping in that these parameters influence the amount of cracking which can take place.

It should be noted in all of the above cases that the damping factor λ increases with amplitude of oscillation. Even in those cases where the initial prestress keeps the entire cross section under compressive stresses during the vibration period, an increase in damping with amplitude of oscillation is observed. The rate of increase with amplitude is, of course, much more pronounced when the amplitudes increase sufficiently to develop tension cracks.

The resonance curves shown in Figures 50 - 53 were obtained from tests conducted on Beams Nos. 17 - 20 which were ordinary reinforced concrete beams (no prestress). Beam No. 17 obviously cracked during testing which resulted in damping factors of over two percent of critical and also resulted in a reduced frequency. Beam No. 18 apparently did not crack during testing as indicated by the low damping factors and by the resonant frequency of 90 cps which is about correct for an uncracked beam of this type. Beams Nos. 19 and 20 were reinforced on both top and bottom as shown in Table I and as a result no cracking took place during testing. Thus low damping factors, i.e. of the order of one percent of critical, were observed.

As pointed out in a previous section of this report, Beams Nos. 1 - 20 were manufactured using concrete Mix No. 1, Beams Nos. 21 and 22 were manufactured using Mix No. 2, and Beams Nos. 23 and 24 were manufactured using Mix No. 3. Therefore, it was the intent to check the effect which concrete ultimate strength has on damping by testing Beams Nos. 21 - 24. It is quite obvious, however, that the effect of this parameter is entirely overshadowed by the effect of cracking.

Beams Nos. 21 and 23 were prestressed and do not show evidence of cracking as shown by their resonance curves (Figs. 54 and 56), i.e. the damping factors are reasonably low and their frequencies are consistent with uncracked sections.

Beams Nos. 22 and 24, which were ordinary reinforced beams, produced the resonance curves shown in Figures 55 and 57. It is quite apparent that both of these beams cracked during the steady state tests as evidenced by the large increase in damping with amplitude and by the reduction of their resonant frequencies with amplitude.

As previously pointed out, all damping factors given on Figures 36 - 57 were based on the measured amplitude of response at resonance. However, the general shape of the resonance curves in these Figures also give an indication of the amount of damping as illustrated by comparing these resonance curves with those presented in Figure 90 for a single degree system.

In concluding this discussion on the steady state test results, it seems appropriate to re-emphasize that the important parameter

which appears to influence damping in prestress or ordinary reinforced concrete elements is the degree to which cracking is permitted to develop. Damping factors seem to be of the order of one percent or less for uncracked members but increase with the degree of cracking permitted. Maximum damping factors measured in these tests were of the order of 2.5 percent of critical. For these extreme cases, cracks were unquestionably produced; however, considering the small amplitudes of oscillation which produced them, it would be impossible to see such cracks with the naked eye even if one could stop the motion of the vibrating beam at its maximum amplitude of motion.

B. Free Vibration Tests

Due to the limited force output of the available excitor used in the steady state test program, it was necessary that each test beam be further tested using the free vibration method previously described so that large amplitude oscillation could be achieved. The results of this investigation are presented in Figures 82 - 89. The applied static load p_0 and resulting deflection $x(0)$ as indicated for each dynamic test is represented by a point on the appropriate static load-deflection curve in Figures 58 - 81.

Each damping coefficient λ shown in Figures 82 - 89 is based on the assumption of viscous damping and has been obtained in the usual way by measuring the decrement of damping directly from the photographs of the decayed free vibration response. This decrement was checked for successive cycles of oscillation for a number of tests to determine if damping was a function of amplitude. While

some variations were observed, generally the damping decrement was reasonably constant over the earlier portion of the decayed response curve. Therefore, all λ 's were calculated by considering the reduction in displacement amplitude over a period of four cycles of oscillation which results in the equation

$$\lambda = \frac{1}{2\pi} \left[1 - \sqrt[4]{\frac{x_{n+4}}{x_n}} \right]$$

where x_n is the displacement amplitude of the n th cycle of oscillation. Due to the accuracy of the amplitude measurements, it is very difficult to measure accurately the damping decrement towards the end of the decayed response curve. Therefore, damping for the relatively low amplitude oscillations could not be measured.

In attempting to correlate the damping factors in Figures 82 - 89 with the various parameters involved, considerably more difficulty arises than in the correlation of the steady state results previously discussed. This difficulty would seem to be due to the fact that in most cases the initial maximum displacements are sufficiently large to produce cracking in the concrete. Since the amount of this cracking can vary over a wide range and since each beam had been loaded only once or twice to the prescribed test load before the actual test was conducted, one might expect considerable differences in the damping factors obtained. This latter statement would imply that past history of loading is an important parameter. To illustrate this point, Test 22-2D (Fig. 88) was initiated at a load of 3.30 kips which was the first time Beam No. 22 had been loaded to this level. From the resulting decayed response curve it is quite clear that cracks were produced on the first cycle of oscillation; thus, a relatively large amount of the strain energy was immediately dissipated.

Obviously for this case any damping factor one might calculate would be meaningless. Test 22-3D is a rerun of Test 22-2D, which gave entirely different results. It can be assumed from these results that Test 22-3D did not produce any additional new cracks.

If one observes only those dynamic tests which were conducted strictly in the linear range (see Figs. 58 - 81), damping factors generally fall in the range 3 - 3 1/2 percent of critical. For those tests conducted in the non-linear range where large cracks develop, damping factors generally fall in the range 3 1/2 - 6 percent of critical. There is, however, one exception to this statement, i.e. for those tests involving Beams Nos. 20, 22, and 24 which were reinforced both top and bottom. For these beams damping seemed to show a decrease for the large amplitude oscillation.

In comparing the low amplitude free vibration results with the steady state results, greater damping factors are observed in the case of free vibration. While this difference is greater than one would expect, there are a number of factors which no doubt contribute to this difference. Some of these contributory factors are the following:

- (1) In the steady state tests, many thousands of cycles of loading were accumulated before the basic test data were recorded, while in the free vibration case, each beam experienced only one or two previous cycles of load. It is expected that damping will decrease with number of load cycles to a given amplitude.
- (2) The displacement amplitudes were higher in the free vibration tests than in the steady state tests.

- (3) The frequency of oscillation was lower in the free vibration tests than in the steady state tests.
- (4) Support damping was higher in the case of free vibration tests. As pointed out in numerous references, support damping can be very important in practical situations and should not be overlooked. To what extent support damping influenced the results presented in this report is unknown; however, considerable effort was made to minimize this effect. It is quite evident that further work is needed to study the effect of this very important parameter.

V. CONCLUSIONS AND RECOMMENDATIONS

Based on the experimental results obtained in this investigation, the following general conclusions have been deduced:

- (1) Under steady state conditions, internal damping in prestressed concrete members may be less than one percent of critical if the initial prestress is sufficient to prevent tension cracks from developing. If tension cracks are allowed to develop, but on a microscopic scale, damping can be expected of the order of two percent of critical. If larger (visible) cracks are permitted to develop, one should expect higher damping.
- (2) Under transient conditions, the amount of internal damping present in prestressed concrete members depends to a great extent on the past history of loading and on the amplitude

of displacements produced. For those cases where members have been dynamically loaded only a few times to a given stress level which produces considerable cracking, damping can be expected anywhere in the range of 3 - 6 percent of critical.

- (3) Magnitude and type of prestress in concrete members have an indirect influence on internal damping only because these parameters control the amount of cracking which can take place.

There are numerous factors which affect the overall damping in a prestressed concrete structural system as pointed out in this report. Those factors which were not included as parameters in this investigation but which need further study are the following:

- (1) Effect of history of loading on internal damping;
- (2) Effect of support conditions on external damping; and
- (3) Effect of frequency on overall damping.

VI. BIBLIOGRAPHY

1. Technical Report 116, "Blast Load Tests on Post-Tensioned Concrete Beams", U. S. Naval Civil Engineering Laboratory, Port Hueneme, California.
2. Report 17, C.U.R., "Vibration Problems in Prestressed Concrete", Netherlands Committee for Concrete Research, January, 1960.
3. Etkin, Y., "A Study of the Resonant Frequencies of Prestressed Concrete", Thesis, London, 1956.
4. Bock, E., "Das Verhalten von Beton-und Stahlbetonbalken bei Biegeschwingungen" ("The Behavior of Concrete and Reinforced Concrete Beams Subjected to Transverse Vibrations"), Zeitschrift des Vereins Deutscher Ingenieure, 1942.
5. Jones, R., "The Effect of Frequency of the Dynamic Modulus and Damping Coefficient of Concrete", Magazine of Concrete Research, Vol. 9, No. 26, August, 1957.
6. Denkhaus, G. and Dück, G., "Über das Verhalten von Spannbetonbalken bei Biegeschwingungen" ("The Behaviour of Prestressed Concrete Beams Subjected to Transverse Vibrations"), Beton-und Stahlbetonbau, 1952.
7. Ruzicka, J., "Structural Damping", The American Society of Mechanical Engineers, 1959.
8. O'Neil, C., "Structural Damping as Influenced by Support Conditions", Thesis, University of California, Berkeley, January, 1962.

Table I

f_c^1 (28 day Compressive Strength), E (Modulus of Elasticity), f_t (Modulus of Rupture)

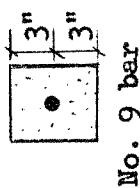

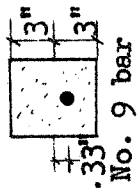



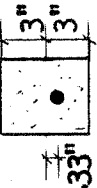

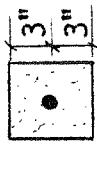

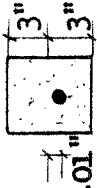
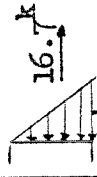
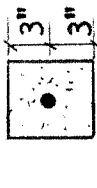
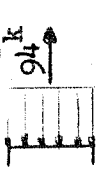
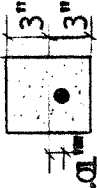

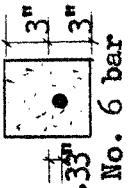
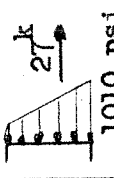
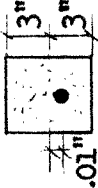
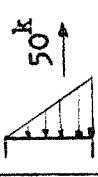


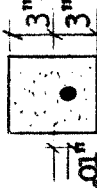

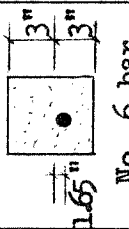

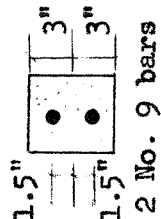
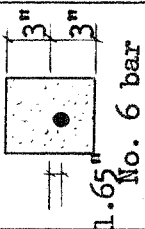
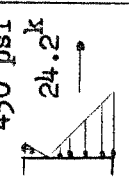
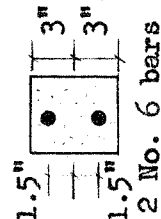
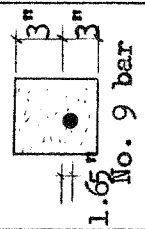
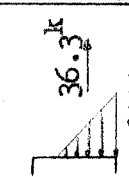
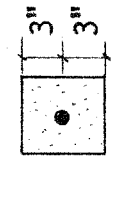

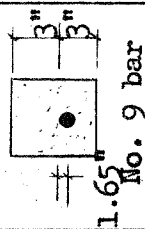
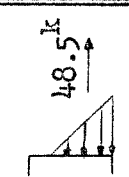
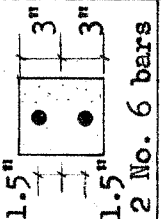
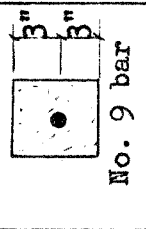
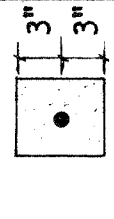
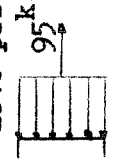
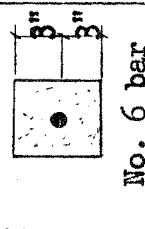
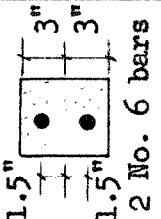
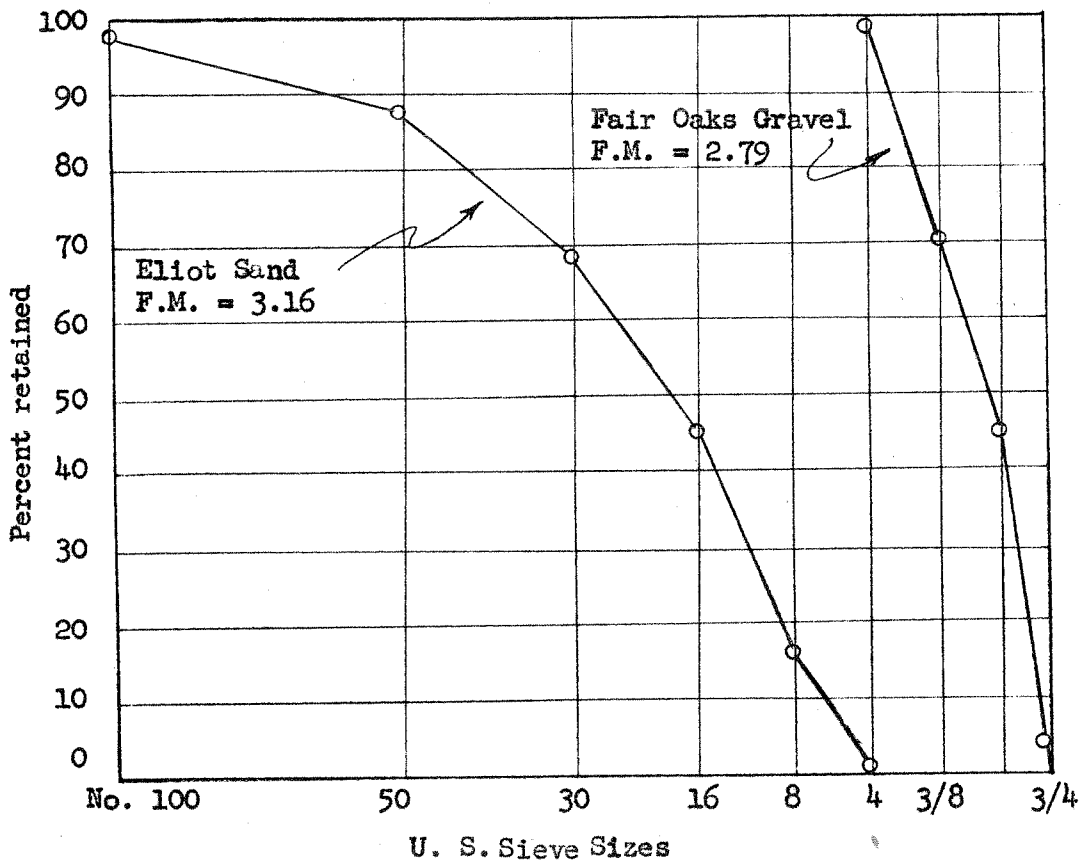
Beam No.	f_c^1 psi	E psi	f_t psi	Cross Section	Initial Prestress Condition	Beam No.	f_c^1 psi	E psi	f_t psi	Cross Section	Initial Prestress Condition
1	5040	3.1×10^6 4.0×10^6	571	 No. 9 bar		7	5310	4.3×10^6 4.3×10^6	675	 No. 9 bar	
2	4920	4.7×10^6 4.7×10^6	550	 No. 9 bar		8	4890	4.2×10^6 4.8×10^6	620	 No. 9 bar	
3	4600	4.3×10^6 4.3×10^6	562	 No. 9 bar		9	5100	3.6×10^6 4.1×10^6	617	 No. 6 bar	
4	4755	3.6×10^6 3.6×10^6	599	 No. 9 bar		10	4780	3.3×10^6 3.3×10^6	637	 No. 9 bar	
5	5020	4.0×10^6 4.0×10^6	606	 No. 6 bar		11	5010	3.6×10^6 3.6×10^6	610	 No. 9 bar	
6	5170	4.2×10^6 4.6×10^6	654	 No. 9 bar		12	4980	4.0×10^6 4.0×10^6	530	 No. 9 bar	

Table I (continued)

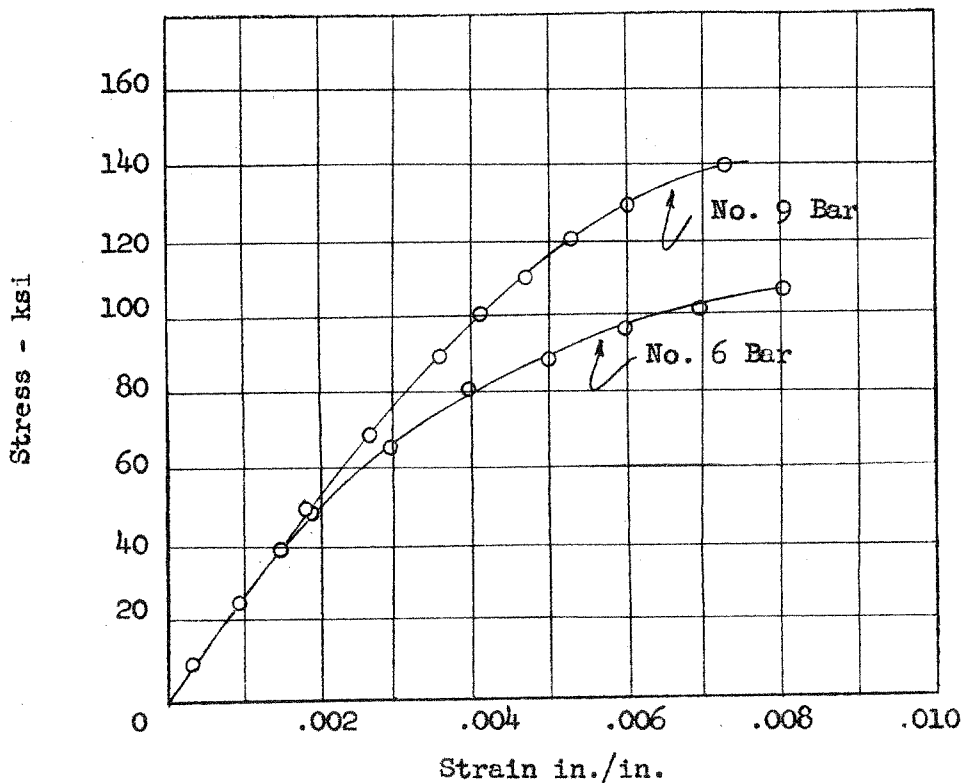
f_c^l (28 day Compressive Strength), E (Modulus of Elasticity), f_t (Modulus of Rupture)

Beam No.	f_c^l psi	E psi	f_t psi	Cross Section	Initial Prestress Condition	Beam No.	f_c^l psi	E psi	f_t psi	Cross Section	Initial Prestress Condition
13	5243	4.1×10^6 4.5×10^6	649	 1.65" No. 6 bar	 220 psi 12.0 k	19	5100	4.0×10^6 4.0×10^6	659	 1.5" 3" 3" 2 No. 9 bars	No prestress
14	5510	4.0×10^6 5.0×10^6	709	 1.65" No. 6 bar	 450 psi 24.2 k	20	5100	3.8×10^6 4.1×10^6	678	 1.5" 3" 3" 2 No. 6 bars	No prestress
15	5330	4.2×10^6 4.2×10^6	580	 1.65" No. 9 bar	 36.3 k 2990 psi	21	4087	3.6×10^6 3.6×10^6	605	 1.5" 3" 3" No. 9 bar	1140 psi 
16	5390	4.3×10^6 4.3×10^6	654	 1.65" No. 9 bar	 48.5 k 4000 psi	22	4087	3.9×10^6 3.9×10^6	616	 1.5" 3" 3" 2 No. 6 bars	No prestress
17	5230	4.0×10^6 4.0×10^6	619	 1.65" No. 9 bar	No prestress	23	6360	5.0×10^6 5.0×10^6	693	 1.5" 3" 3" No. 9 bar	2640 psi 
18	5250	4.2×10^6 4.6×10^6	535	 1.65" No. 6 bar	No prestress	24	5983	5.1×10^6 5.5×10^6	686	 1.5" 3" 3" 2 No. 6 bars	No prestress



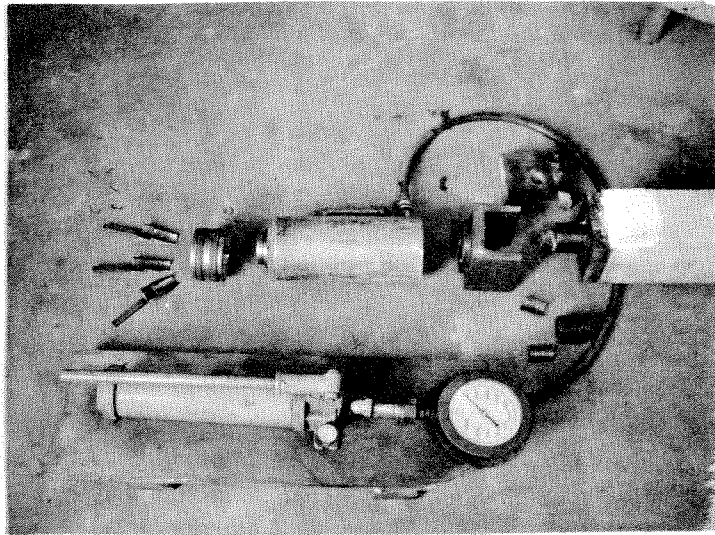
Gradation curves for aggregates

Figure 1



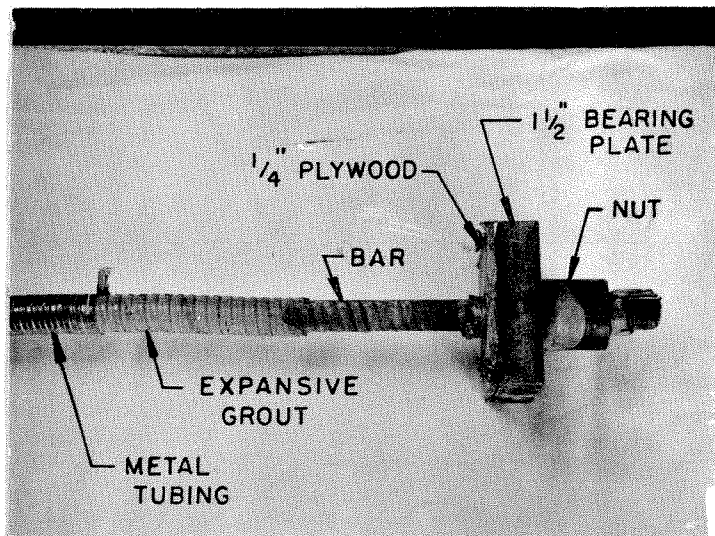
Stress-strain relationships for reinforcing bars

Figure 2



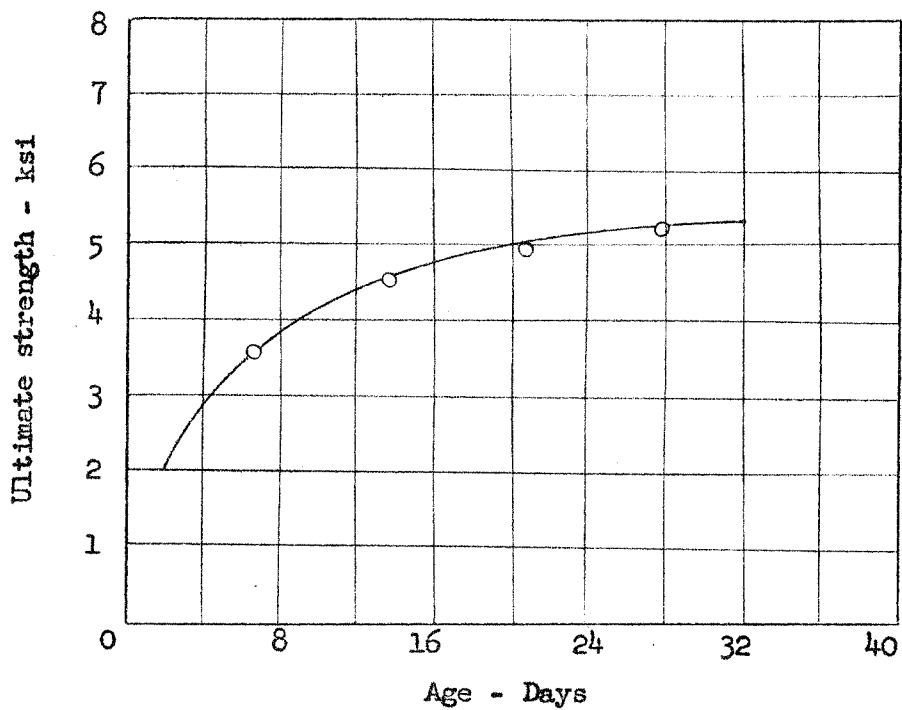
Prestressing equipment

Figure 3



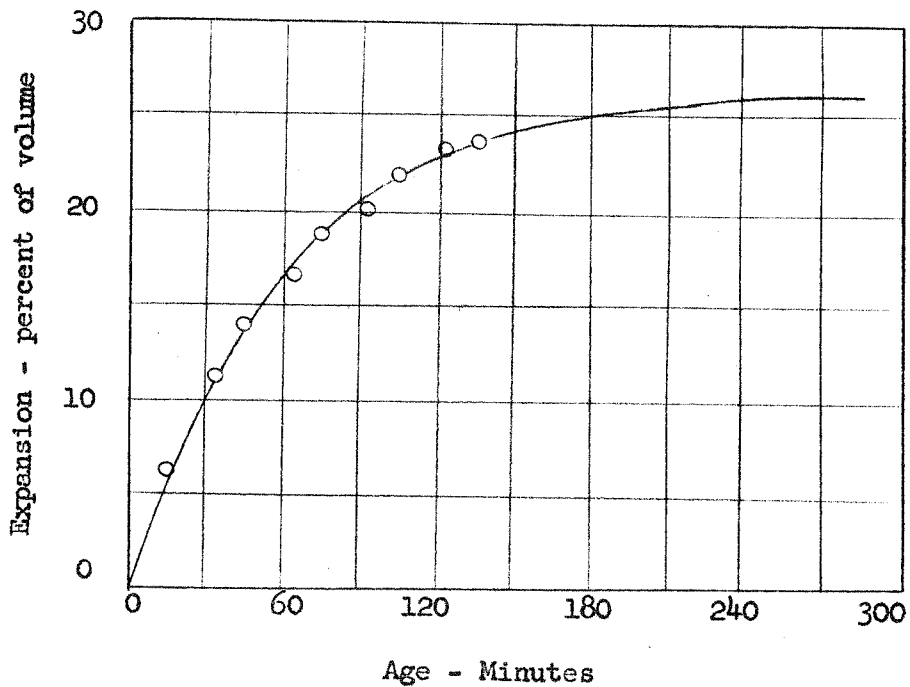
Prestressing bar after removal from beam

Figure 4



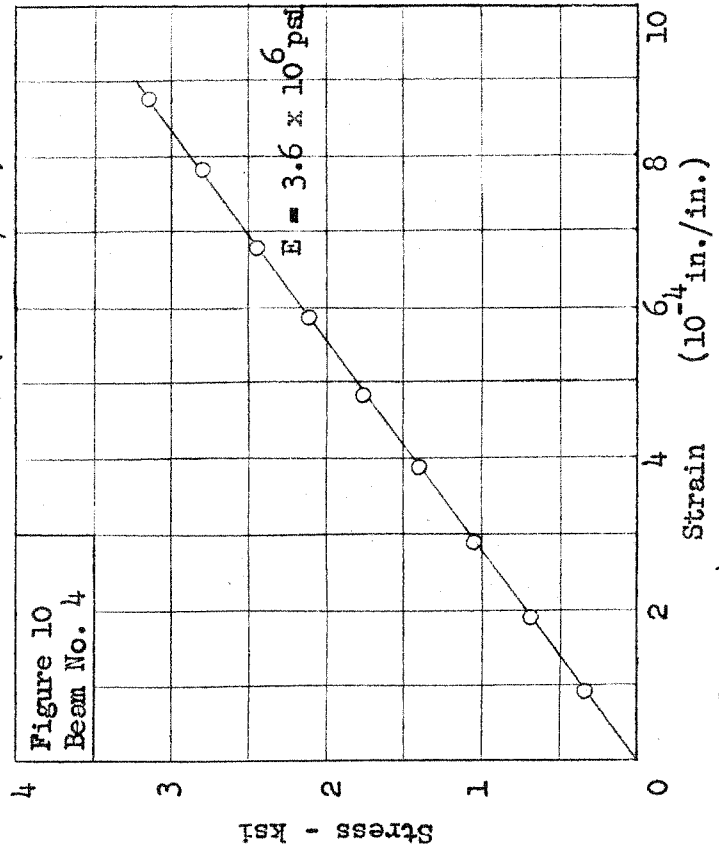
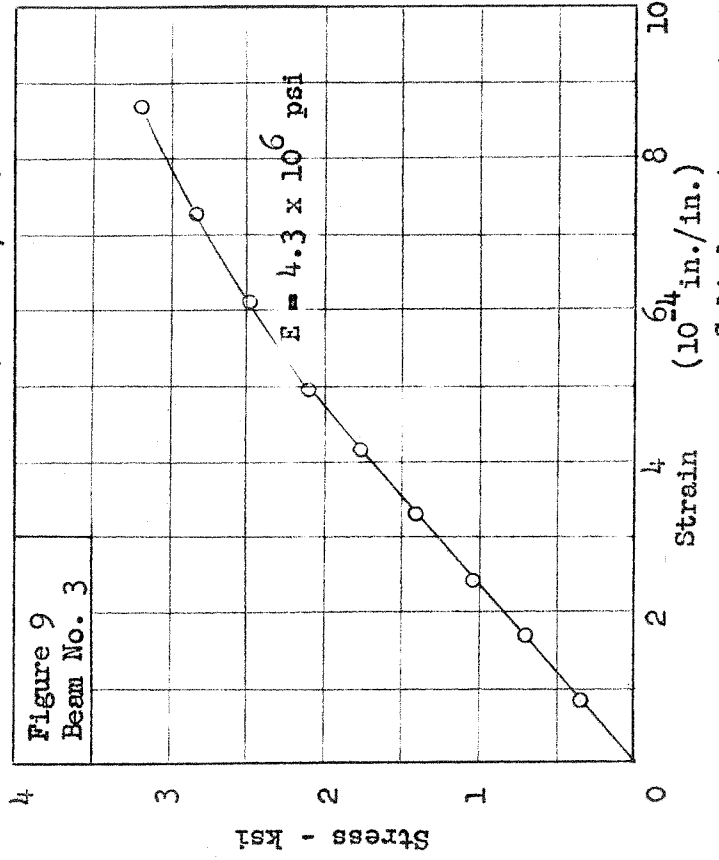
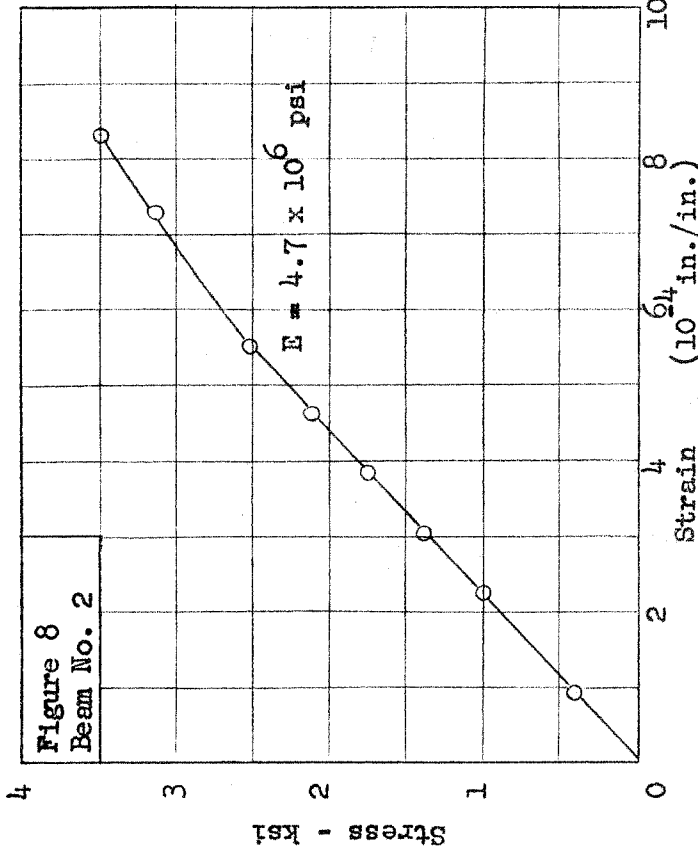
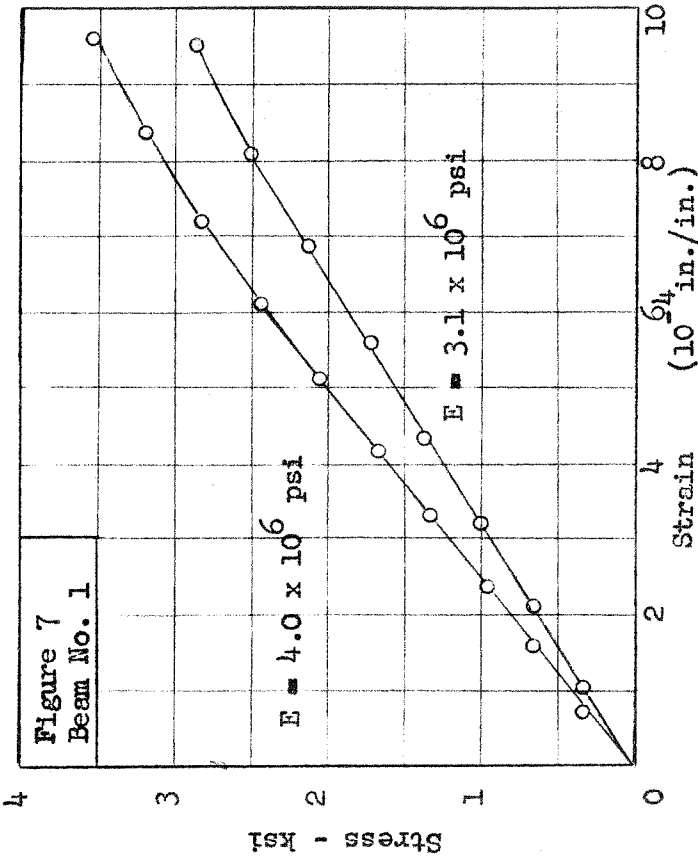
Ultimate compressive strength versus age for Mix No. 2

Figure 5

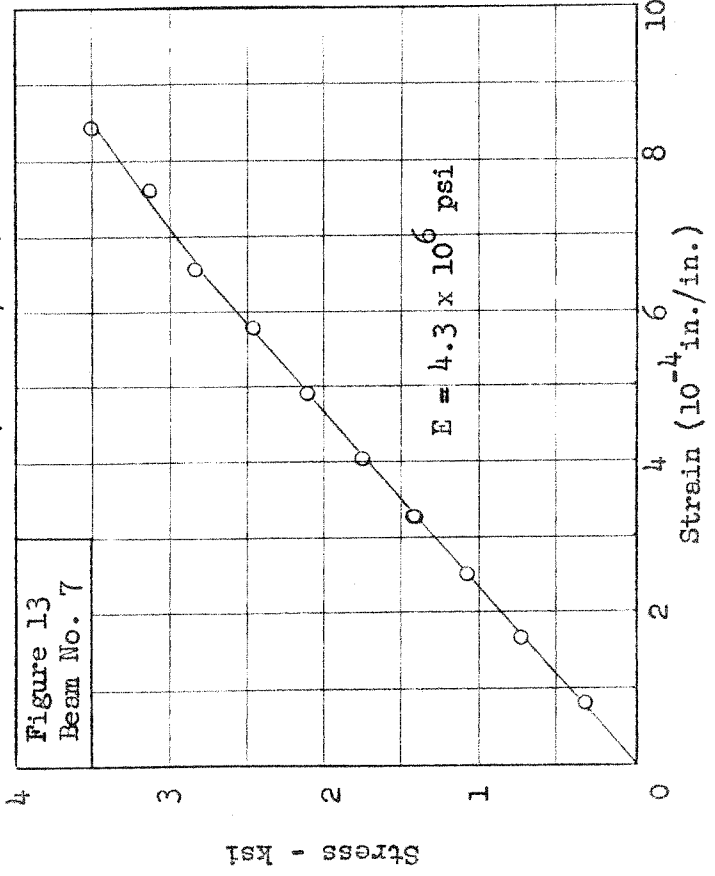
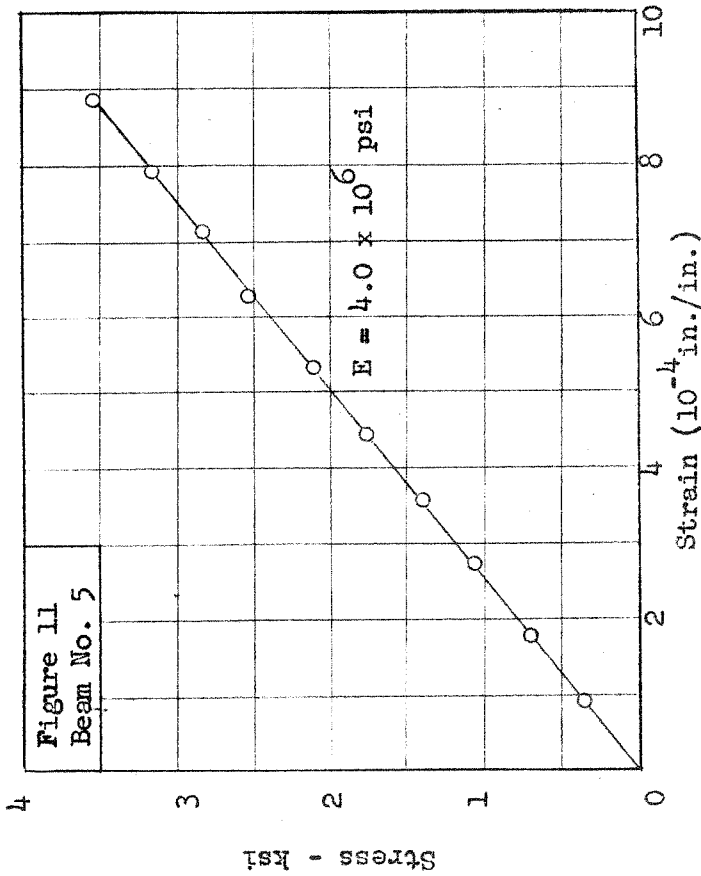
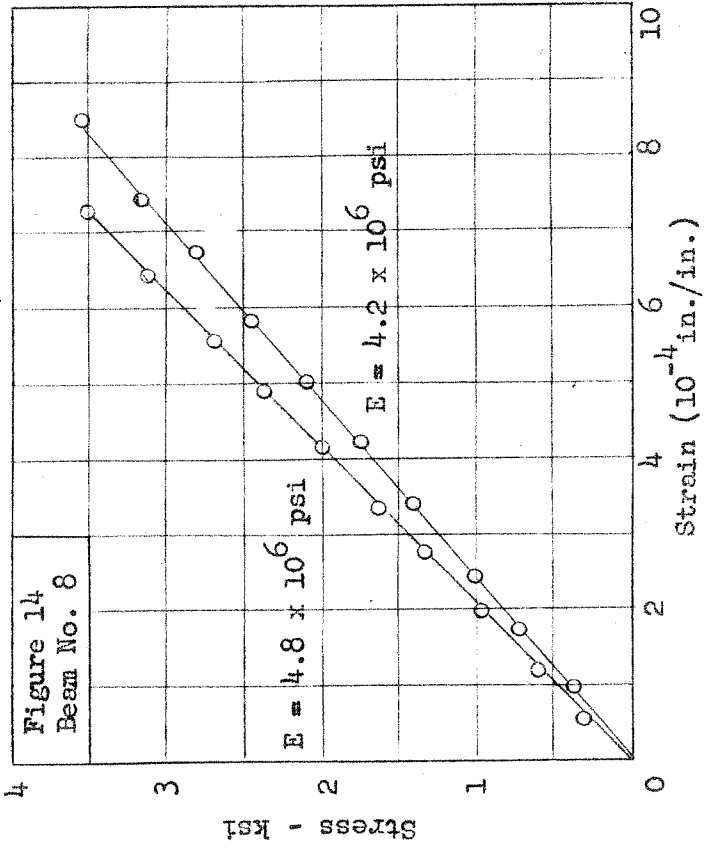
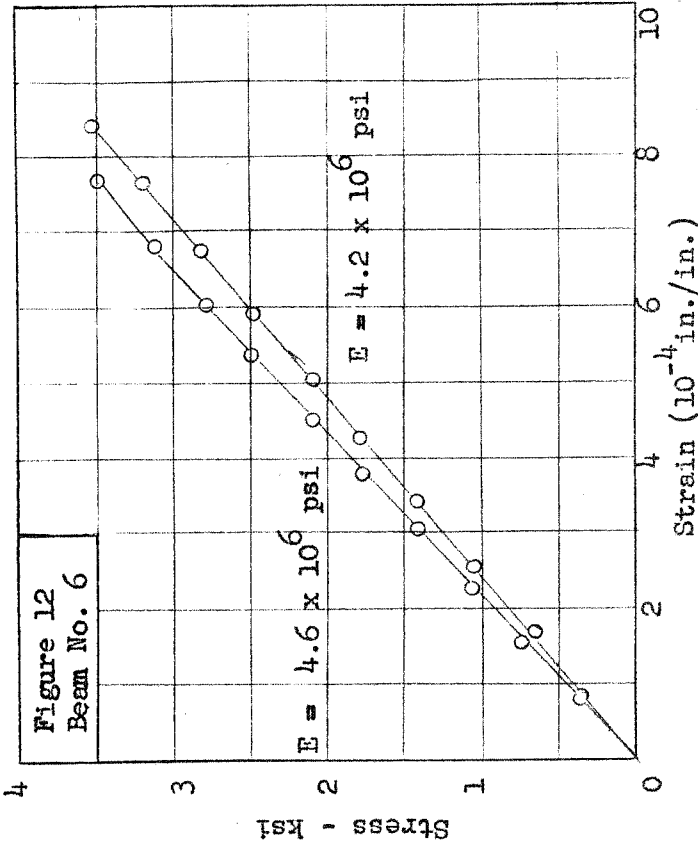


Unrestrained expansion of grout versus age

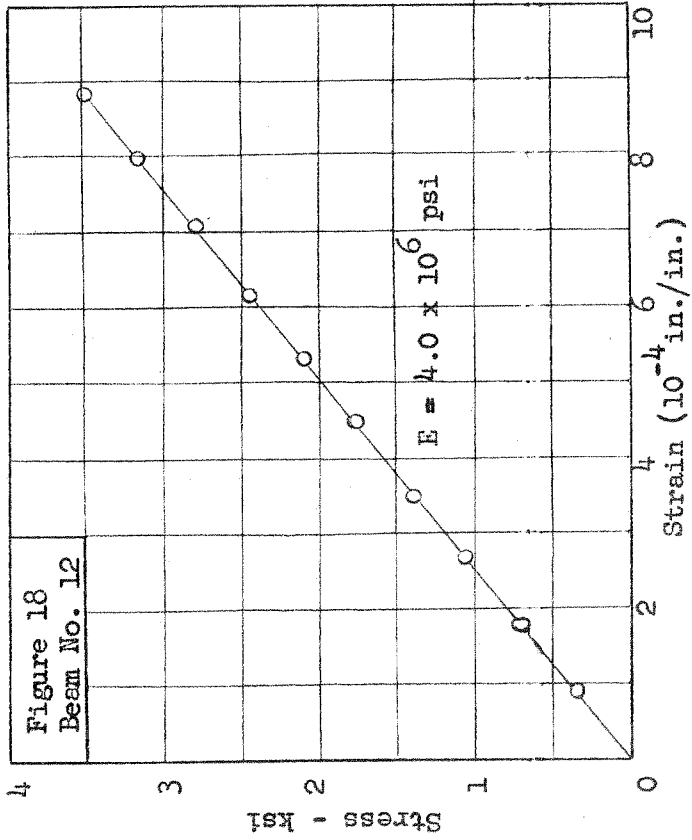
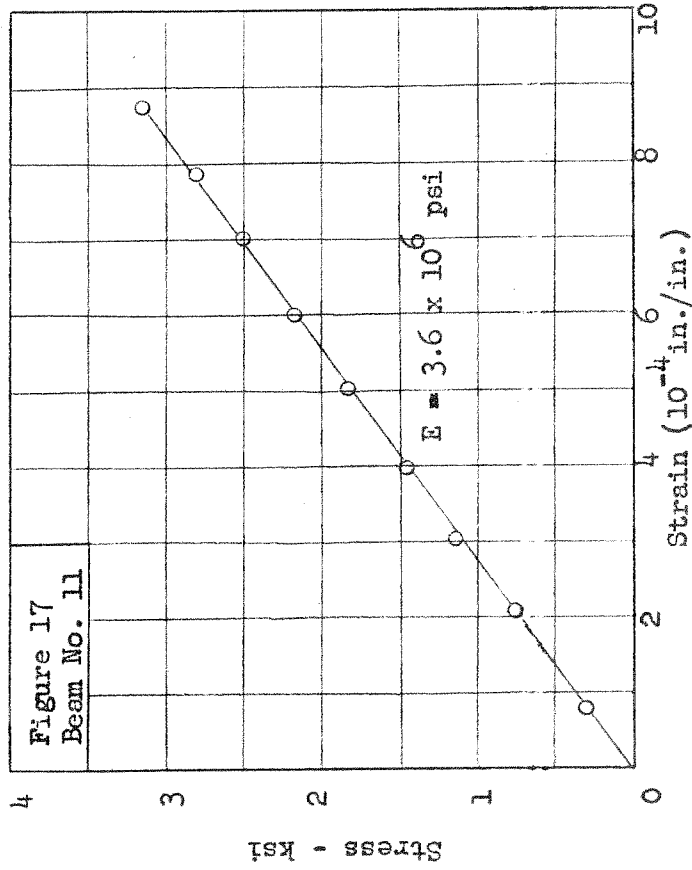
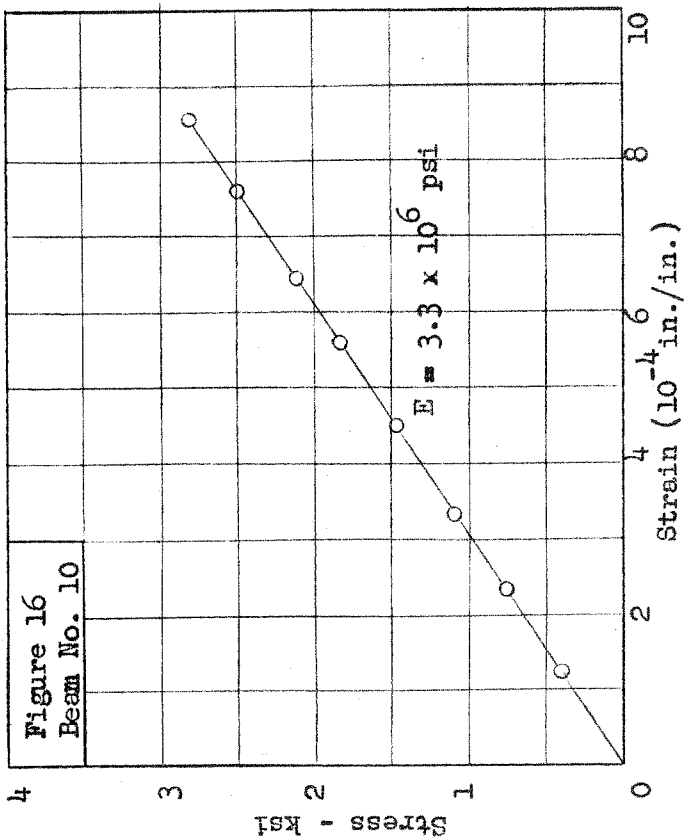
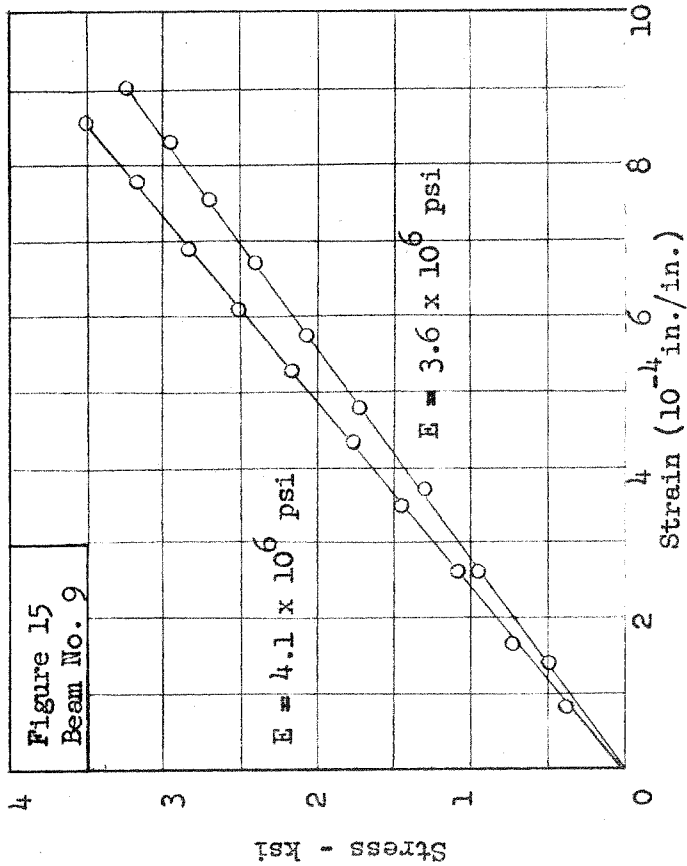
Figure 6



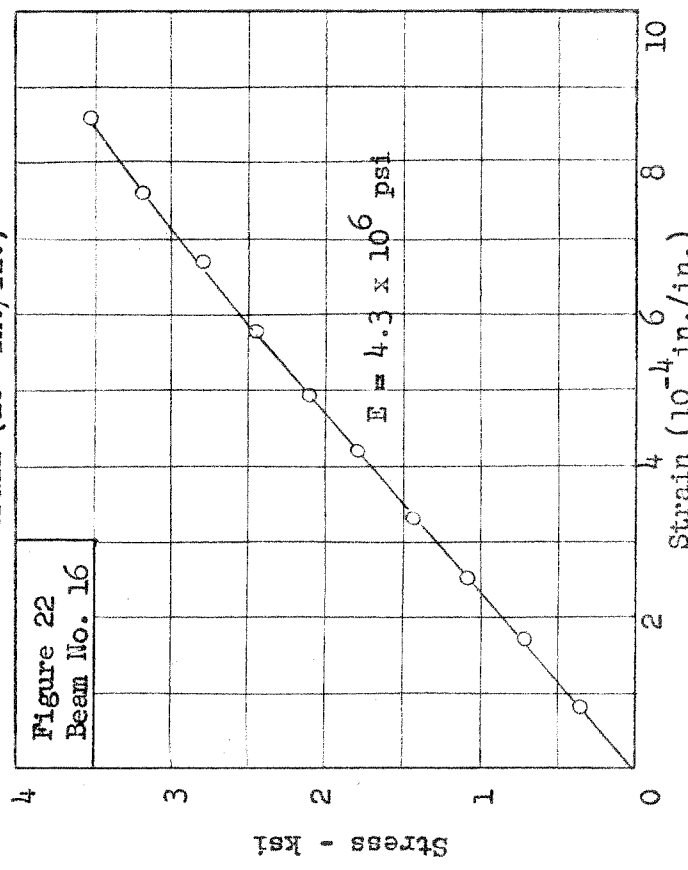
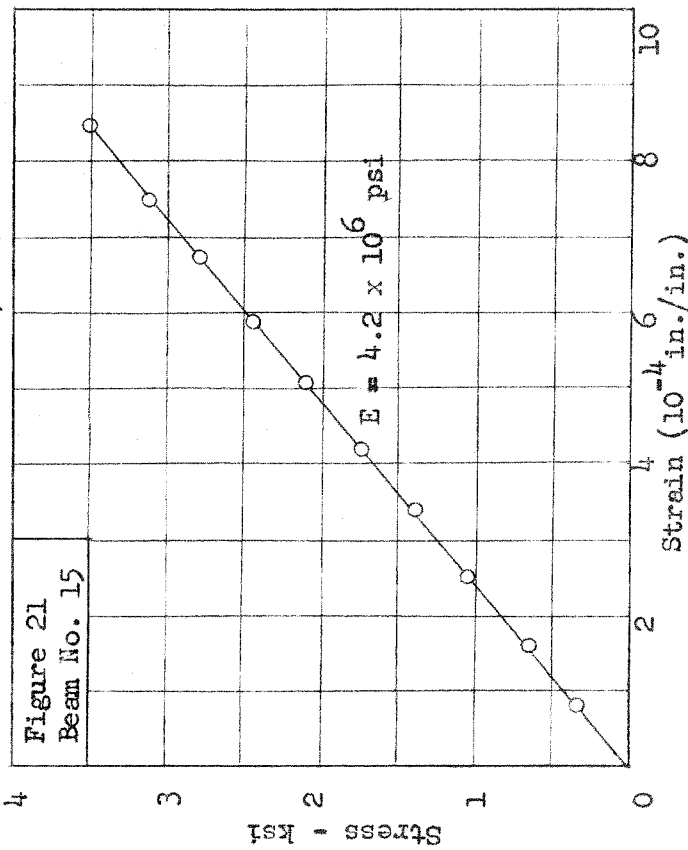
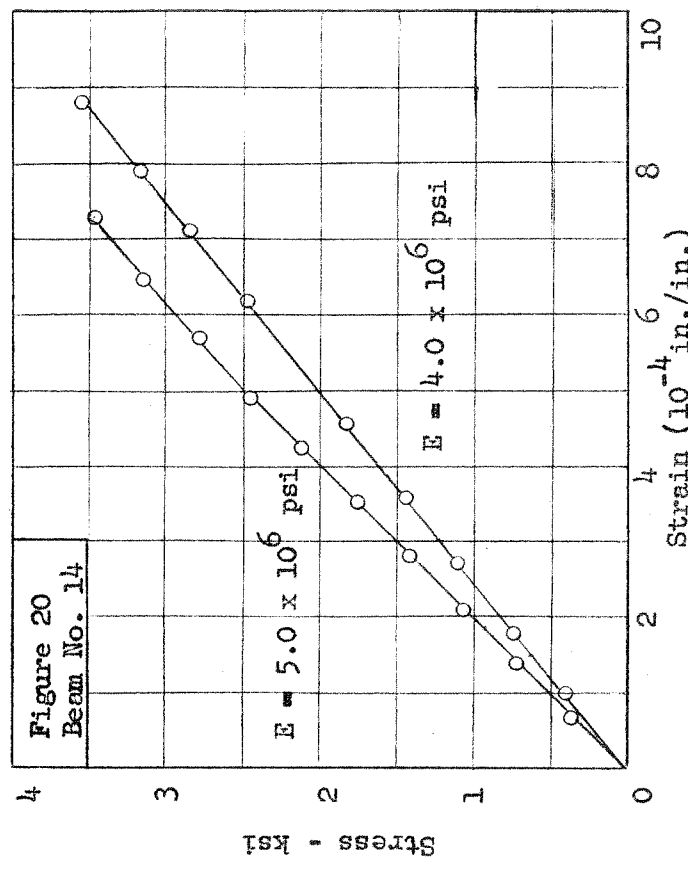
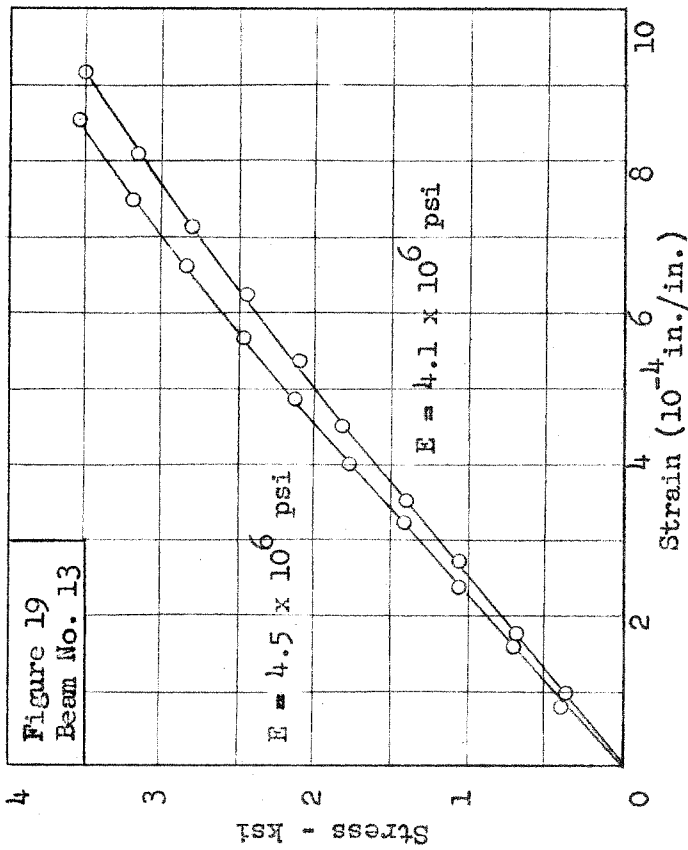
Cylinder stress-strain curves for Beams 1-4

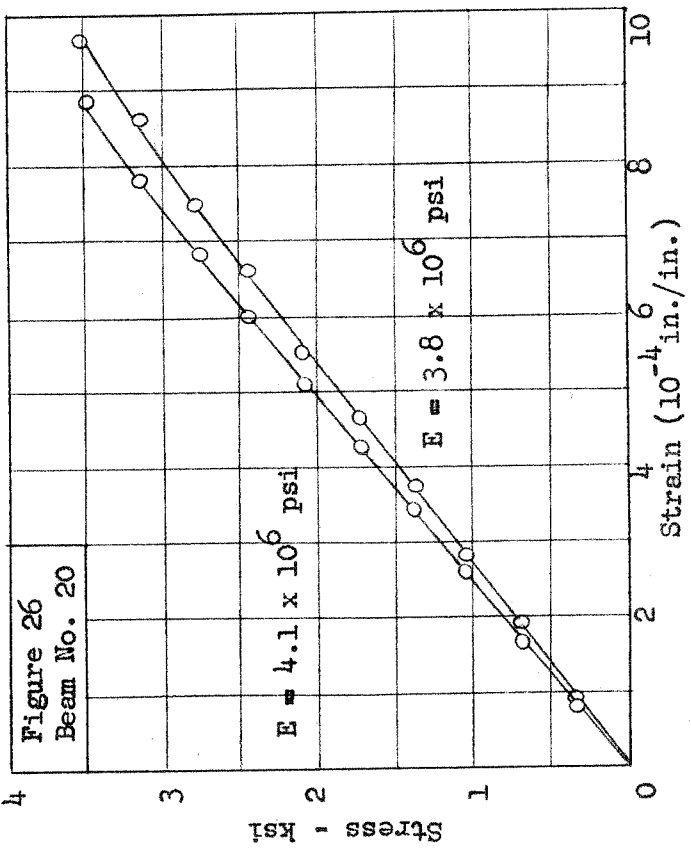
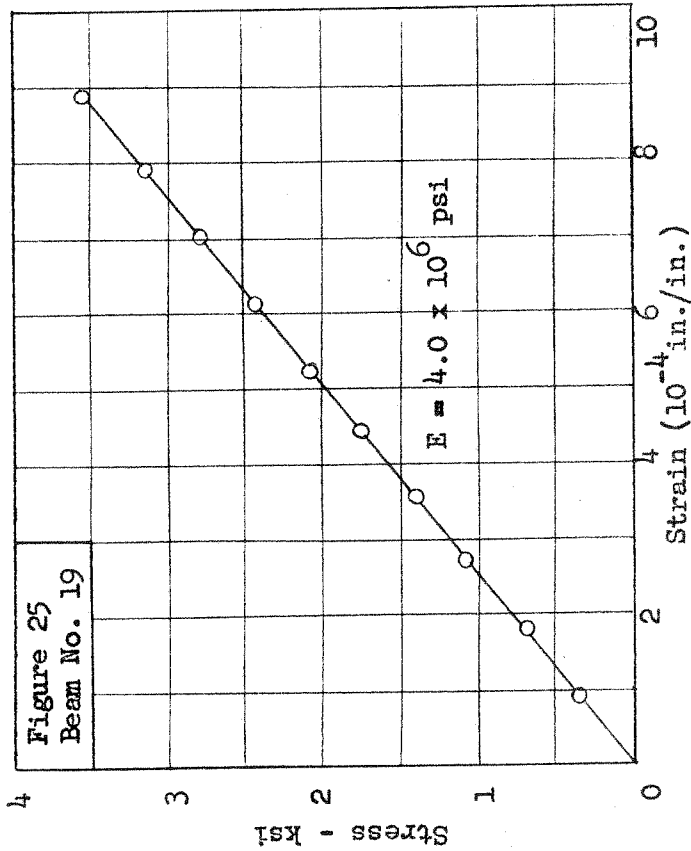
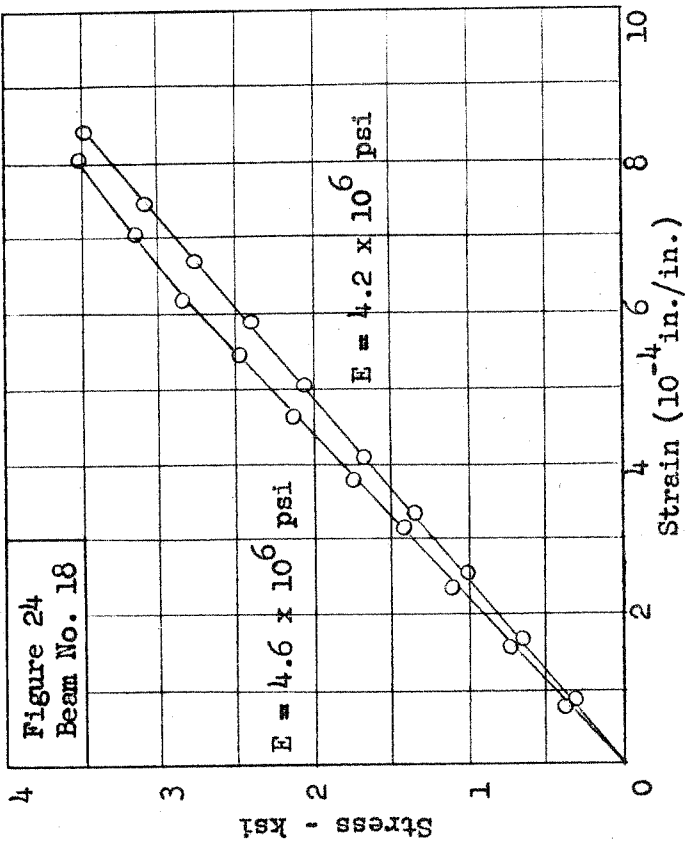
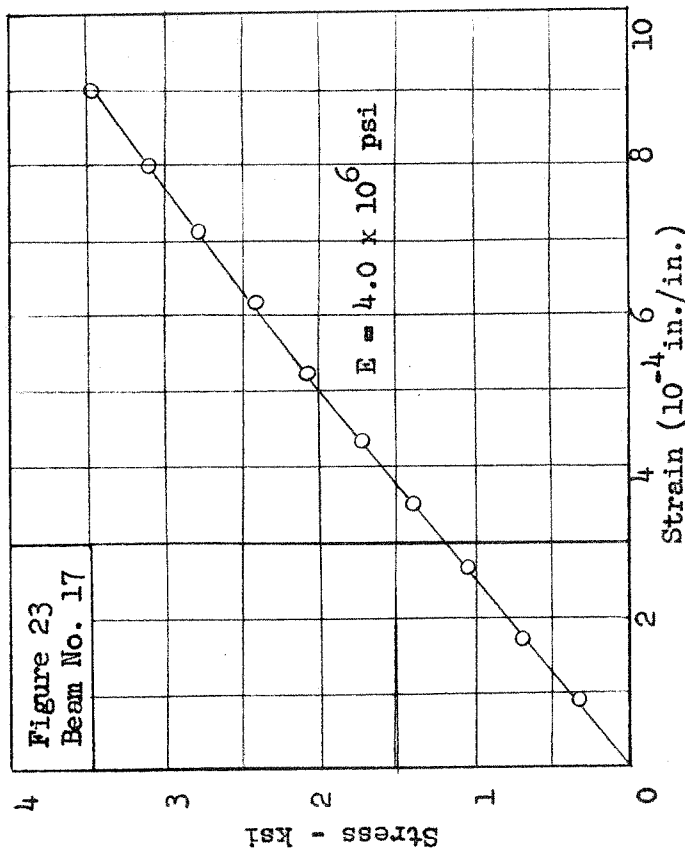


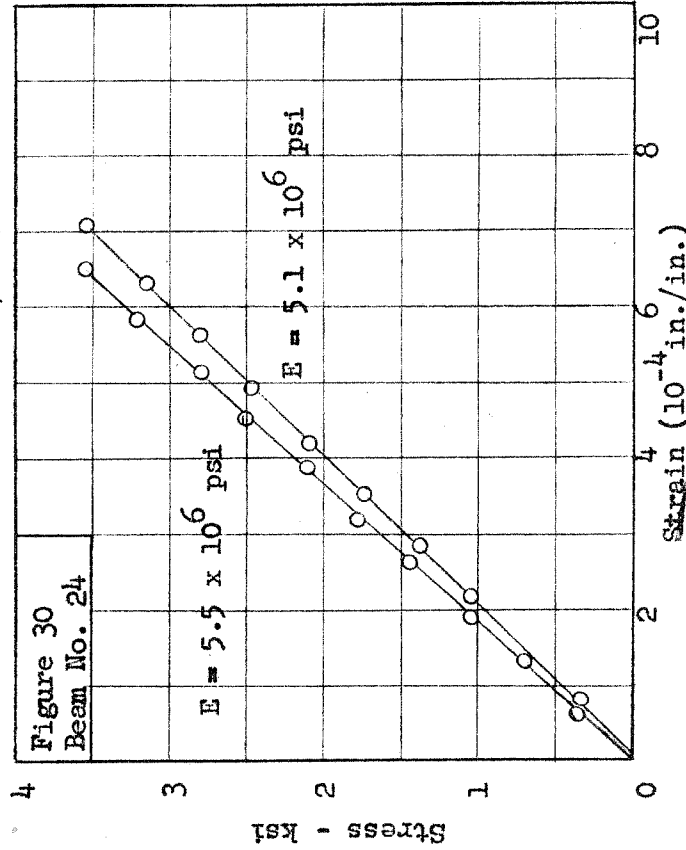
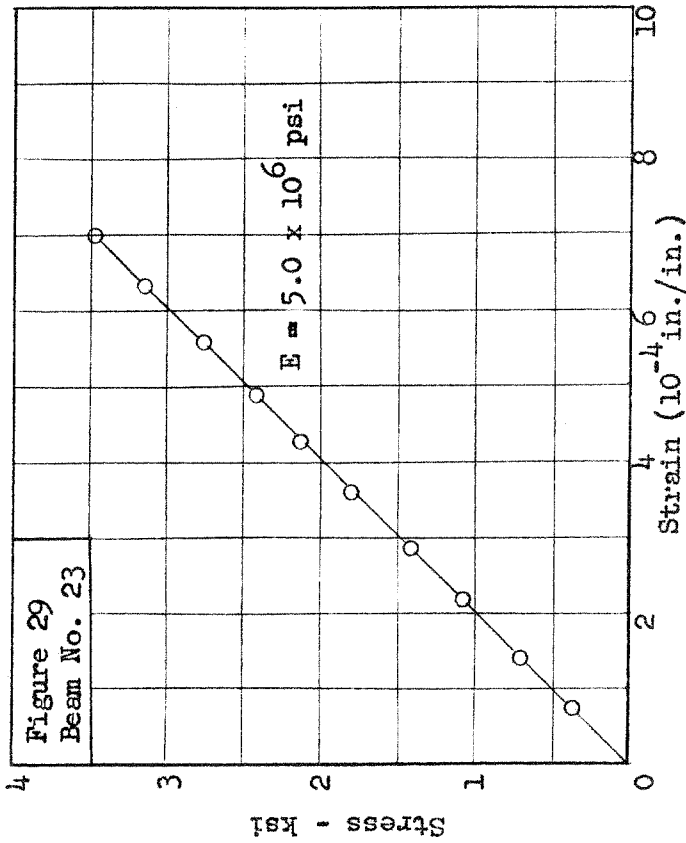
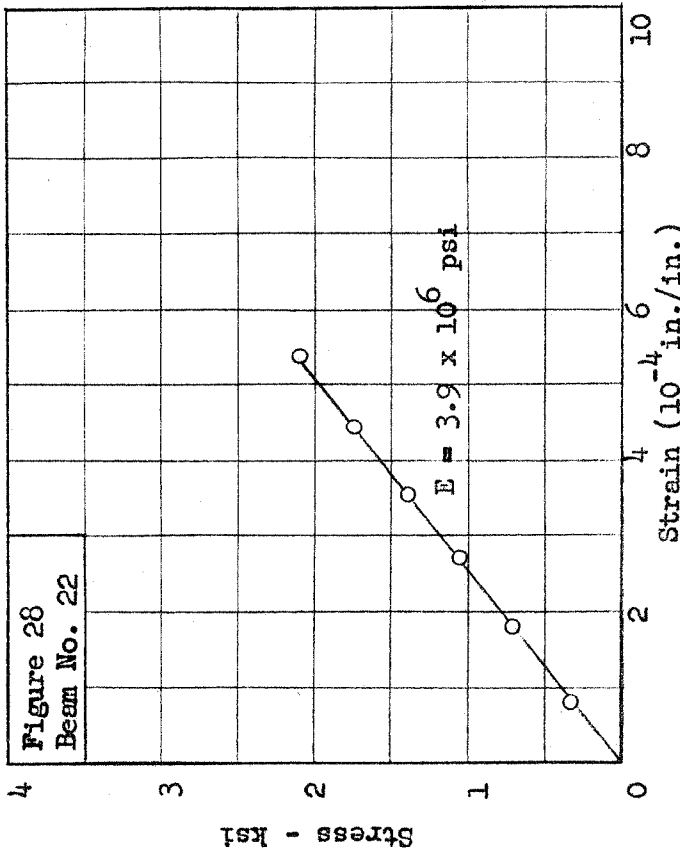
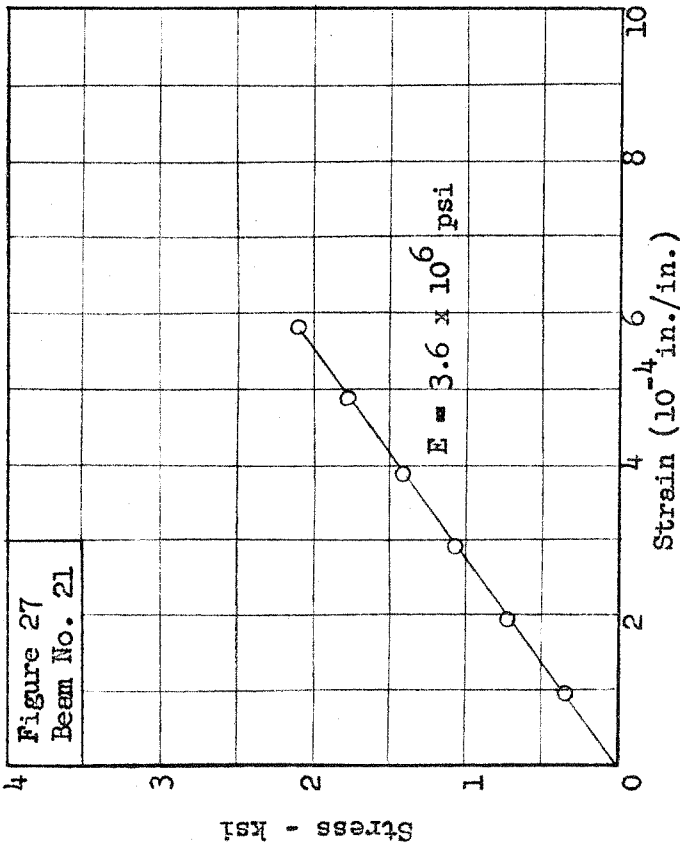
Cylinder stress-strain curves for Beams 5-8

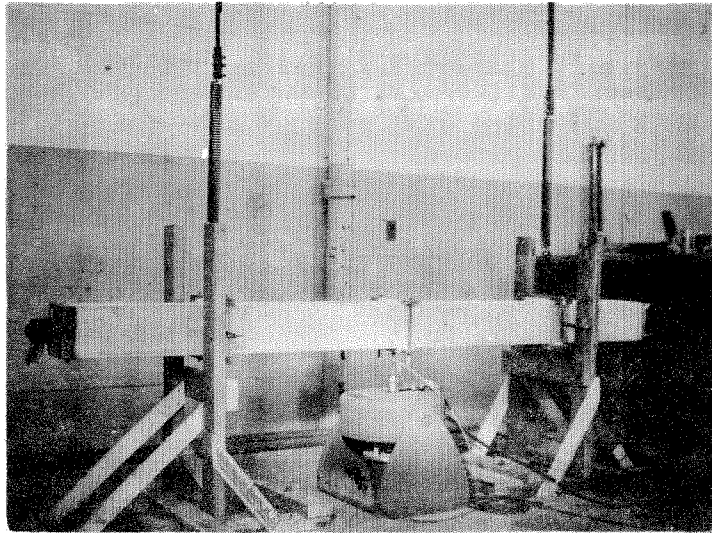


Cylinder stress-strain curves for Beams 9-12



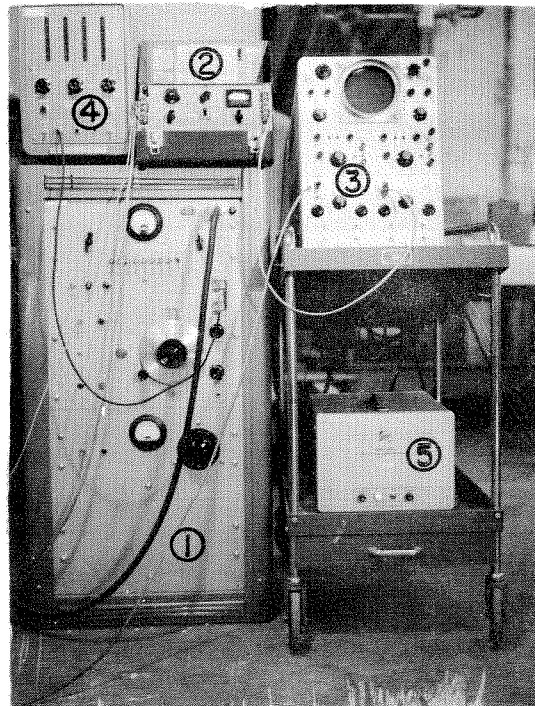






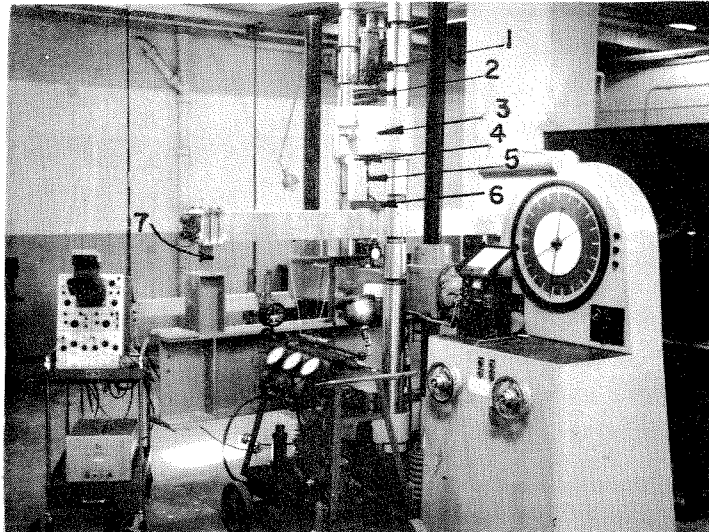
Free-free beam attached to exciter

Figure 31



Exciter power supply unit and electronic recording equipment for steady state tests

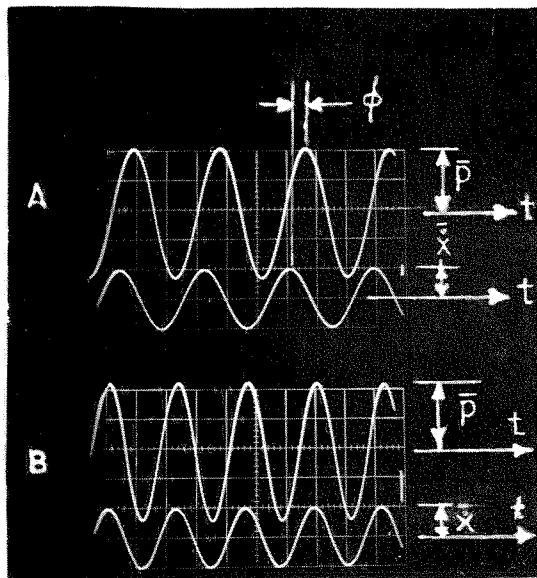
Figure 32



1. Loading jack.
2. Railroad car spring.
3. Upper head Baldwin machine.
4. Lower end 1" bolt.
5. Fractured load bar.
6. Rigid bracket.
7. Flexible support plates.

Concrete beam mounted and ready for free-vibration testing

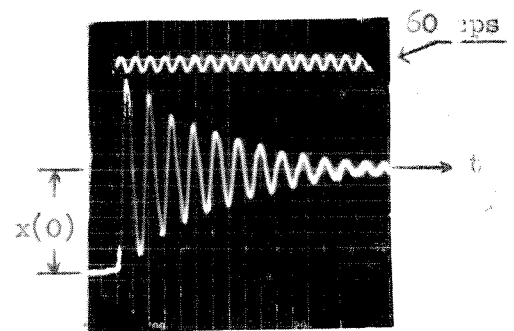
Figure 33



ϕ - PHASE ANGLE
 \bar{P} - FORCE AMPLITUDE
 $\dot{\bar{X}}$ - VELOCITY AMPLITUDE
 t - TIME

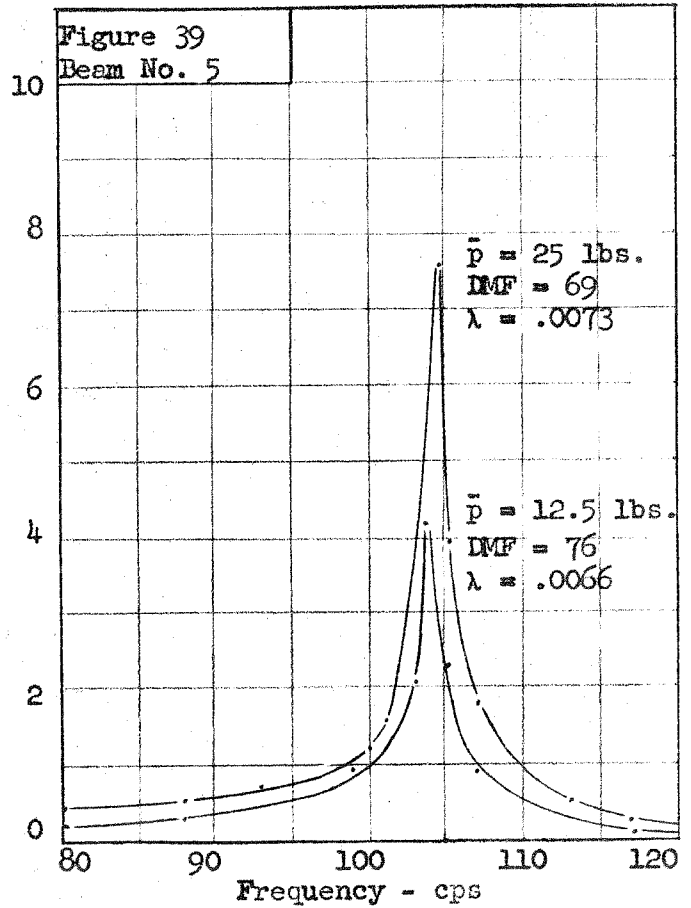
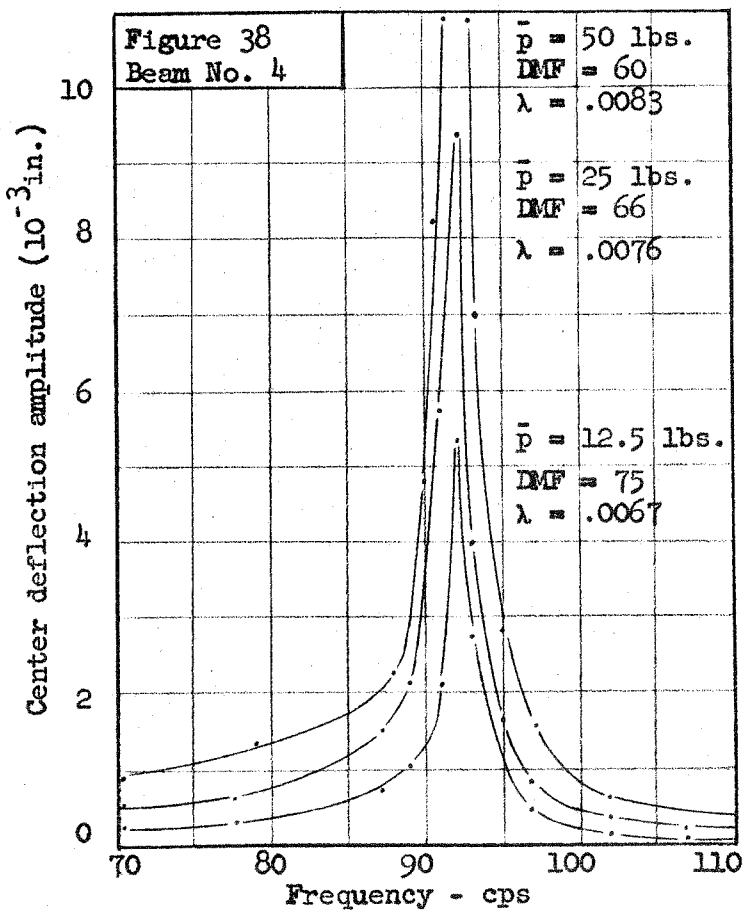
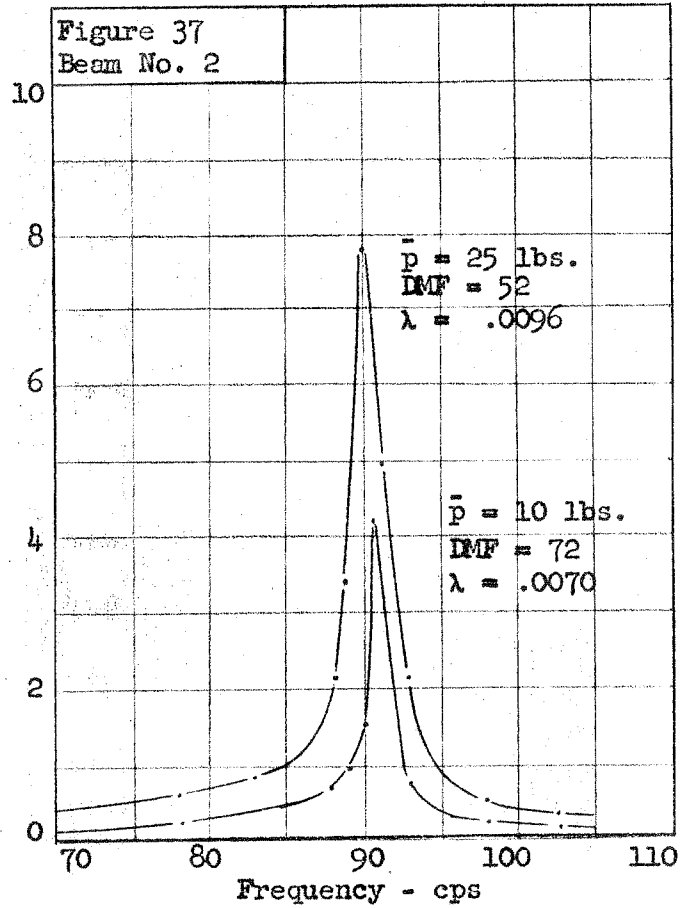
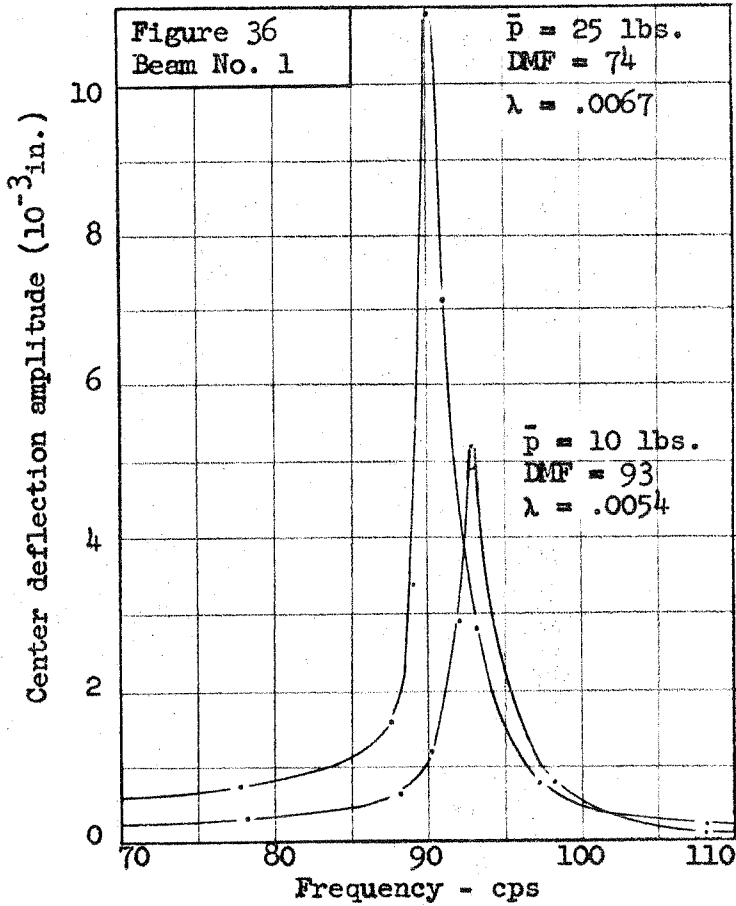
Exciter force and vertical velocity of center of beam under steady state vibration

Figure 34

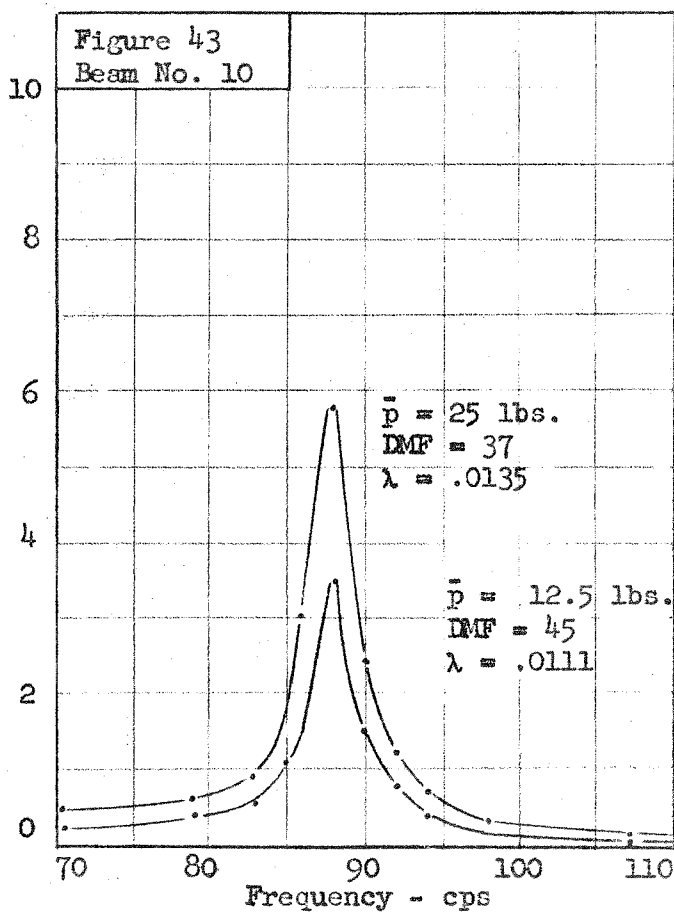
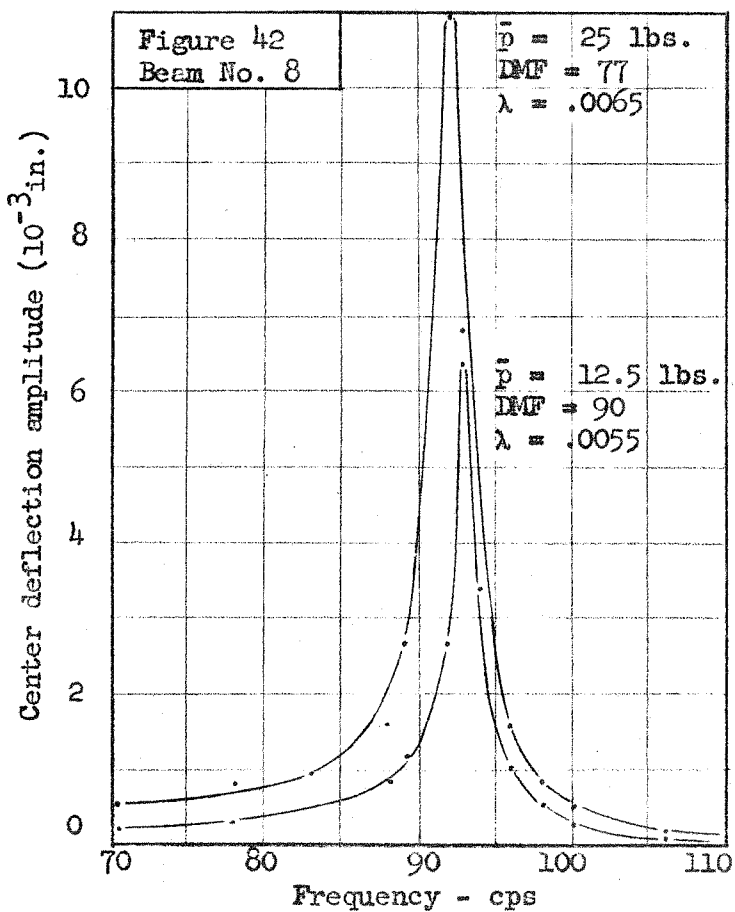
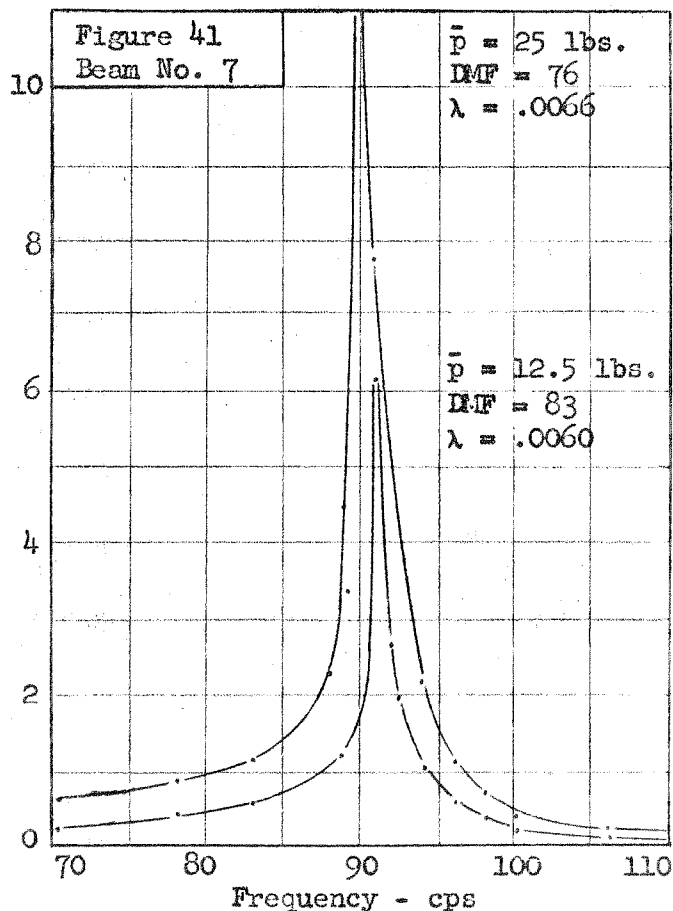
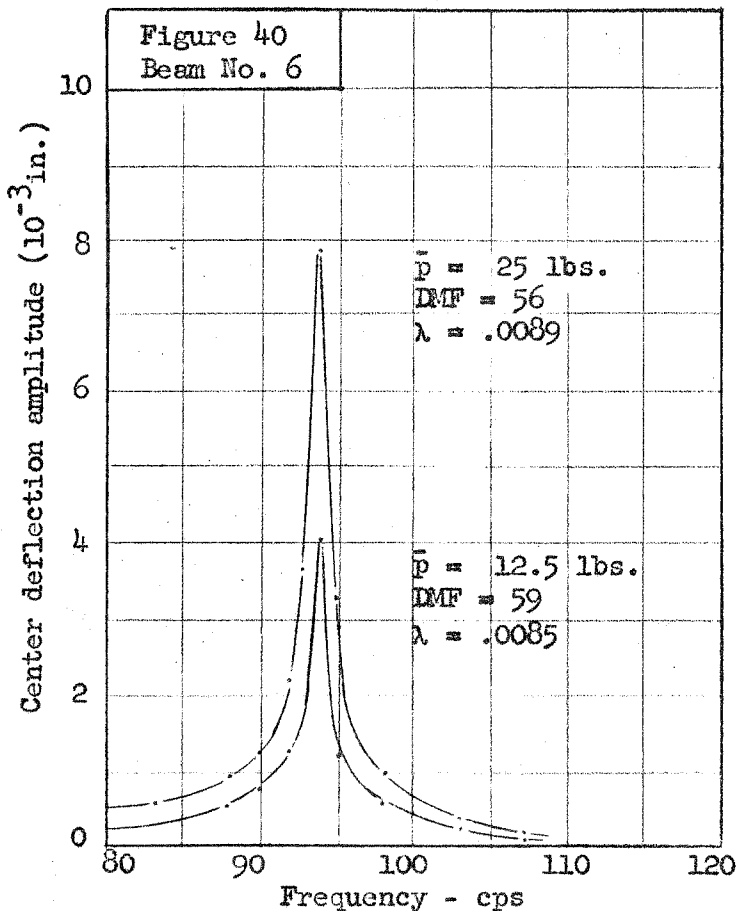


Beam deflection versus time under free vibration

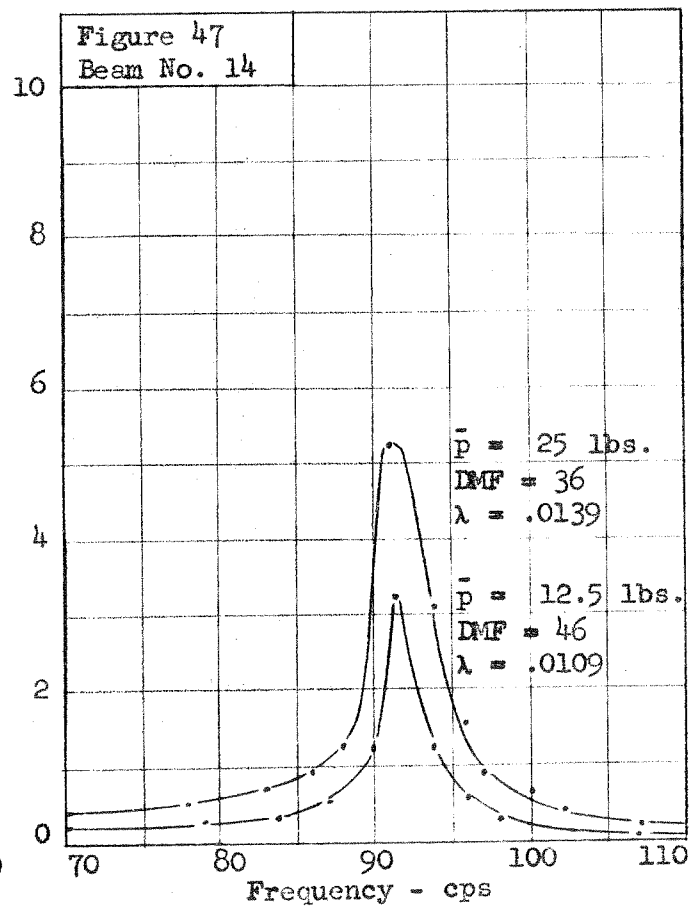
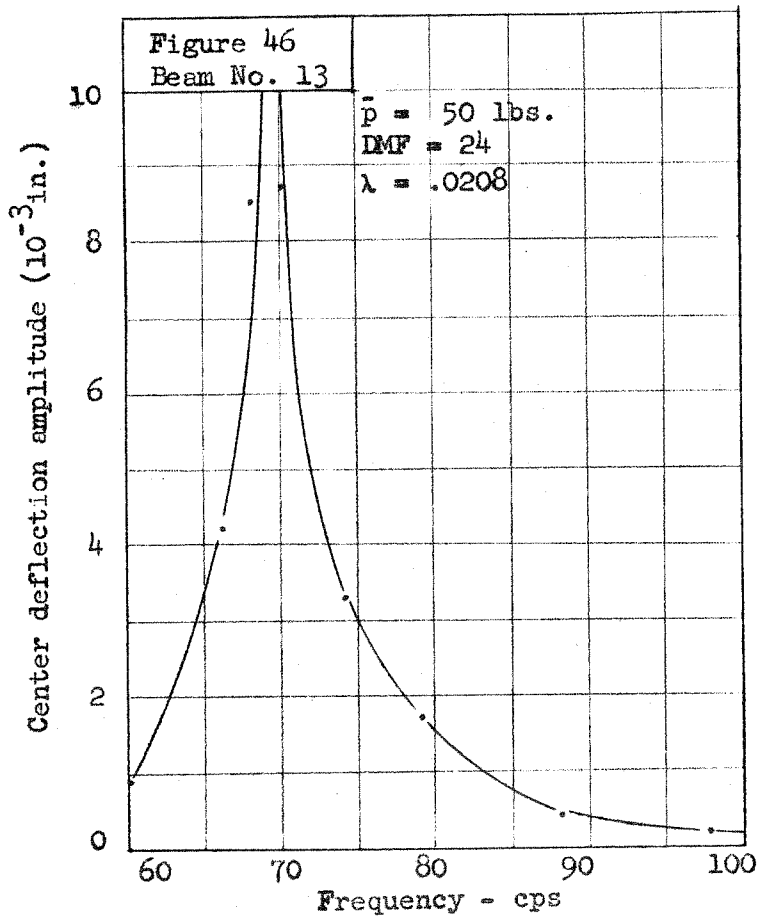
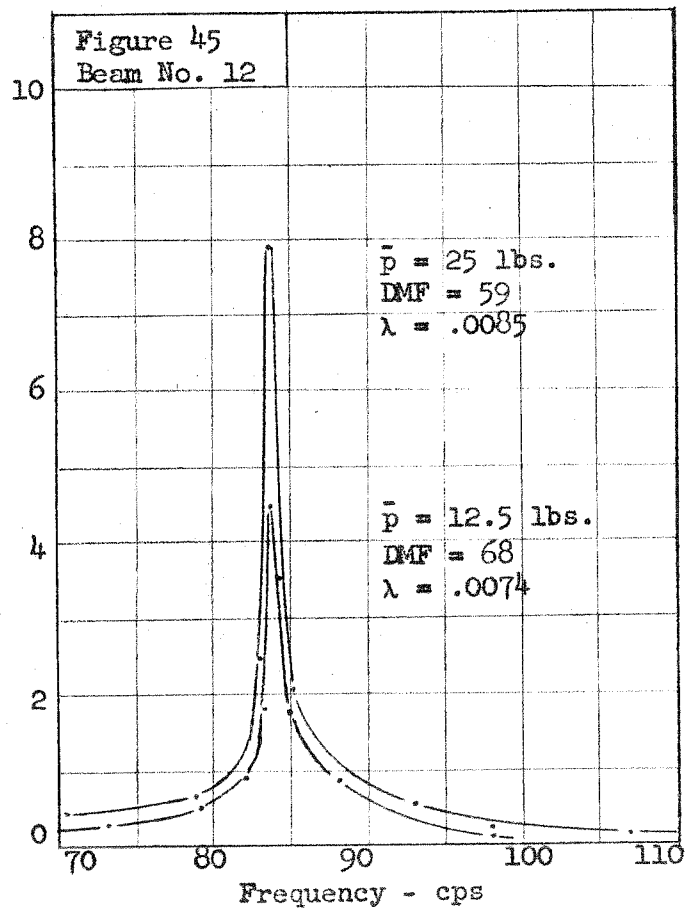
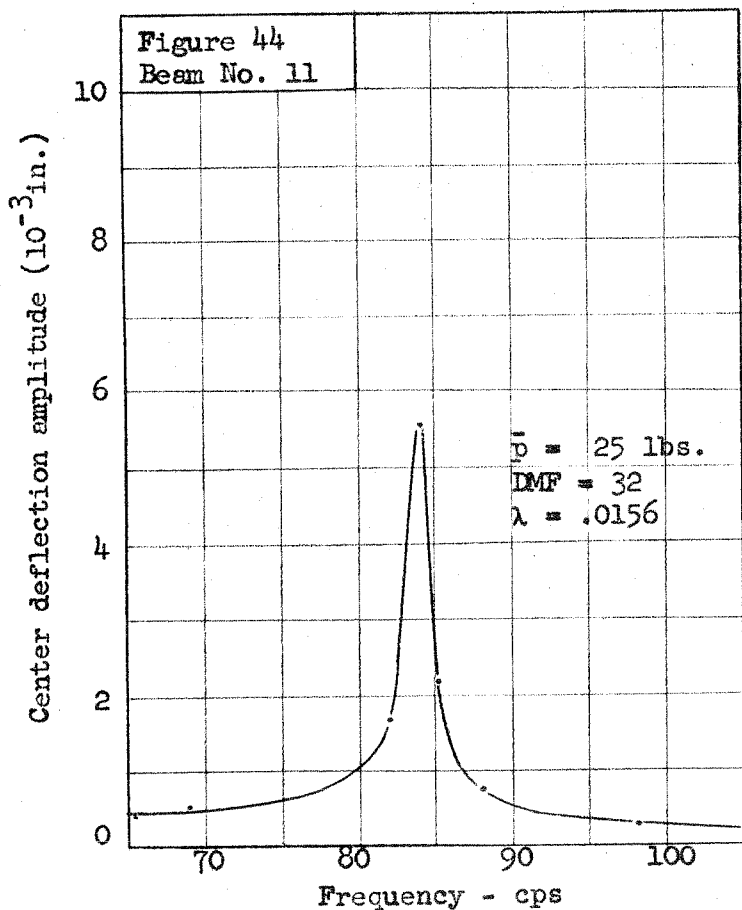
Figure 35

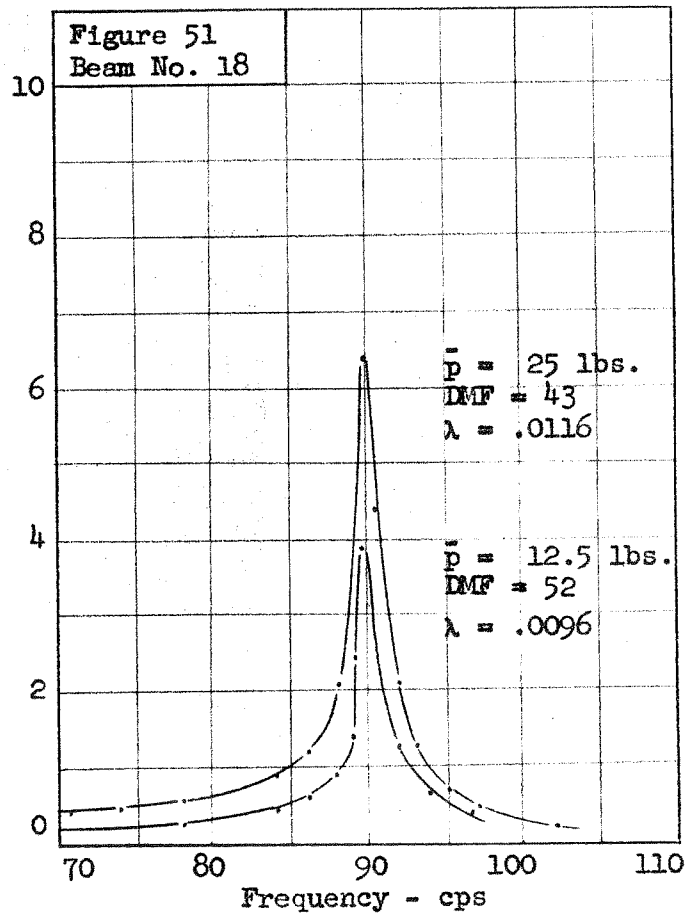
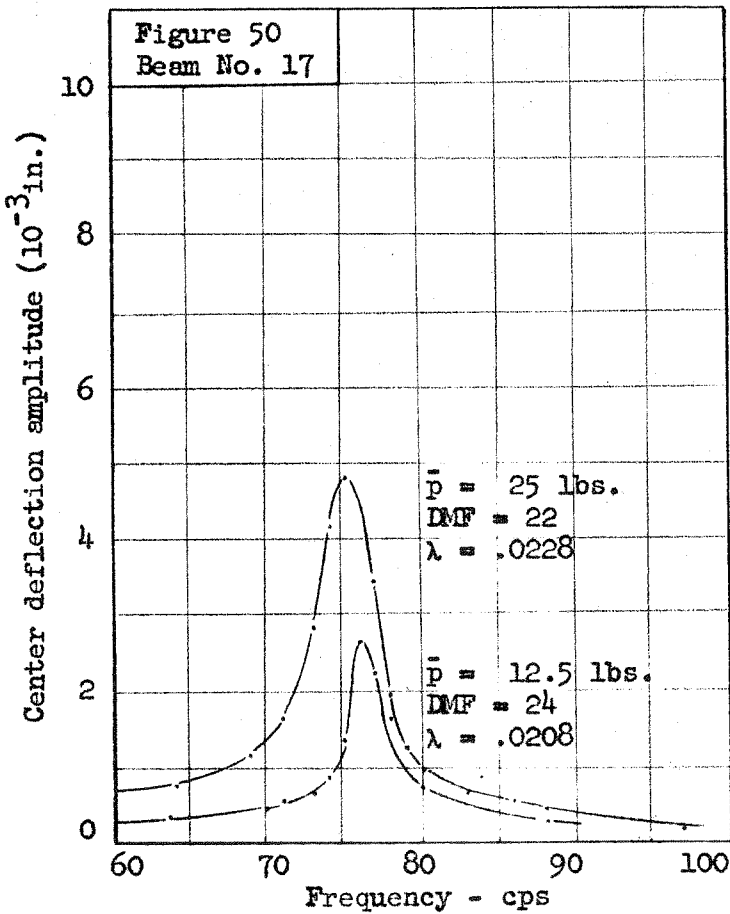
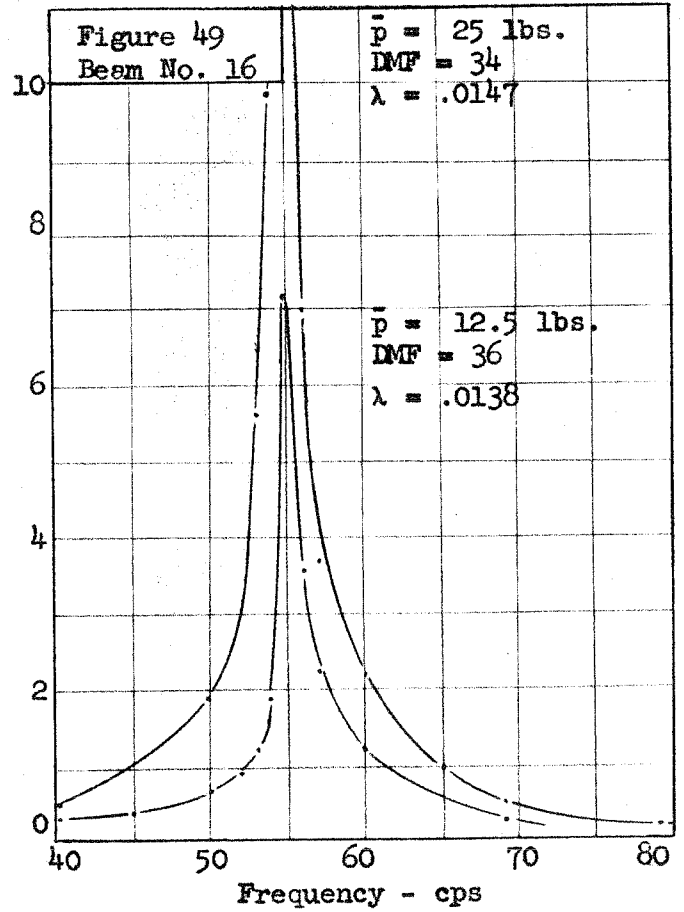
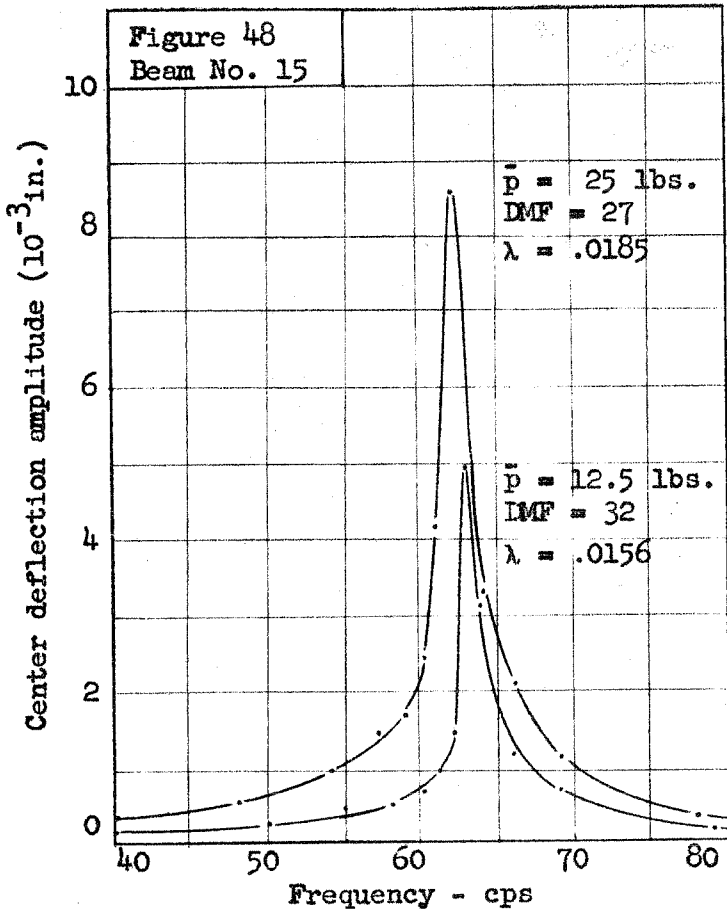


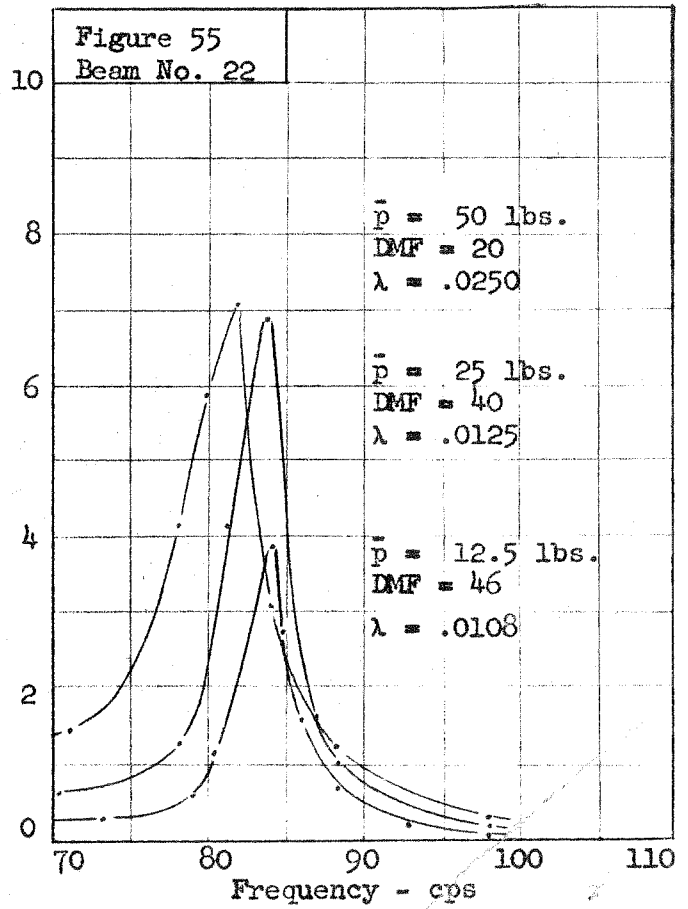
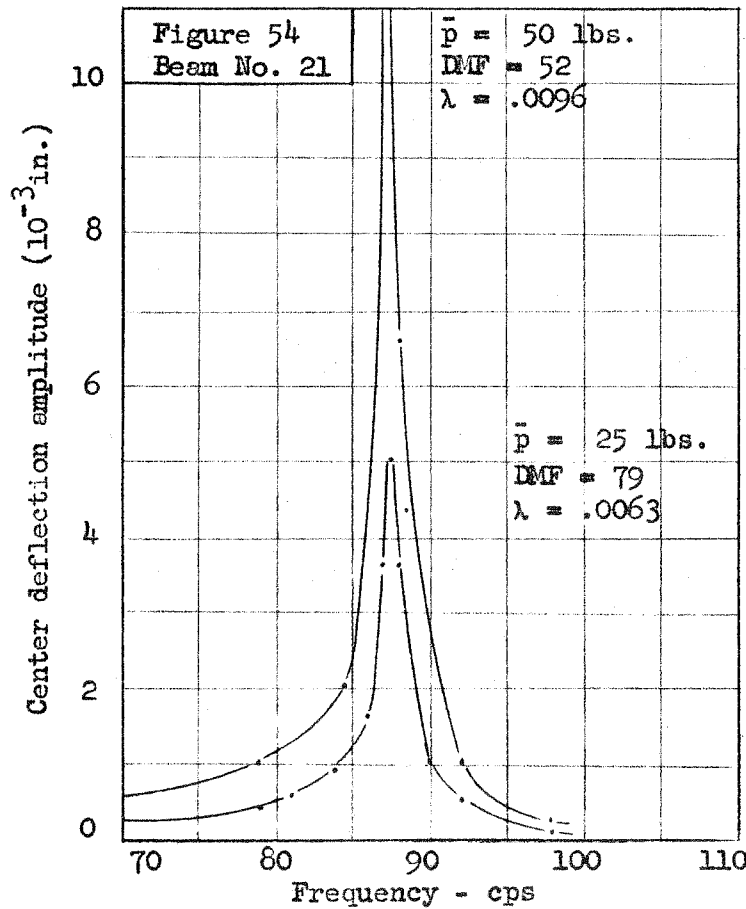
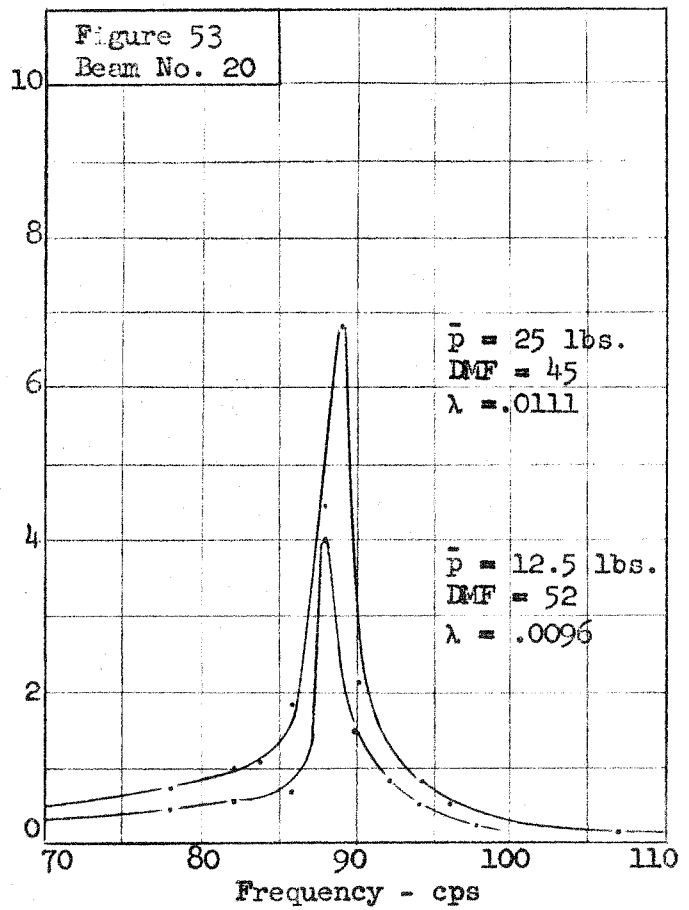
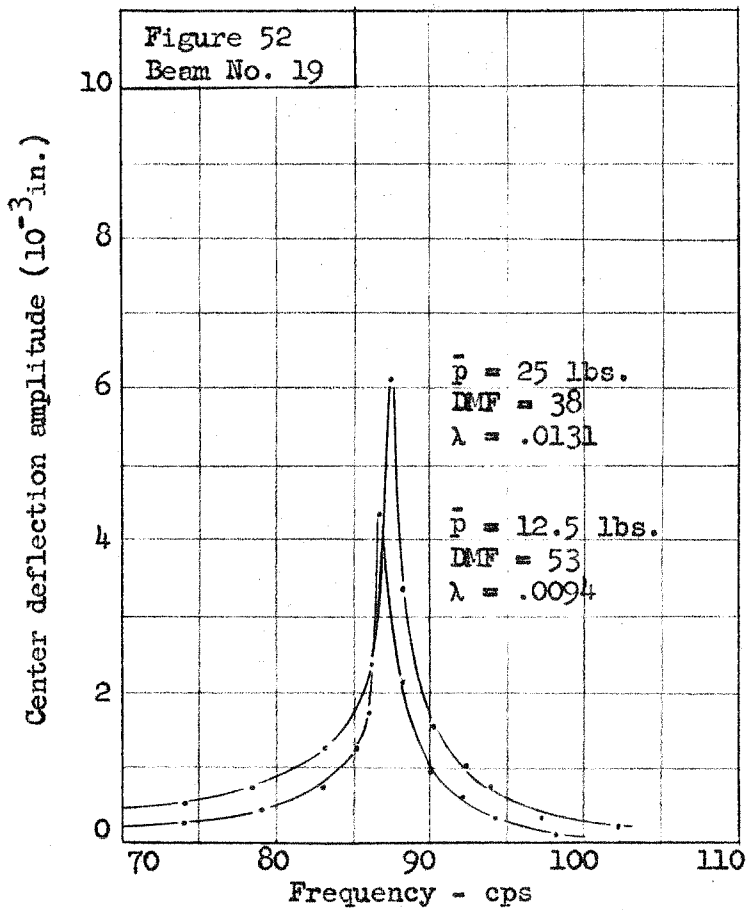
Resonance curves - Beam Nos. 1, 2, 4, and 5

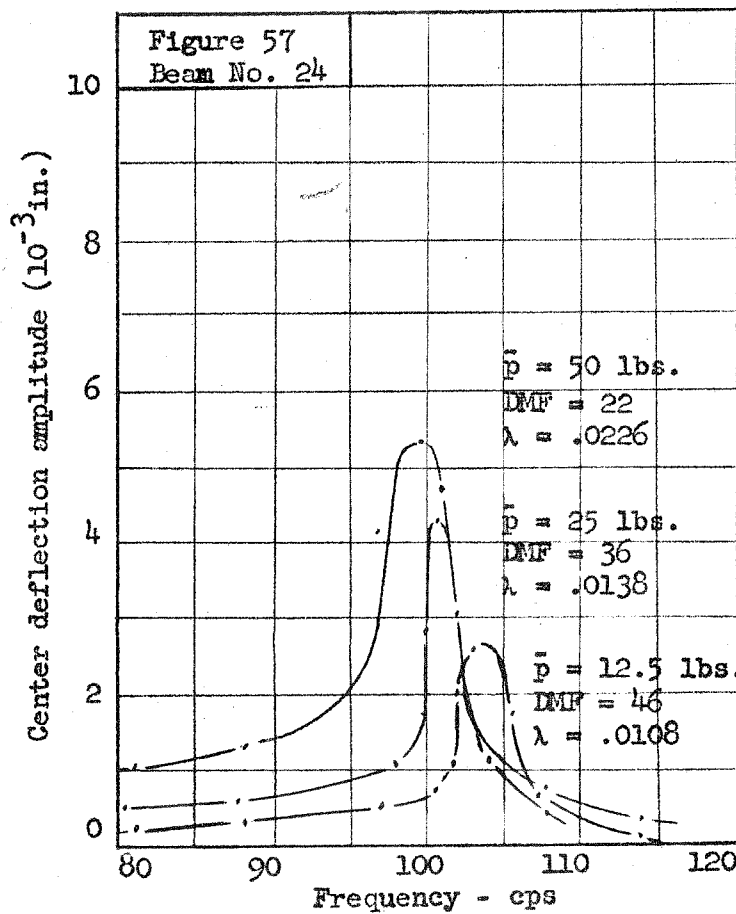
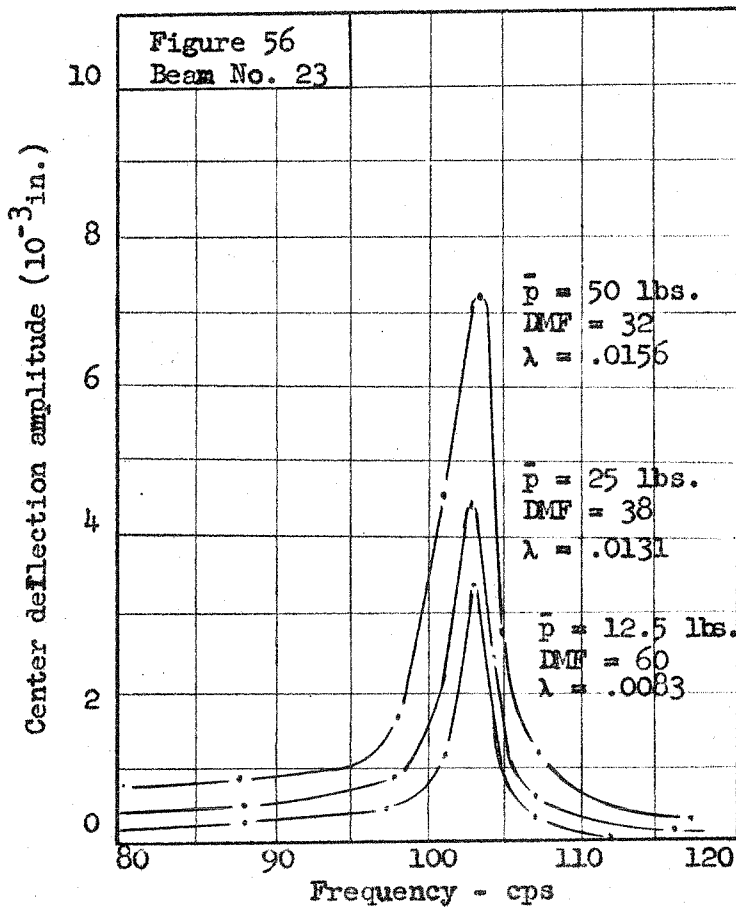


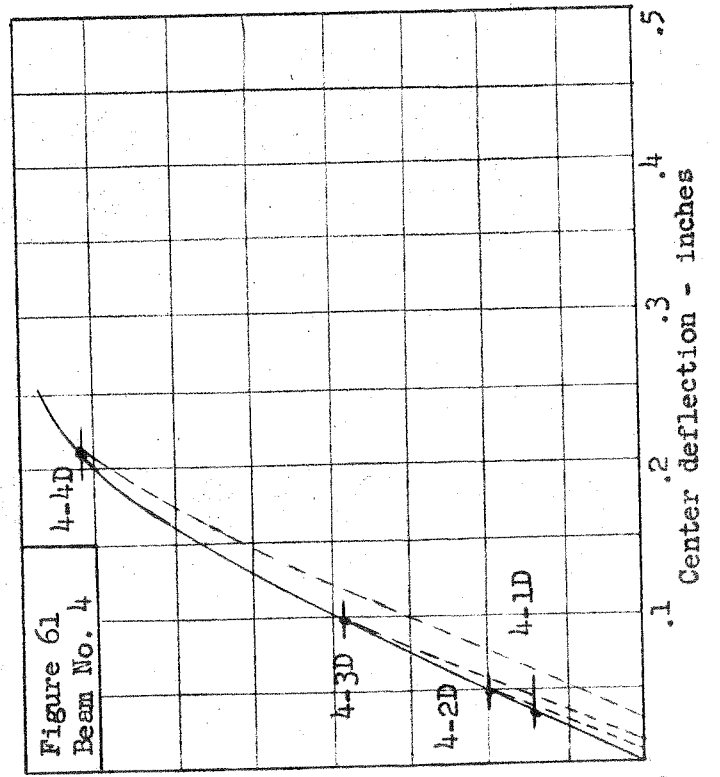
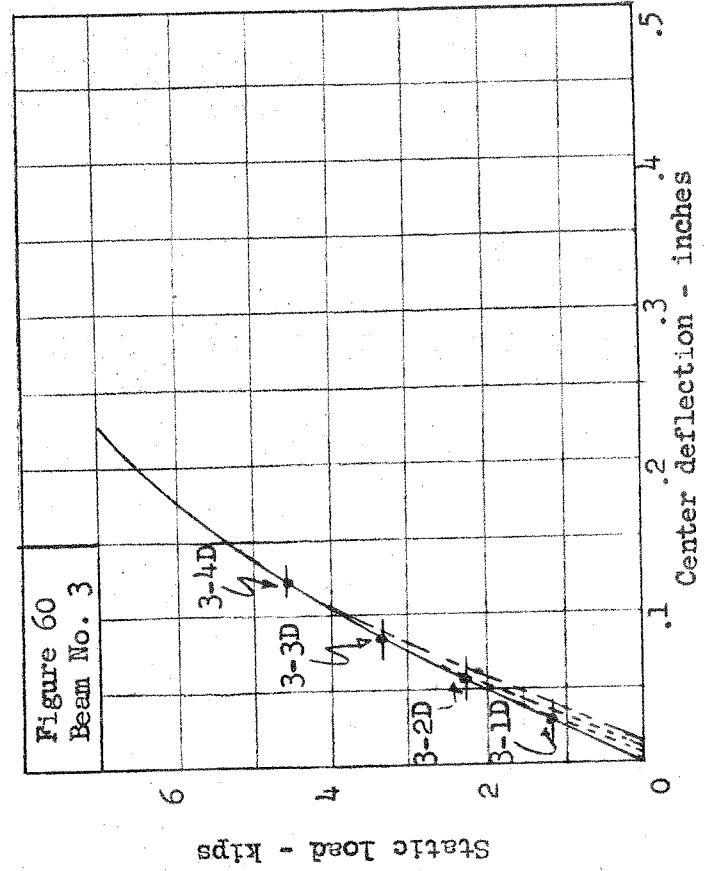
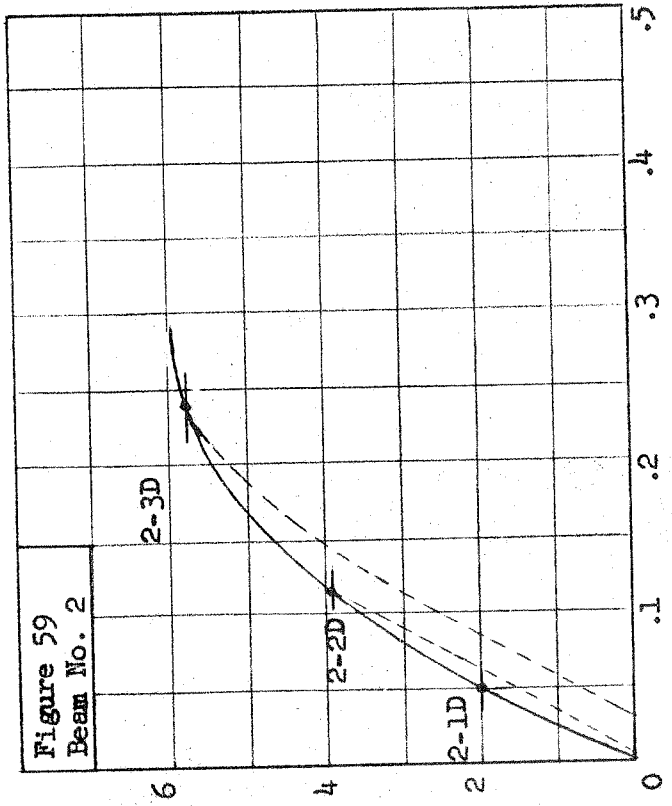
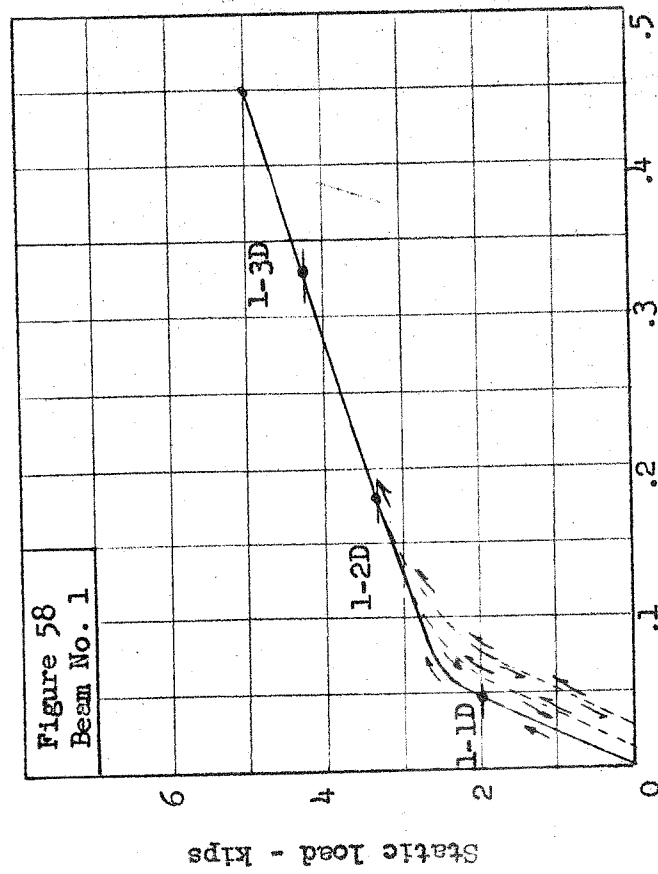
Resonance curves - Beam Nos. 6, 7, 8, and 10



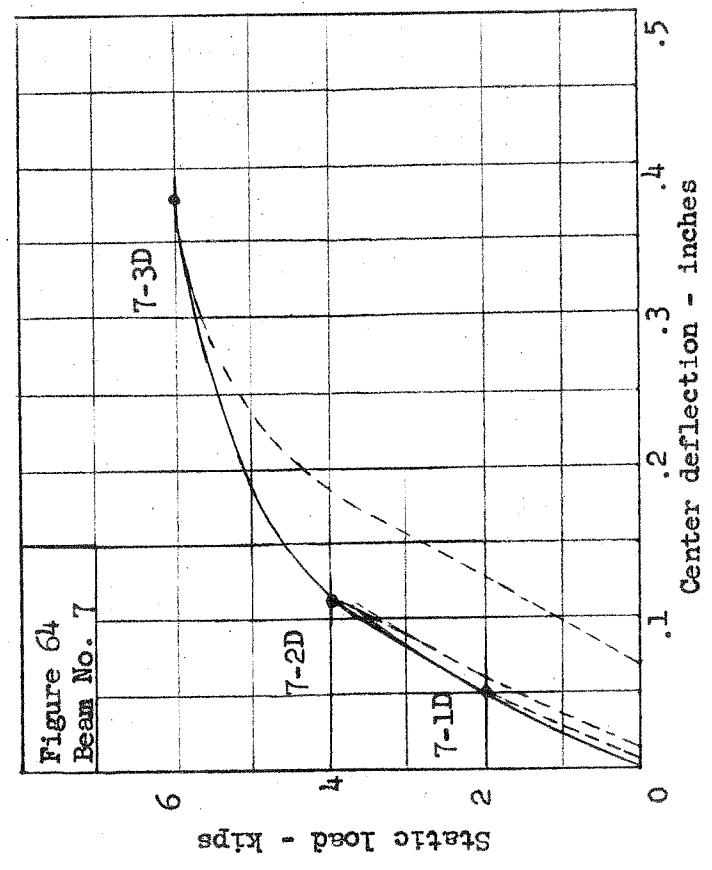
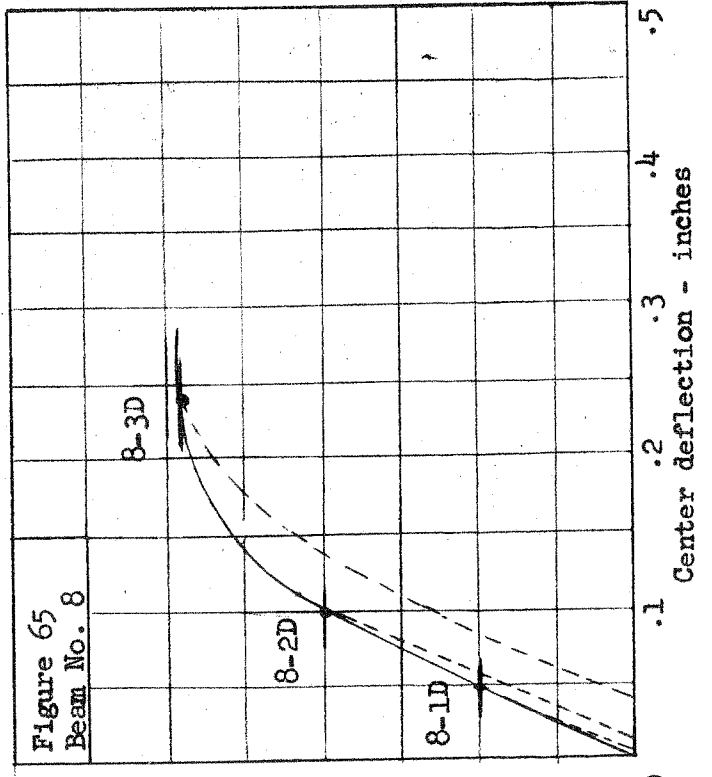
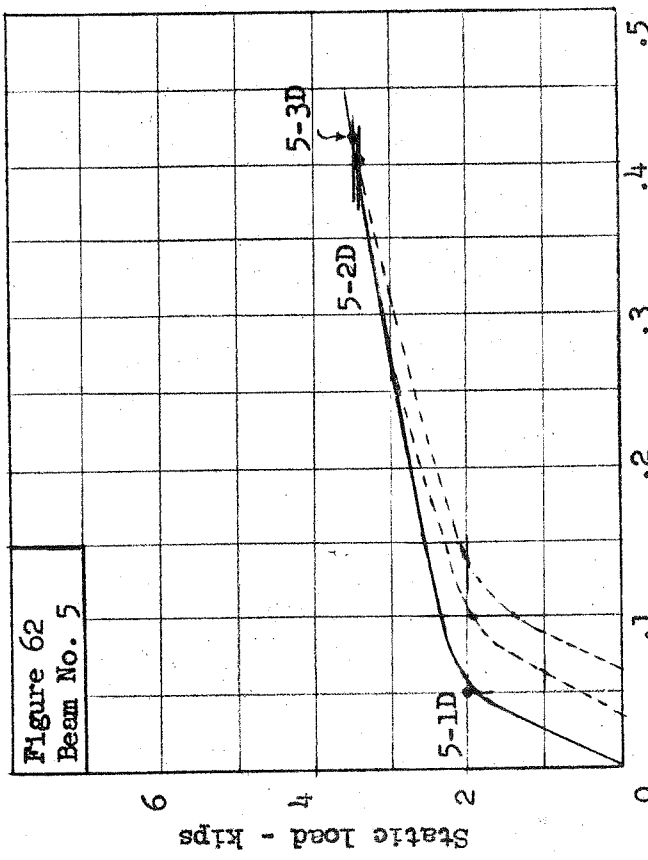
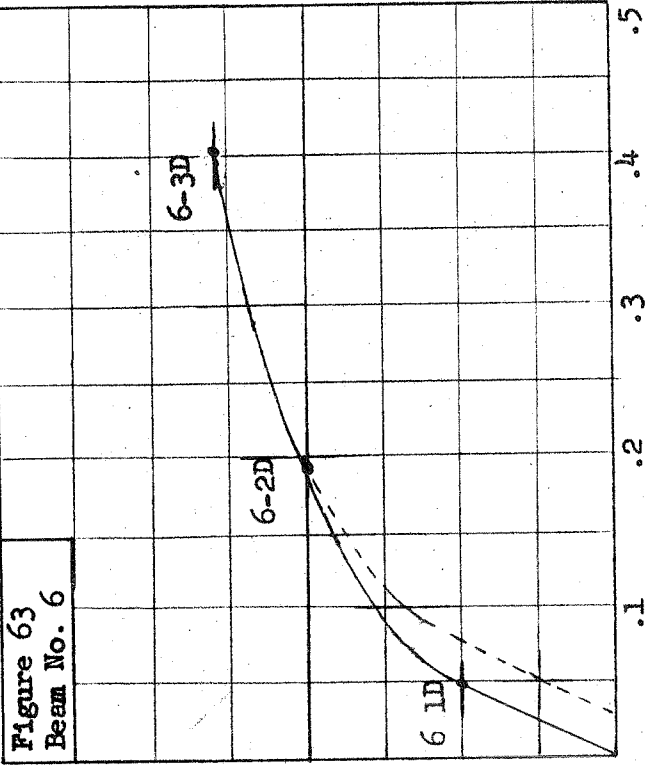




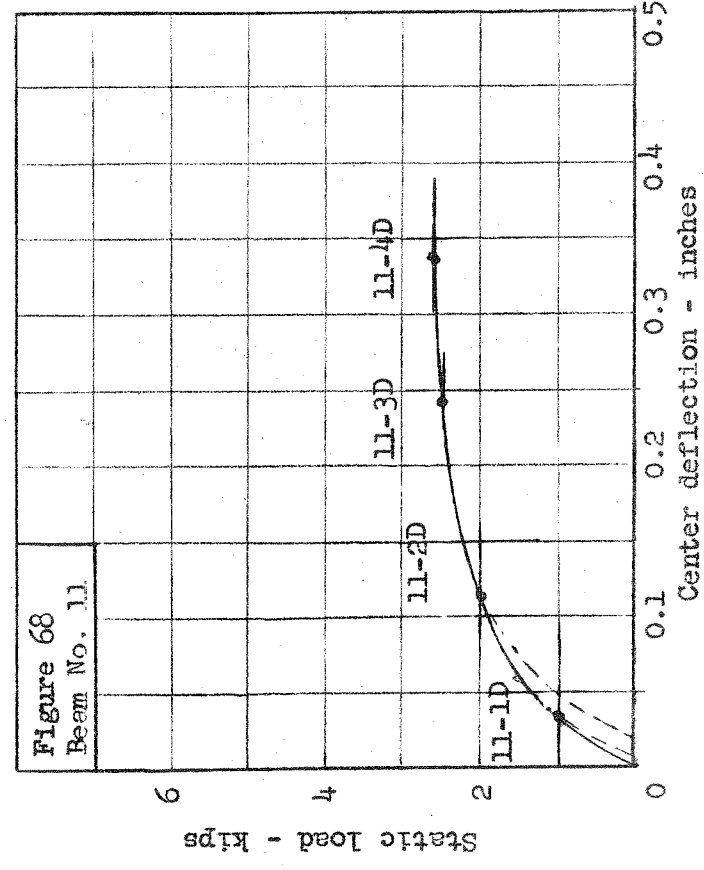
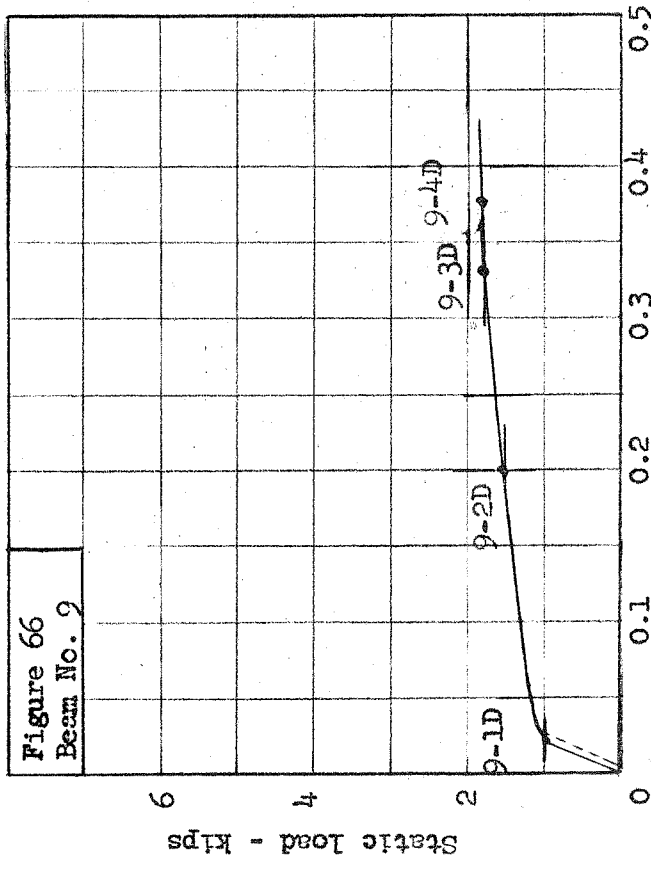
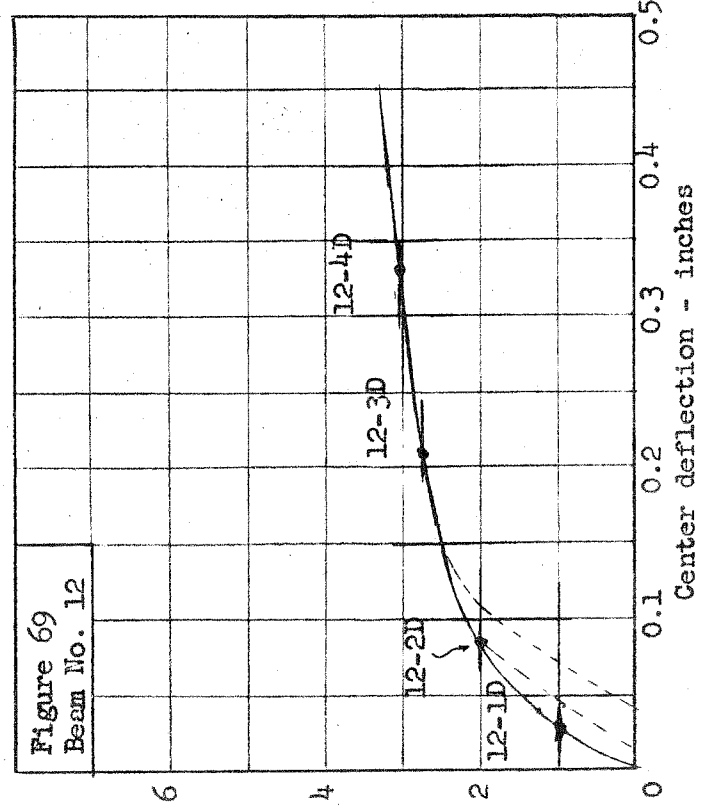
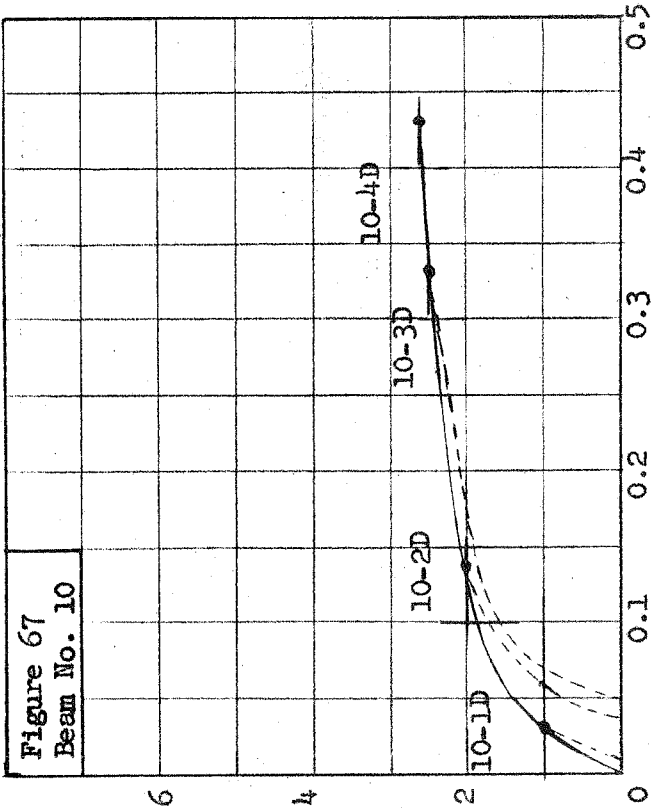


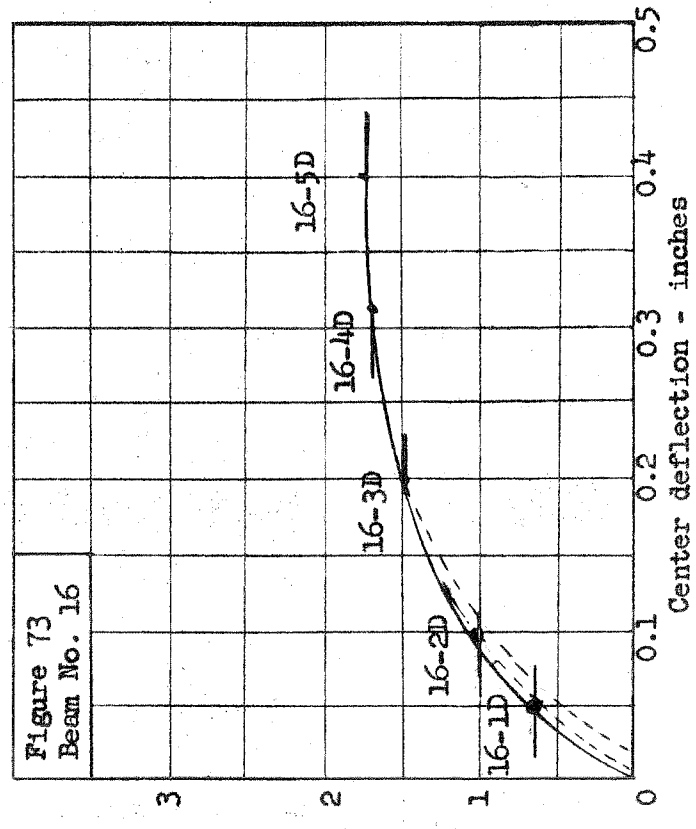
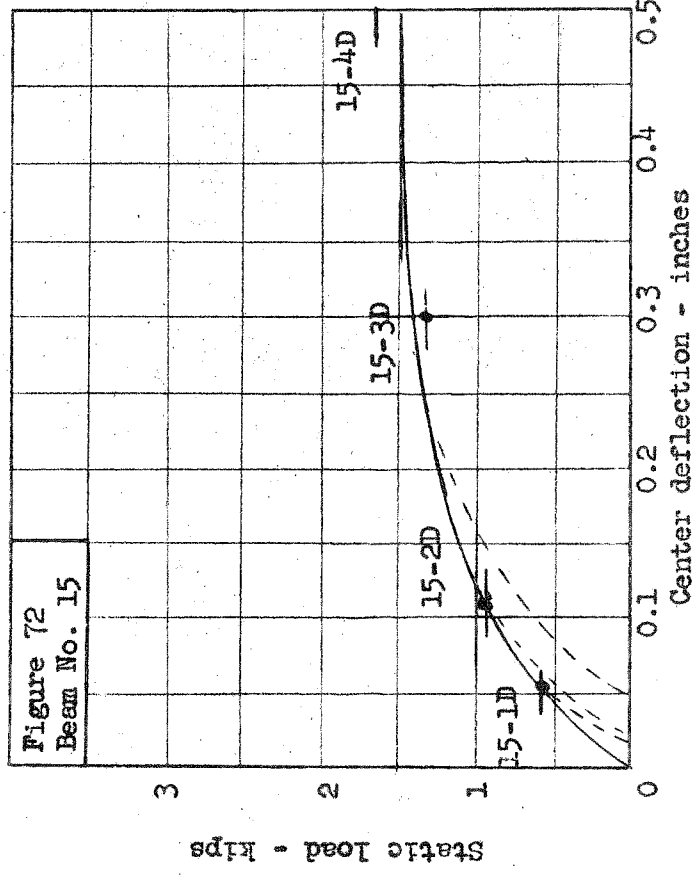
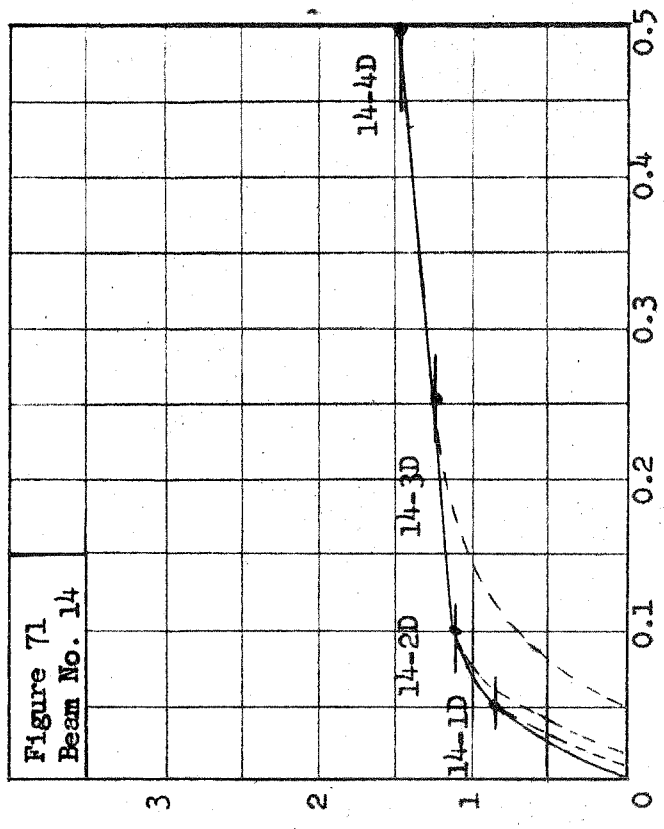
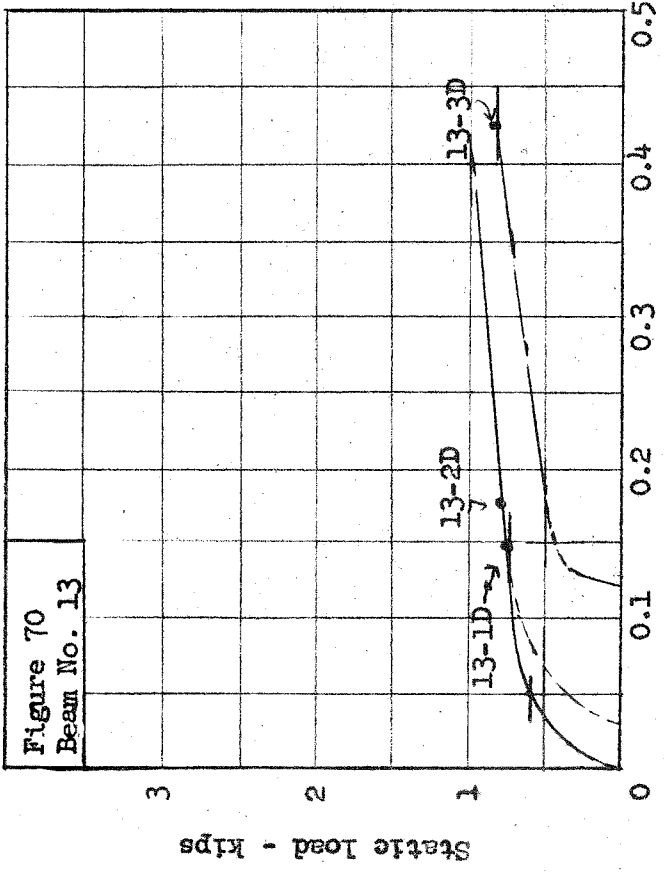


Static load - deflection curves - Beams 1-4

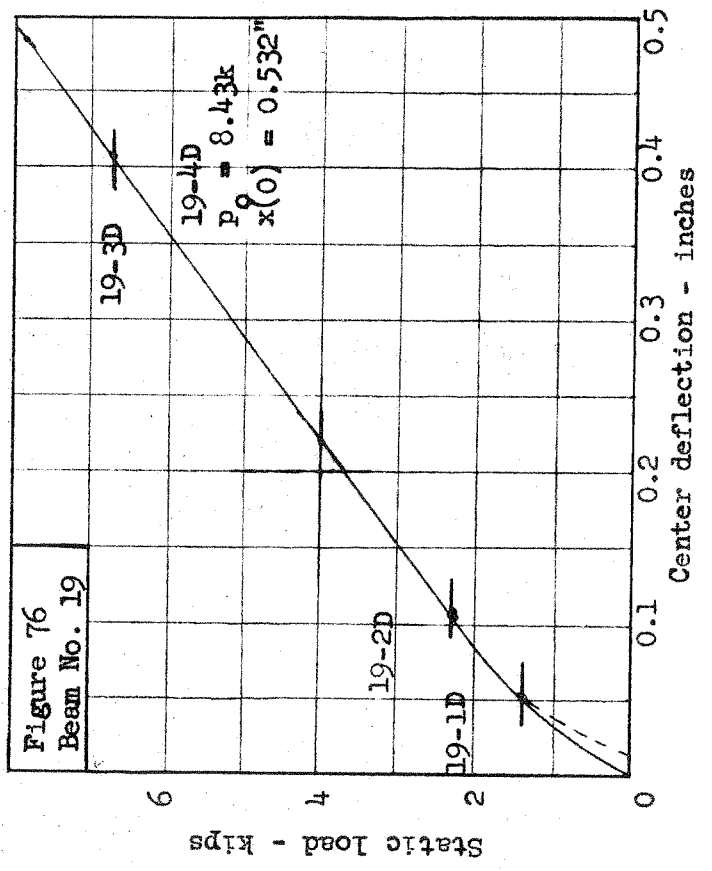
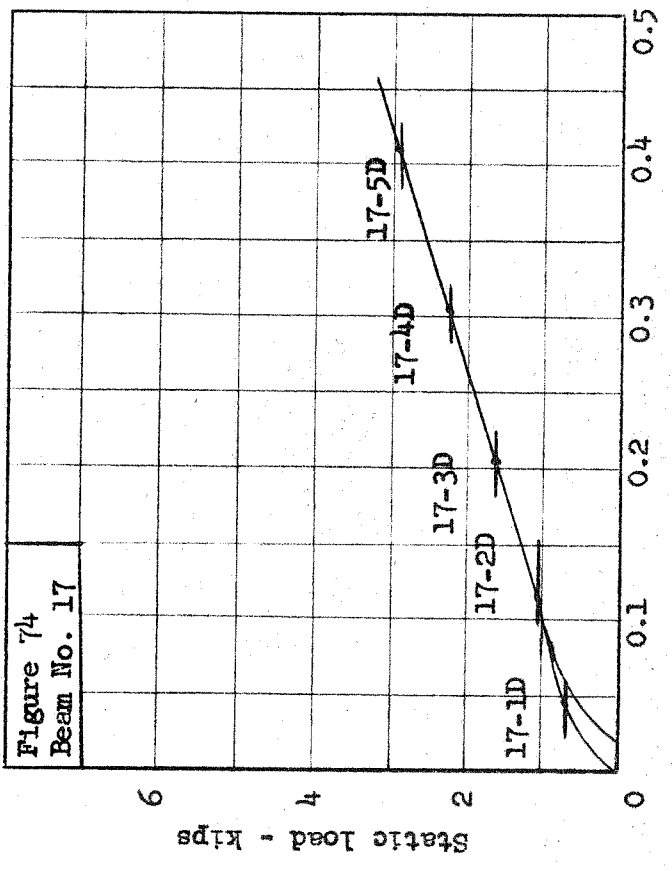
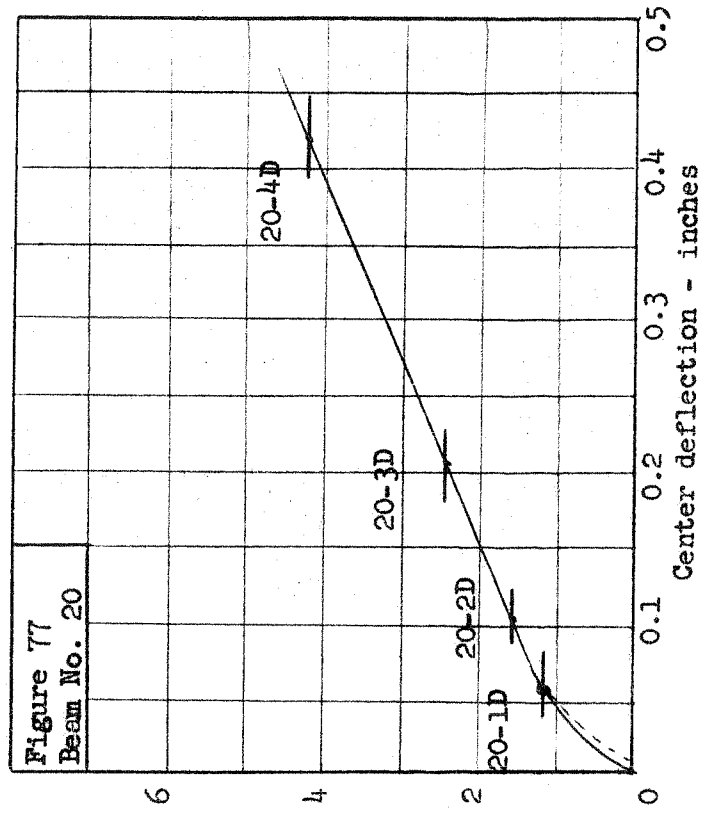
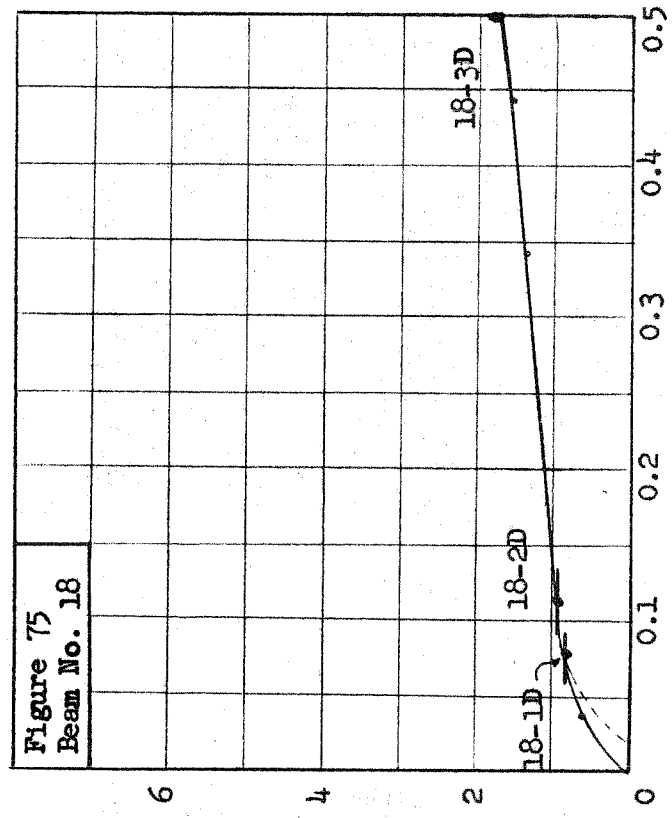


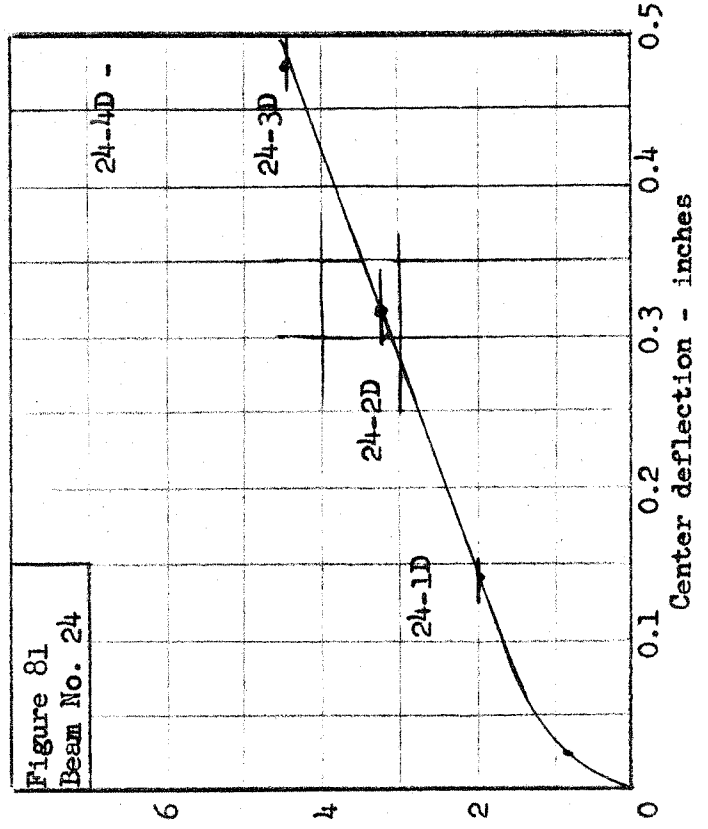
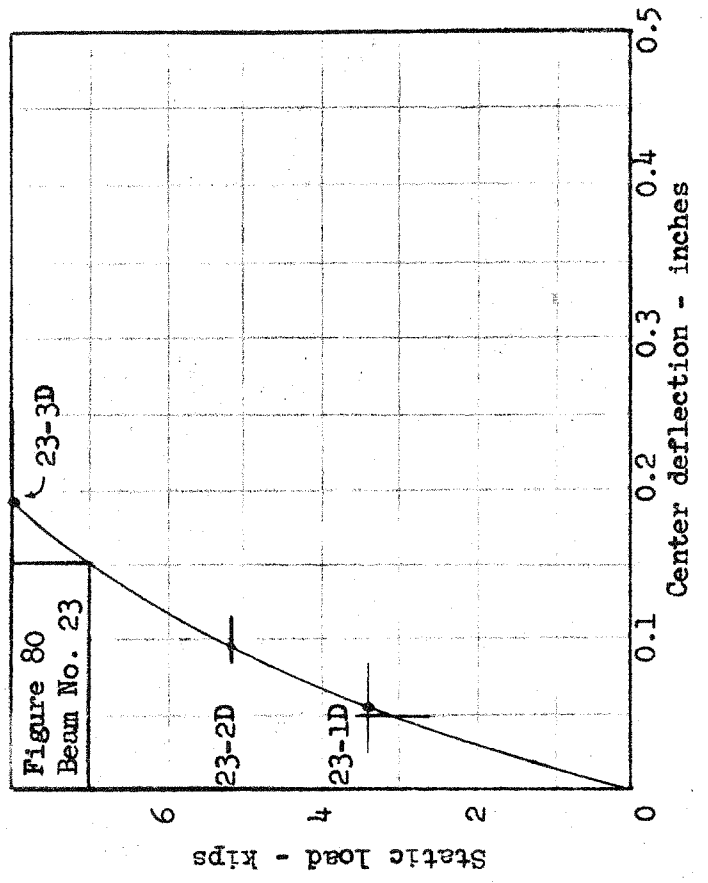
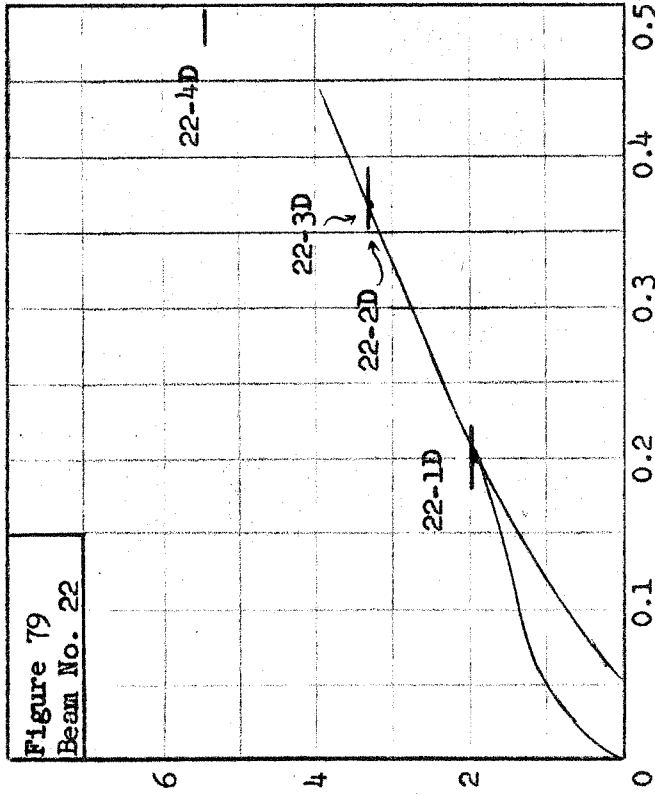
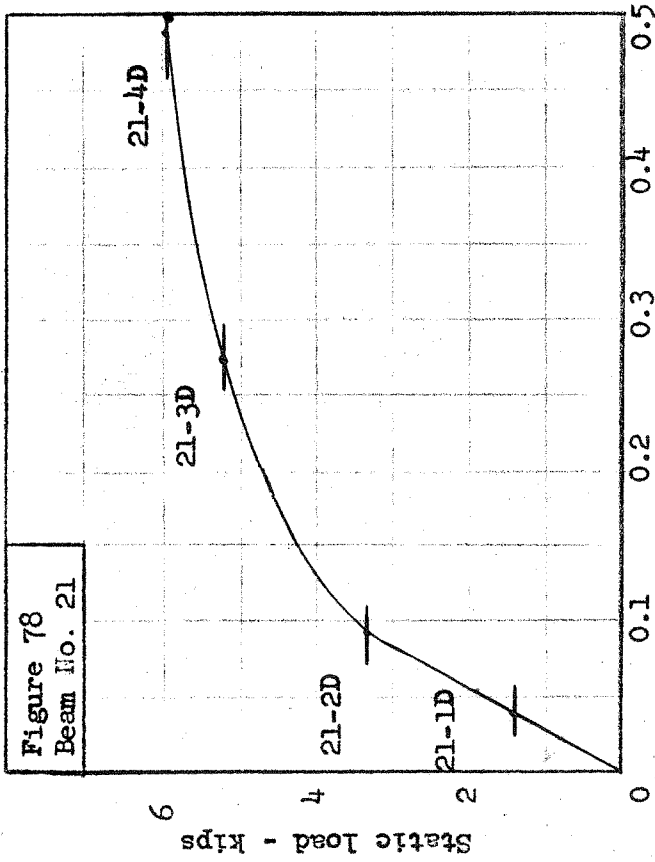
Static load - deflection curves - Beams 5-8

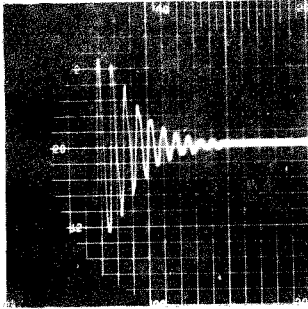




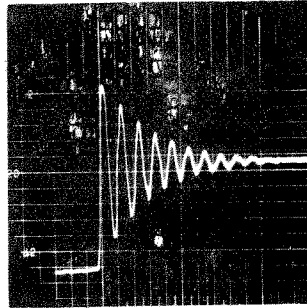
Static load - deflection curves - Beams 13-16



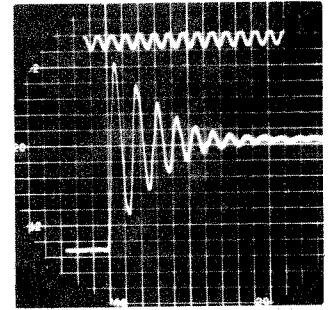




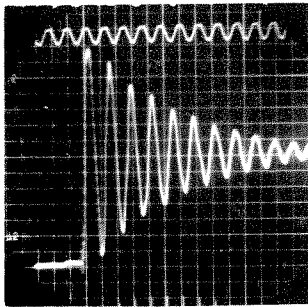
Test 1-1D $\lambda = 0.047$
 $x(0) = 0.047''$ $p_0 = 2.00k$



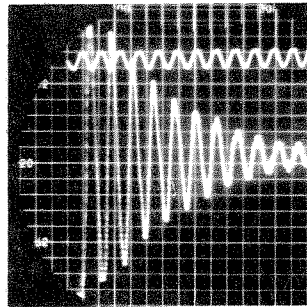
Test 1-2D $\lambda = 0.049$
 $x(0) = 0.178''$ $p_0 = 3.30k$



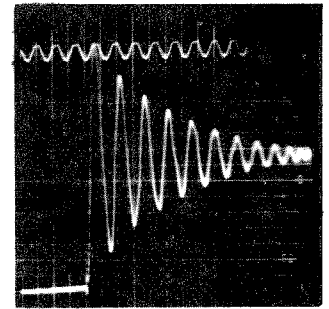
Test 1-3D $\lambda = 0.064$
 $x(0) = 0.330''$ $p_0 = 4.25k$



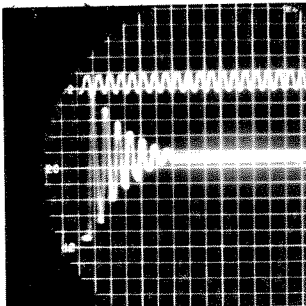
Test 2-1D $\lambda = 0.038$
 $x(0) = 0.050''$ $p_0 = 2.00k$



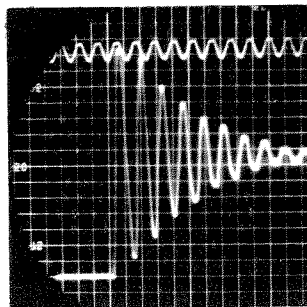
Test 2-2D $\lambda = 0.033$
 $x(0) = 0.115''$ $p_0 = 3.93k$



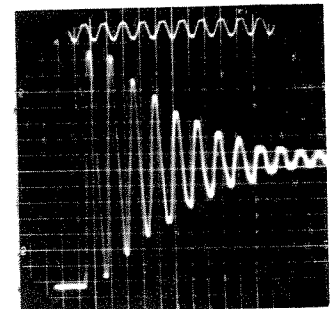
Test 2-3D $\lambda = 0.041$
 $x(0) = 0.240''$ $p_0 = 5.82k$



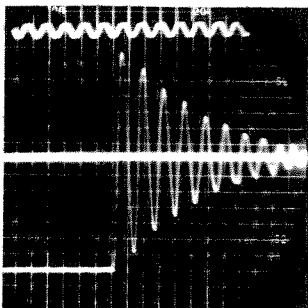
Test 3-1D $\lambda = 0.052$
 $x(0) = 0.030''$ $p_0 = 1.20k$



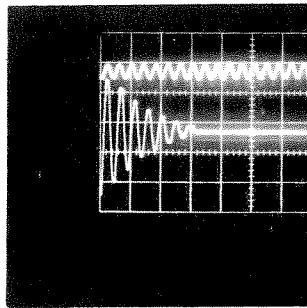
Test 3-2D $\lambda = 0.043$
 $x(0) = 0.060''$ $p_0 = 2.32k$



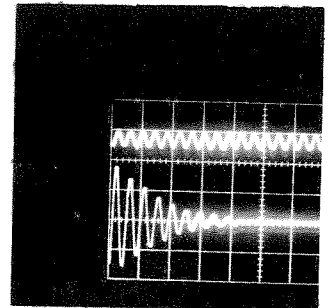
Test 3-3D $\lambda = 0.035$
 $x(0) = 0.085''$ $p_0 = 3.30k$



Test 3-4D $\lambda = 0.037$
 $x(0) = 0.125''$ $p_0 = 4.60k$



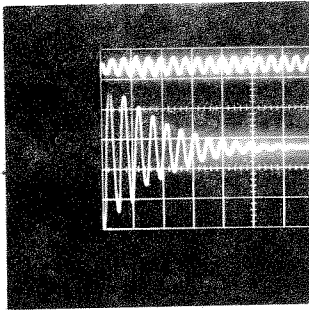
Test 4-1D $\lambda = 0.047$
 $x(0) = 0.033''$ $p_0 = 1.40k$



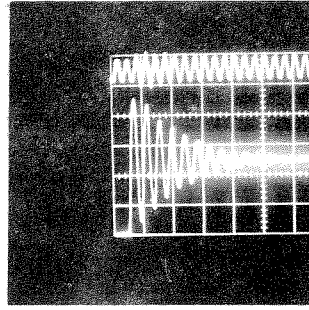
Test 4-2D $\lambda = 0.045$
 $x(0) = 0.045''$ $p_0 = 2.00k$

Figure 82

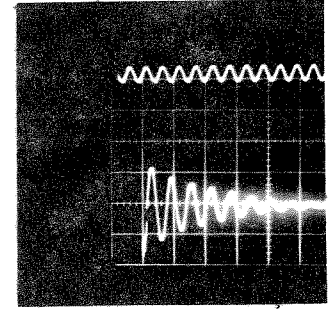
Free vibration response - Beam Nos. 1-4



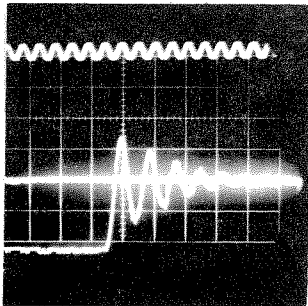
Test 4-3D $\lambda = 0.040$
 $x(0) = 0.100''$ $p_0 = 3.92k$



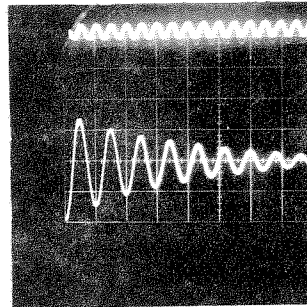
Test 4-4D $\lambda = 0.039$
 $x(0) = 0.210''$ $p_0 = 7.10k$



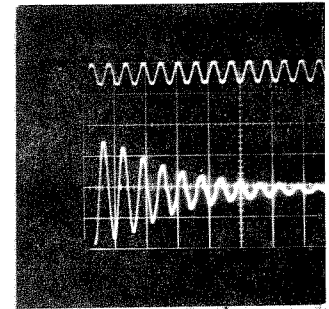
Test 5-1D $\lambda = 0.043$
 $x(0) = 0.050''$ $p_0 = 2.00k$



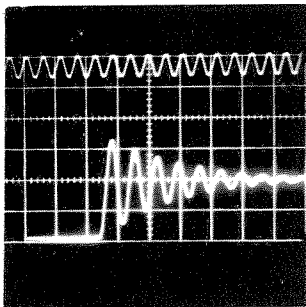
Test 5-2D $\lambda = 0.066$
 $x(0) = 0.405''$ $p_0 = 3.50k$



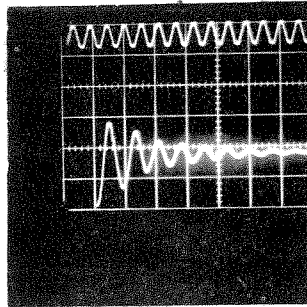
Test 5-3D $\lambda = 0.037$
 $x(0) = 0.435''$ $p_0 = 3.55k$



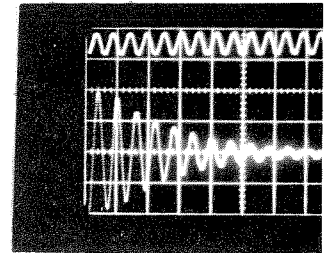
Test 6-1D $\lambda = 0.032$
 $x(0) = 0.050''$ $p_0 = 2.00k$



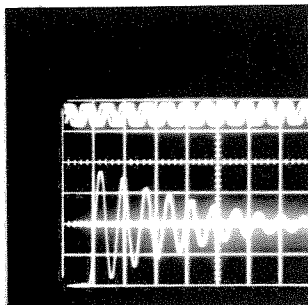
Test 6-2D $\lambda = 0.044$
 $x(0) = 0.195''$ $p_0 = 4.00k$



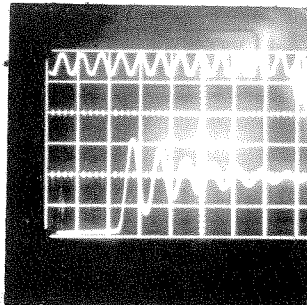
Test 6-3D $\lambda = 0.063$
 $x(0) = 0.405''$ $p_0 = 5.20k$



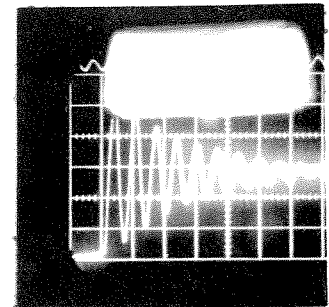
Test 7-1D $\lambda = 0.031$
 $x(0) = 0.050''$ $p_0 = 2.00k$



Test 7-2D $\lambda = 0.032$
 $x(0) = 0.115''$ $p_0 = 4.00k$



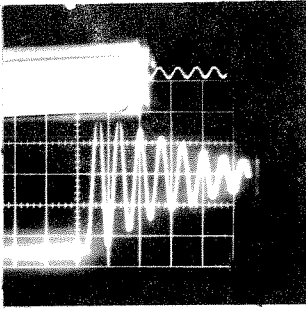
Test 7-3D $\lambda = 0.050$
 $x(0) = 0.380''$ $p_0 = 6.00k$



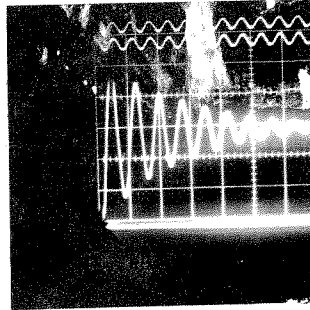
Test 8-1D $\lambda = 0.034$
 $x(0) = 0.049''$ $p_0 = 2.00k$

Figure 83

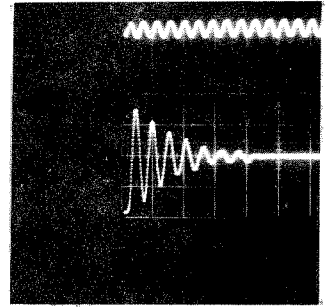
Free vibration response - Beam Nos. 4-8



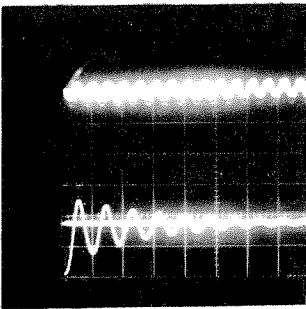
Test 8-2D $\lambda = 0.034$
 $x(0) = 0.100''$ $p_0 = 4.00k$



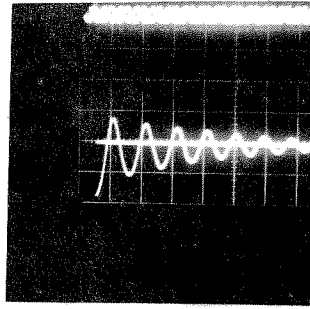
Test 8-3D $\lambda = 0.040$
 $x(0) = 0.235''$ $p_0 = 5.80k$



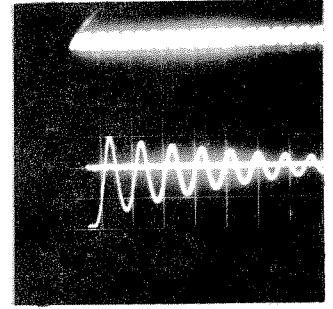
Test 9-1D $\lambda = 0.056$
 $x(0) = 0.030''$ $p_0 = 1.00k$



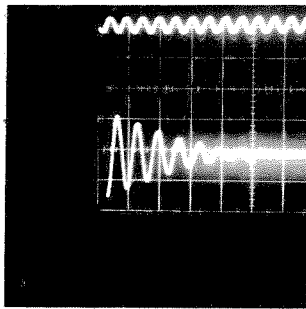
Test 9-2D $\lambda = 0.043$
 $x(0) = 0.20''$ $p_0 = 1.45k$



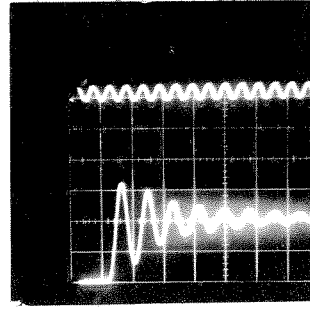
Test 9-3D $\lambda = 0.040$
 $x(0) = 0.333''$ $p_0 = 1.70k$



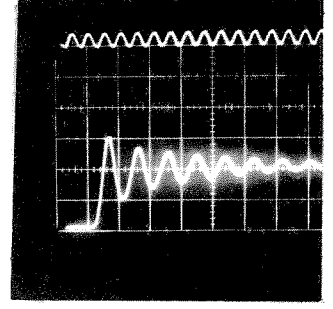
Test 9-4D $\lambda = 0.030$
 $x(0) = 0.375''$ $p_0 = 1.75k$



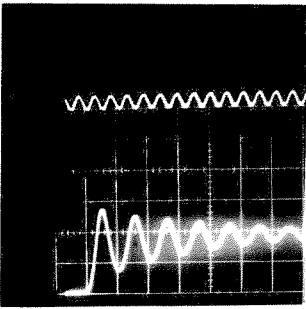
Test 10-1D $\lambda = 0.052$
 $x(0) = 0.032''$ $p_0 = 1.00k$



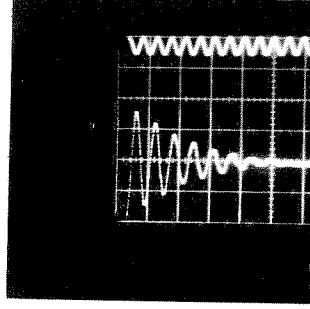
Test 10-2D $\lambda = 0.060$
 $x(0) = 0.145''$ $p_0 = 2.00k$



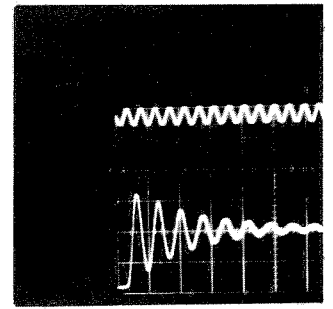
Test 10-3D $\lambda = 0.050$
 $x(0) = 0.335''$ $p_0 = 2.40k$



Test 10-4D $\lambda = 0.050$
 $x(0) = 0.435''$ $p_0 = 2.55k$



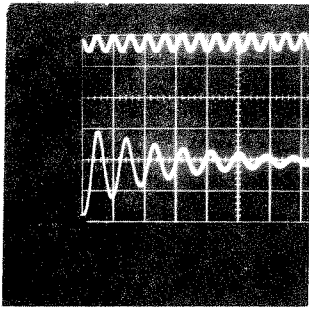
Test 11-1D $\lambda = 0.047$
 $x(0) = 0.032''$ $p_0 = 1.00k$



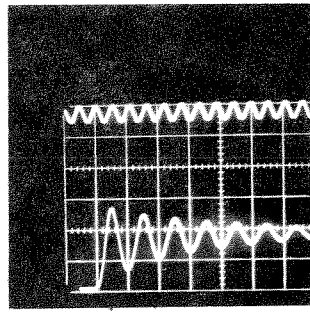
Test 11-2D $\lambda = 0.054$
 $x(0) = 0.120''$ $p_0 = 2.00k$

Figure 84

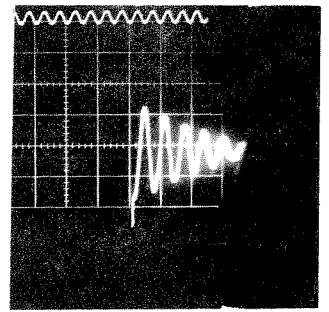
Free vibration response - Beam Nos. 8-11



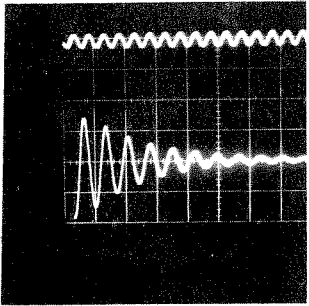
Test 11-3D $\lambda = 0.049$
 $x(0) = 0.245''$ $p_0 = 2.45k$



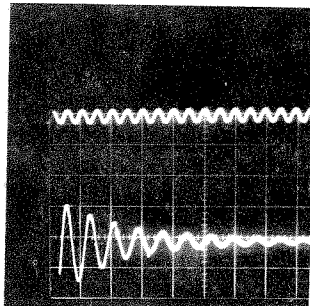
Test 11-4D $\lambda = 0.042$
 $x(0) = 0.355''$ $p_0 = 2.80k$



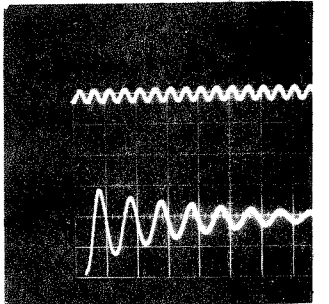
Test 12-1D $\lambda = 0.046$
 $x(0) = 0.032''$ $p_0 = 1.00k$



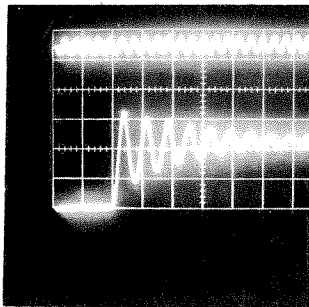
Test 12-2D $\lambda = 0.048$
 $x(0) = 0.084''$ $p_0 = 2.00k$



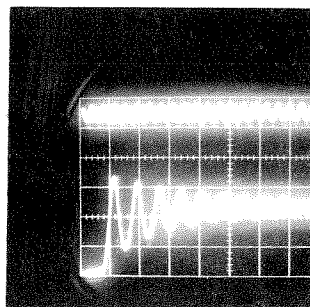
Test 12-3D $\lambda = 0.049$
 $x(0) = 0.212''$ $p_0 = 2.70k$



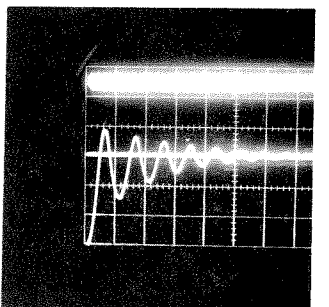
Test 12-4D $\lambda = 0.045$
 $x(0) = 0.330''$ $p_0 = 3.05k$



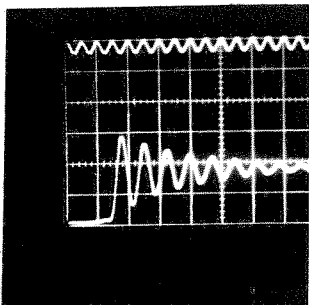
Test 13-1D $\lambda = 0.038$
 $x(0) = 0.145''$ $p_0 = 0.78k$



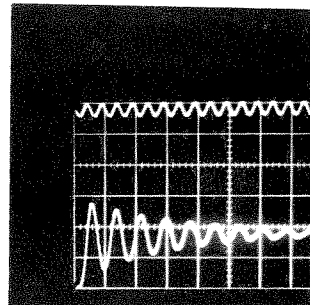
Test 13-2D $\lambda = 0.041$
 $x(0) = 0.170''$ $p_0 = 0.78k$



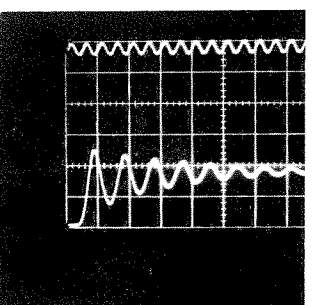
Test 13-3D $\lambda = 0.058$
 $x(0) = 0.430''$ $p_0 = 0.87k$



Test 14-1D $\lambda = 0.041$
 $x(0) = 0.050''$ $p_0 = 0.83k$



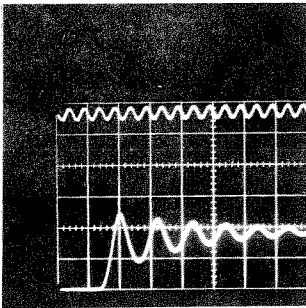
Test 14-2D $\lambda = 0.040$
 $x(0) = 0.100''$ $p_0 = 1.10k$



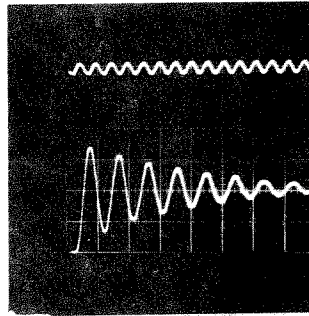
Test 14-3D $\lambda = 0.046$
 $x(0) = 0.253''$ $p_0 = 1.27k$

Figure 85

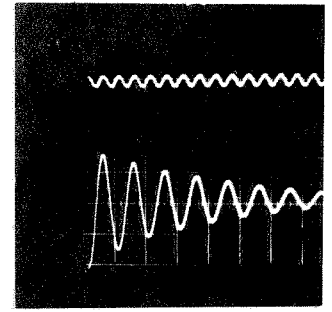
Free vibration response - Beam Nos. 11-14



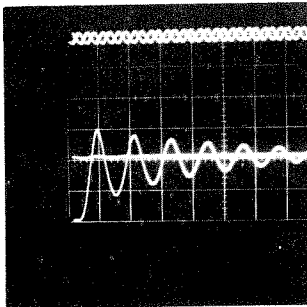
Test 14-4D $\lambda = 0.050$
 $x(0) = 0.500''$ $p_o = 1.50k$



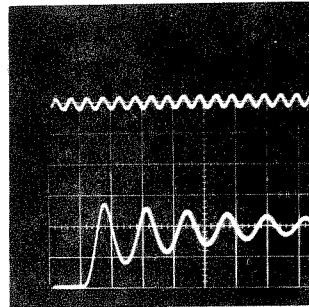
Test 15-1D $\lambda = 0.043$
 $x(0) = 0.065''$ $p_o = 0.64k$



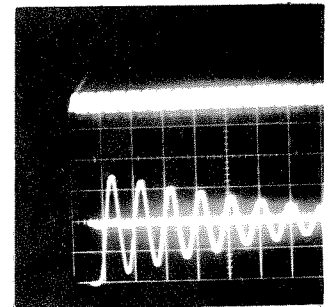
Test 15-2D $\lambda = 0.038$
 $x(0) = 0.115''$ $p_o = 0.98k$



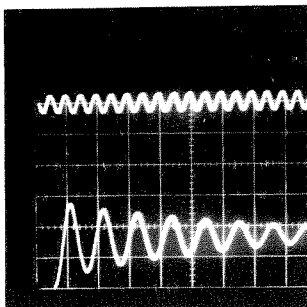
Test 15-3D $\lambda = 0.047$
 $x(0) = 0.300''$ $p_o = 1.35k$



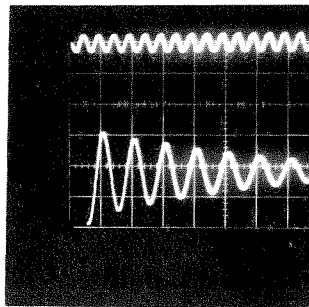
Test 15-4D $\lambda = 0.041$
 $x(0) = 0.525''$ $p_o = 1.60k$



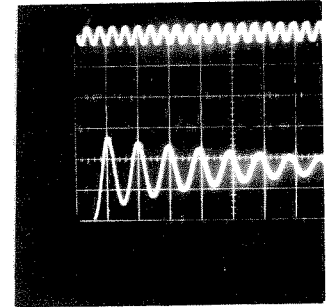
Test 16-1D $\lambda = 0.027$
 $x(0) = 0.050''$ $p_o = 0.61k$



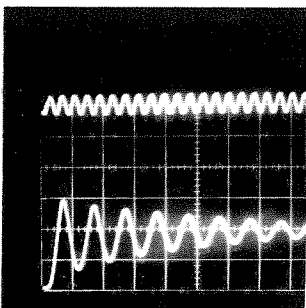
Test 16-2D $\lambda = 0.030$
 $x(0) = 0.100''$ $p_o = 1.00k$



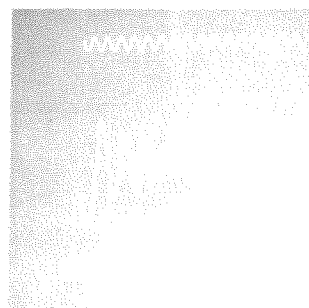
Test 16-3D $\lambda = 0.030$
 $x(0) = 0.200''$ $p_o = 1.50k$



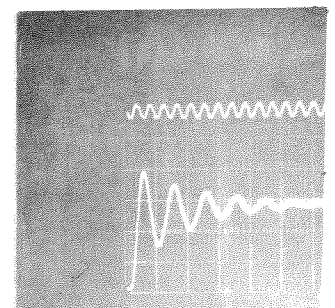
Test 16-4D $\lambda = 0.031$
 $x(0) = 0.312''$ $p_o = 1.68k$



Test 16-5D $\lambda = 0.035$
 $x(0) = 0.400''$ $p_o = 1.75k$



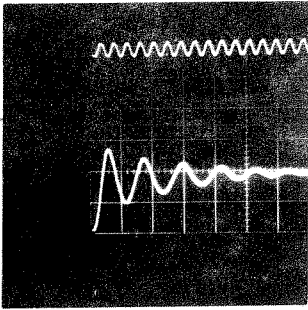
Test 17-1D $\lambda = 0.051$
 $x(0) = 0.044''$ $p_o = 0.78k$



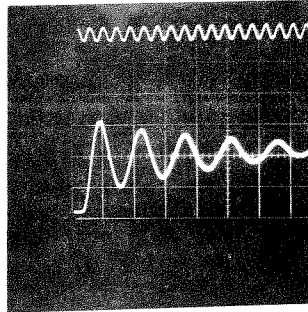
Test 17-2D $\lambda = 0.064$
 $x(0) = 0.114''$ $p_o = 1.10k$

Figure 86

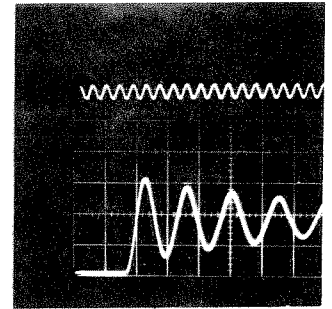
Free vibration response - Beam Nos. 14-17



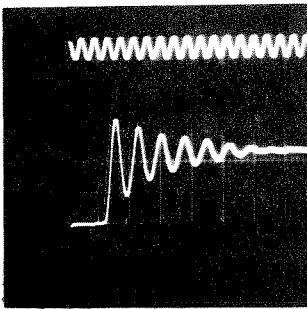
Test 17-3D $\lambda = 0.060$
 $x(0) = 0.204''$ $p_0 = 1.65k$



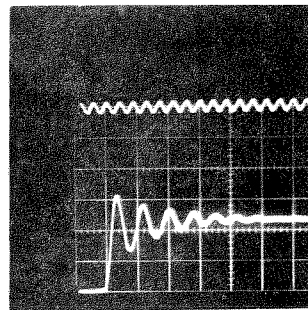
Test 17-4D $\lambda = 0.050$
 $x(0) = 0.302''$ $p_0 = 2.28k$



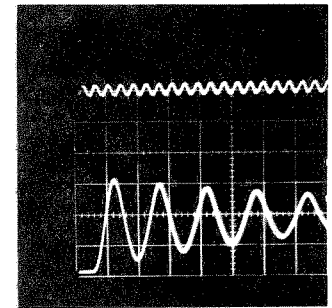
Test 17-5D $\lambda = 0.034$
 $x(0) = 0.410''$ $p_0 = 2.90k$



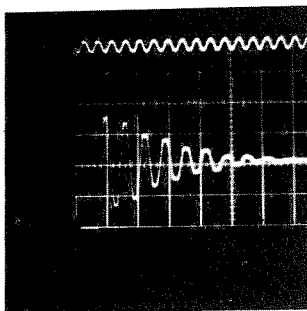
Test 18-1D $\lambda = 0.051$
 $x(0) = 0.070''$ $p_0 = 0.70k$



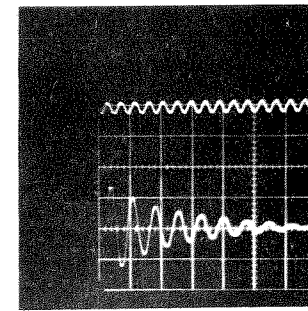
Test 18-2D $\lambda = 0.063$
 $x(0) = 0.111''$ $p_0 = 0.95k$



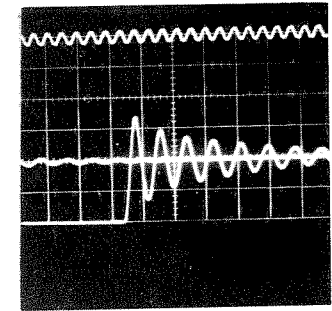
Test 18-3D $\lambda = 0.029$
 $x(0) = 0.500''$ $p_0 = 1.90k$



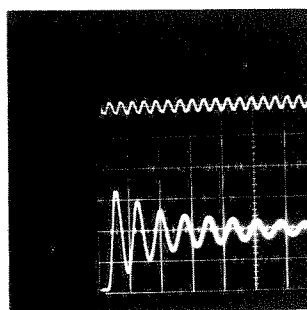
Test 19-1D $\lambda = 0.042$
 $x(0) = 0.050''$ $p_0 = 1.48k$



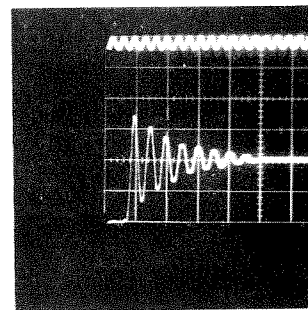
Test 19-2D $\lambda = 0.047$
 $x(0) = 0.109''$ $p_0 = 2.30k$



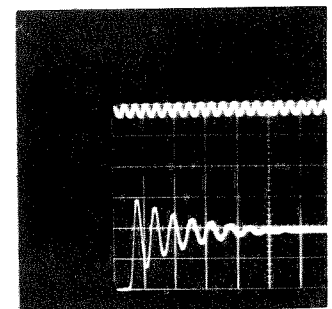
Test 19-3D $\lambda = 0.044$
 $x(0) = 0.210''$ $p_0 = 4.10k$



Test 19-4D $\lambda = 0.044$
 $x(0) = 0.530''$ $p_0 = 8.43k$



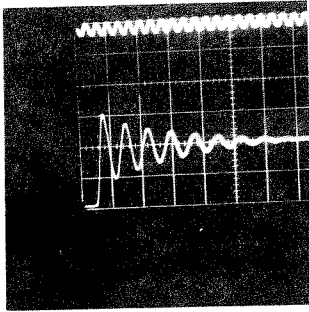
Test 20-1D $\lambda = 0.048$
 $x(0) = 0.060''$ $p_0 = 1.28k$



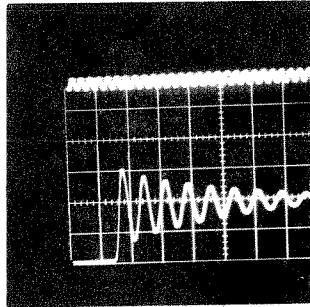
Test 20-2D $\lambda = 0.051$
 $x(0) = 0.102''$ $p_0 = 1.52k$

Figure 87

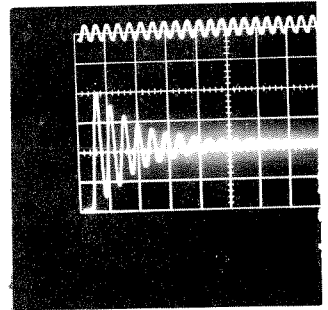
Free vibration response - Beam Nos. 17-20



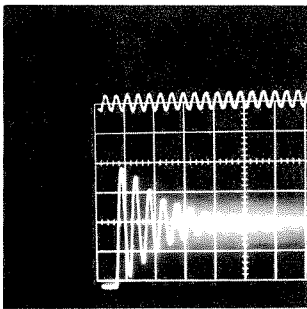
Test 20-3D $\lambda = 0.046$
 $x(0) = 0.205''$ $p_0 = 2.40k$



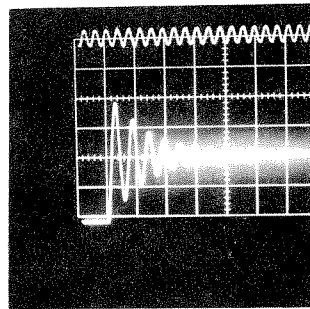
Test 20-4D $\lambda = 0.032$
 $x(0) = 0.420''$ $p_0 = 4.20k$



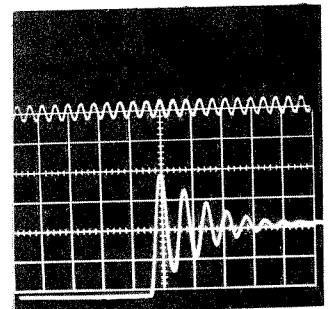
Test 21-1D $\lambda = 0.042$
 $x(0) = 0.039''$ $p_0 = 1.40k$



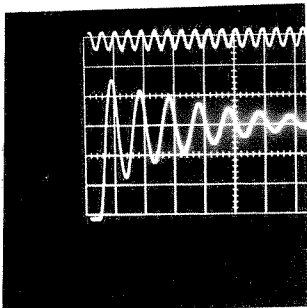
Test 21-2D $\lambda = 0.043$
 $x(0) = 0.94''$ $p_0 = 3.30k$



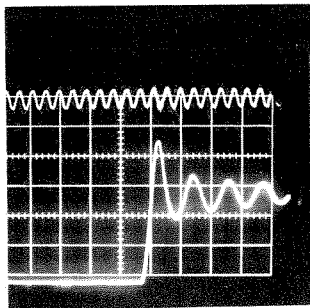
Test 21-3D $\lambda = 0.052$
 $x(0) = 0.274''$ $p_0 = 5.20k$



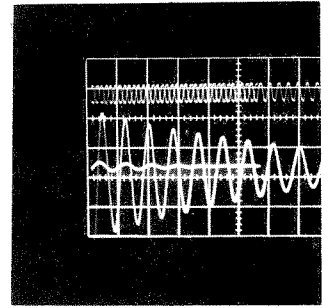
Test 21-4D $\lambda = 0.060$
 $x(0) = 0.500''$ $p_0 = 6.00k$



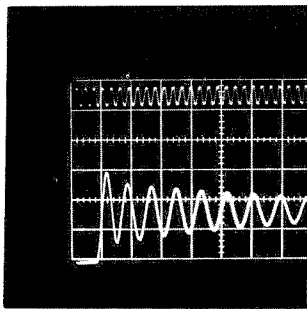
Test 22-1D $\lambda = 0.050$
 $x(0) = 0.200''$ $p_0 = 2.00k$



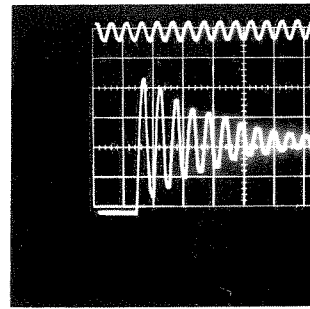
Test 22-2D $\lambda = 0.020$
 $x(0) = 0.369''$ $p_0 = 3.30k$



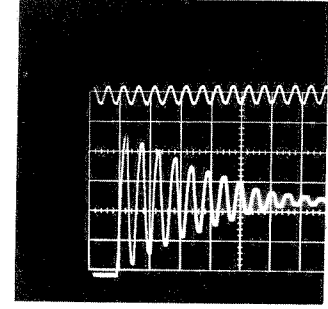
Test 22-3D $\lambda = 0.020$
 $x(0) = 0.369''$ $p_0 = 3.30k$



Test 22-4D $\lambda = 0.024$
 $x(0) = 0.560''$ $p_0 = 5.20k$



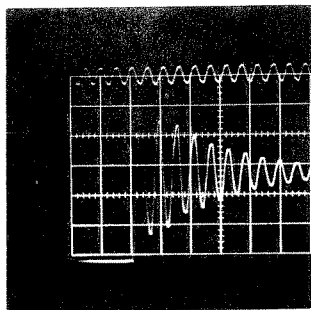
Test 23-1D $\lambda = 0.030$
 $x(0) = 0.060''$ $p_0 = 3.28k$



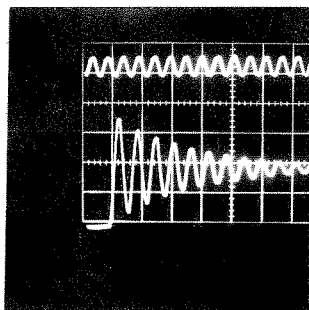
Test 23-2D $\lambda = 0.024$
 $x(0) = 0.095''$ $p_0 = 5.20k$

Figure 88

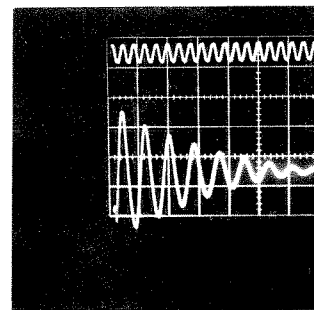
Free vibration response - Beam Nos. 20-23



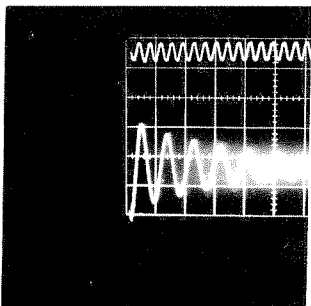
Test 23-3D $\lambda = 0.029$
 $x(0) = 0.104$ $p_0 = 0.05k$



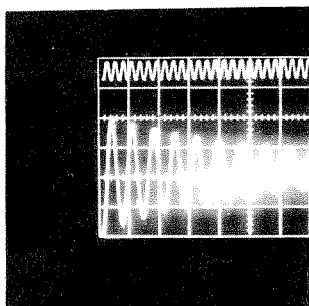
Test 23-4D $\lambda = 0.035$
 $x(0) = 0.250$ $p_0 = 9.00k$



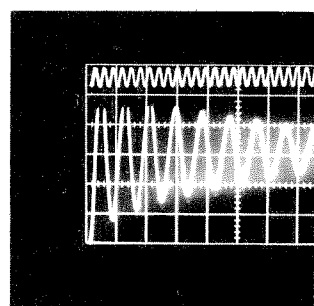
Test 24-1D $\lambda = 0.044$
 $x(0) = 0.160$ $p_0 = 2.00k$



Test 24-2D $\lambda = 0.037$
 $x(0) = 0.216$ $p_0 = 3.25k$

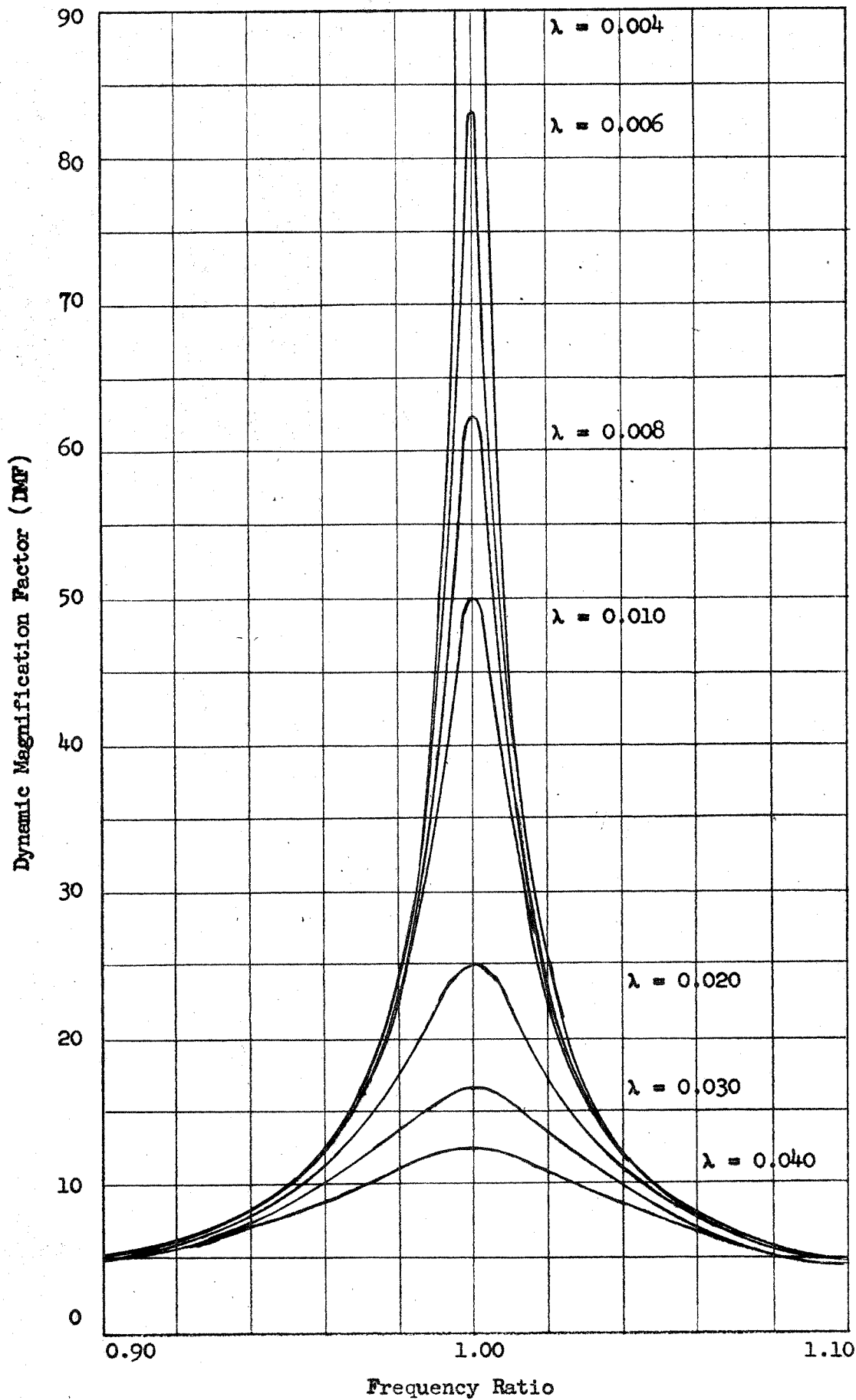


Test 24-3D $\lambda = 0.041$
 $x(0) = 0.477$ $p_0 = 4.95k$



Test 24-4D $\lambda = 0.025$
 $x(0) = 0.430$ $p_0 = 6.60k$

Figure 89 Free vibration response - Beam Nos. 23-24



Dynamic Magnification Factor vs. Frequency Ratio
for a single degree system

Figure 90